TECHNISCHE UNIVERSITÄT
ILMENAU

Technische Universität Ilmenau
Fakultät für Informatik und Automatisierung
Institut für Automatisierungs- und Systemtechnik
Fachgebiet Prozessoptimierung

Model-Based Optimization of PV-Based Microgrids Considering Grid Blackout and Battery Lifetime

Dissertation zur Erlangung des akademischen Grades Doktoringenieur (Dr.-Ing)

Mansour Alramlawi

Gutachter

Prof. Dr.-Ing habil. Pu Li (Technische Universität Ilmenau, Germany).

Prof. Dr.-Ing Georg Frey (Universität des Saarlandes, Germany).

Prof. Dr.-Ing. Peter Bretschneider (Fraunhofer Institut für Angewandte Systemtechnik, Germany).

Tag der Einreichung: 05.06.2020
Tag der wissenschaftlichen Aussprache: 16.12.2020

urn:nbn:de:gbv:ilm1-2020000668

Printed and/or published with the support of the German Academic exchange service.

Erklärung

Ich versichere, dass ich die vorliegende Arbeit ohne unzulässige Hilfe Dritter und ohne Benutzung anderer als der angegebenen Hilfsmittel angefertigt habe. Die aus anderen Quellen direkt oder indirekt übernommenen Daten und Konzepte sind unter Angabe der Quelle gekennzeichnet.
Weitere Personen waren an der inhaltlich-materiellen Erstellung der vorliegenden Arbeit nicht beteiligt. Insbesondere habe ich hierfür nicht die entgeltliche Hilfe von Vermittlungsbzw. Beratungsdiensten (Promotionsberater oder anderer Personen) in Anspruch genommen. Niemand hat von mir unmittelbar oder mittelbar geldwerte Leistungen für Arbeiten erhalten, die im Zusammenhang mit dem Inhalt der vorgelegten Dissertation stehen.
Die Arbeit wurde bisher weder im In- noch im Ausland in gleicher oder ähnlicher Form einer Prüfungsbehörde vorgelegt.
Ich bin darauf hingewiesen worden, dass die Unrichtigkeit der vorstehenden Erklärung als Täuschungsversuch bewertet wird und gemäß § 7 Abs. 10 der Promotionsordnung den Abbruch des Promotionsverfahrens zur Folge hat.

Ilmenau, June 5, 2020

Dedication

To the memory of my beloved mother, ***Wasfia Alramlawi***, who always believed in my ability to be successful man in the practical and academic life. You are gone, but your belief in me has made this journey possible.

Acknowledgements

Foremost, I wish to express my sincere thanks and gratitude to my advisor Prof. Pu Li for his continuous support of my research for his patience, guidance, and encouragement.

My profound thanks also go to Prof. Georg Frey from Saarland University and Prof. Peter Bretschneider from Fraunhofer-Institut for their precious time in reviewing my thesis and their insightful comments.

I am very grateful to my colleagues in Process Optimization Group at Technische Universität Ilmenau. In particular, I am very thankful to Dr. Siegbert Hopfgarten and Dr. Abebe Geletu for their continuous help and support in my practical and academic life. Sincere thanks to Mr. Kibru Teka Nida, Mr. Gbalimene-Richard Ileberi, Mr. Xujiang Huang, Mr. Björn Töpper, Mr. Qais Yousef, Mr. Bernd Juris, and Mr. Jens Hollandmoritz for their support, friendship and sharing beautiful memories in Ilmenau.

Special thanks to my friends Dr. Khaled Ardah and Dr. Erfan Mohagheghi, for their outstanding help and support. Furthermore, I appreciatively acknowledge the German Academic Exchange Service (DAAD) for funding my research.

Last but by no means least, I am incredibly grateful to my family from the bottom of my heart:my father, Yasser; my beloved wife, Nisreen; my sons Yamin and Adam, as well as my sisters and brothers for their love, endurance, and continuous support.

Abstract

The interest in installing photovoltaic (PV)-based microgrids (MGs) has increased significantly in the last few years due to the urgent need for reducing greenhouse gas emissions and improving the reliability as well as the quality of power supply, particularly in developing countries. However, the critical potential for low-cost operation and uninterrupted power supply lies in the optimal operation and design of such MGs.

This dissertation presents novel mathematical models and new formulations of optimal operation and design for both the residential and industrial MGs. Based on sophisticated and practical models of the considered MGs, different optimization problems are formulated and solved to address the grid blackout problem which is a significant problem in several countries worldwide.

The standard residential PV-Battery is enhanced by adding controllable switches to handle the practical constraints of the MG operation. Then an optimal power dispatch strategy based on the concept of an economic model predictive controller (EMPC) is proposed. The proposed operation strategy aims to cover the load and meanwhile minimize the total cost of the energy and prolong the battery lifetime considering the grid blackout problem.

On the other hand, it is well-known that the industrial loads have low power factors; therefore, the reactive power consumption of the load cannot be neglected. In this sense, a cost model for the dispatched reactive power from the PV-system and battery storage system is introduced. Furthermore, a novel cost model for reactive power generation from the diesel generator is developed. Consequently, a new active-reactive optimal power dispatch (AR-OPD) strategy for PV-battery-diesel MGs is introduced to decrease the costs of the dispatched active and reactive power.

The existence of the nonlinear cost function and nonlinear constraints leads to a dynamic mixed-integer nonlinear programming (MINLP) optimization problem, which

is solved by metaheuristic optimization techniques. The computation result shows that the proposed EMPC framework is able to manage the power dispatch in the MG cost-effectively and reliably for both grid-connected and islanded mode. Moreover, the proposed operation strategy leads to a significant reduction in the total costs of the dispatched active-reactive power and battery lifetime loss in comparison to the traditional rule-based operation strategies. Furthermore, it is approved that the PV-inverter is able to generate reactive power with very low cost compared to other energy sources in the MG.

From another perspective, optimizing the sizes of MG components is essential to guarantee the best performance and maximize the MG profitability. Therefore, a comprehensive method for the optimal design of both the residential and industrial MGs is proposed. The proposed method aims to minimize the Levelized cost of energy ($LCOE$) considering the limitation of the annual total loss of the power supply ($TLPS$) and the MG operational constraints. In the proposed method, special attention is given to estimate the battery bank lifetime accurately. For that, a comprehensive model for the lead-acid battery is utilized to simulate the battery operation and aging, based on the Physico-chemical processes of the battery.

However, considering the uncertainty of the input parameters play a vital role in increasing the optimal design accuracy. Therefore, the uncertainties of solar irradiance, ambient temperature, blackouts starting time, and blackouts duration are modeled and added to the optimization problem. However, due to the existence of random parameters in the optimization problem, it is uncertain to satisfy the problem constraints. Therefore, the new optimization problem is formulated as a chance-constrained optimization problem and solved by a stochastic simulation-based optimization method incorporating Monte-Carlo simulation.

The results showed that neglecting the uncertainties of the input parameter can lead to a significant error in calculating the optimum size, which drives to a considerable decrement in the reliability level of the MG. Moreover, it could lead to a wrong estimation for the $LCOE$ over the MG life, which could lead to wrong investment decisions. Moreover, it is observed that considering the uncertainty of grid blackouts plays the most crucial role in ensuring the reliability of the MG.

Zusammenfassung

Das Interesse an der Installation von auf Photovoltaik (PV) basierenden Mikronetzen (MGs) hat in den letzten Jahren deutlich zugenommen, da die dringende Notwendigkeit besteht, die Treibhausgasemissionen zu reduzieren und die Zuverlässigkeit sowie die Qualität der Stromversorgung, insbesondere in Entwicklungsländern, zu verbessern. Das entscheidende Potenzial für einen kostengünstigen Betrieb und eine unterbrechungsfreie Stromversorgung liegt jedoch im optimalen Betrieb und Design solcher MGs.

In dieser Dissertation werden neue mathematische Modelle und neue Formulierungen für den optimalen Betrieb und die optimale Auslegung von MGs sowohl für Wohnviertel als auch für die Industrie vorgestellt. Basierend auf hochentwickelten und praktischen Modellen der betrachteten MGs werden verschiedene Optimierungsprobleme formuliert und gelöst, um das Netzausfallproblem anzugehen, das in mehreren Ländern weltweit ein bedeutendes Problem darstellt.

Die Standard- PV-Batterie für Privathaushalte wird um steuerbare Schalter erweitert, um den praktischen Einschränkungen des MG -Betriebs gerecht zu werden. Dann wird eine optimale Leistungsabgabestrategie vorgeschlagen, die auf dem Konzept eines prädiktiven Reglers mit einem ökonomischen Modell (EMPC) basiert. Die vorgeschlagene Betriebsstrategie zielt darauf ab, die Last abzudecken und in der Zwischenzeit die Gesamtkosten der Energie zu minimieren und die Lebensdauer der Batterie unter Berücksichtigung des Netzausfallproblems zu verlängern.

Andererseits ist bekannt, dass die industriellen Lasten niedrige Leistungsfaktoren haben; daher kann der Blindleistungsverbrauch der Last nicht vernachlässigt werden. In diesem Sinne wird ein Kostenmodell für die abgegebene Blindleistung aus dem PV-System und dem Batteriespeichersystem vorgestellt. Darüber hinaus wird ein

neuartiges Kostenmodell für die Blindleistungserzeugung aus dem Dieselgenerator entwickelt. Folglich wird eine neue optimale Wirk-Blindleistungsverteilungsstrategie (AR-OPD) für PV-Batterie-Diesel-MGs eingeführt, um die Kosten der abgegebenen Wirk- und Blindleistung zu senken. Die Existenz der nichtlinearen Kostenfunktion und nichtlinearer Nebenbedingungen führt zu einem Optimierungsproblem der dynamischen gemischt-ganzzahligen nichtlinearen Programmierung (MINLP), das durch metaheuristische Optimierungstechniken gelöst wird. Das Berechnungsergebnis zeigt, dass das vorgeschlagene EMPC-Rahmenwerk in der Lage ist, die Leistungsverteilung im MG sowohl für den netzgekoppelten als auch für den Inselbetrieb kosteneffizient und zuverlässig zu steuern. Darüber hinaus führt die vorgeschlagene Betriebsstrategie im Vergleich zu den traditionellen regelbasierten Betriebsstrategien zu einer signifikanten Reduzierung der Gesamtkosten der abgegebenen Wirk-Blindleistung und des Batterie-Lebensdauerverlusts. Darüber hinaus wird gezeigt , dass der PV-Wechselrichter in der Lage ist, Blindleistung mit sehr geringen Kosten im Vergleich zu anderen Energiequellen im MG zu erzeugen. Aus einer anderen Perspektive ist die Optimierung der Größe der MG-Komponenten von wesentlicher Bedeutung, um die beste Leistung zu garantieren und die Rentabilität des MG zu maximieren. Daher wird eine umfassende Methode für die optimale Auslegung sowohl der Wohnviertel- als auch der Industrie-MGs vorgeschlagen. Die vorgeschlagene Methode zielt darauf ab, die nivellierten Energiekosten (LCOE) unter Berücksichtigung der Begrenzung des jährlichen Gesamtverlustes der Stromversorgung (TLPS) und der betrieblichen Einschränkungen des MG zu minimieren. Bei der vorgeschlagenen Methode wird besonders darauf geachtet, die Lebensdauer der Batteriebank genau abzuschätzen. Dazu wird ein umfassendes Modell für die Blei-Säure-Batterie verwendet, um den Betrieb und die Alterung der Batterie zu simulieren, basierend auf den physikalisch-chemischen Prozessen der Batterie.

Die Berücksichtigung der Unsicherheit der Eingabeparameter spielt jedoch eine entscheidende Rolle bei der Erhöhung der optimalen Entwurfsgenauigkeit. Daher werden die Unsicherheiten der Sonneneinstrahlung, der Umgebungstemperatur, der Blackout-Startzeit und der Blackout-Dauer modelliert und zum Optimierungsproblem hinzugefügt. Aufgrund der Existenz von Zufallsparametern im Optimierungsprob-

lem ist es jedoch unsicher, die Randbedingungen des Problems zu erfüllen. Daher wird das neue Optimierungsproblem als ein wahrscheinlichkeitsbeschränktes Optimierungsproblem formuliert und durch eine auf stochastischer Simulation basierende Optimierungsmethode unter Einbeziehung der Monte-Carlo-Simulation gelöst. Die Ergebnisse zeigten, dass die Vernachlässigung der Unsicherheit der Eingangsparameter zu einem signifikanten Fehler bei der Berechnung der optimalen Größe führen kann, was zu einer erheblichen Verminderung des Zuverlässigkeitsniveaus des MG führt. Darüber hinaus könnte dies zu einer falschen Schätzung für den LCOE über die Lebensdauer des MG führen, was zu falschen Investitionsentscheidungen führen könnte. Darüber hinaus ist zu beobachten, dass die Berücksichtigung der Unsicherheit von Netzausfällen die entscheidende Rolle bei der Gewährleistung der Zuverlässigkeit des MG spielt.

Contents

Nomenclature

Battery Storage System

$\Delta W(t)$	The growth in the corrosion layer thickness in lead acid battery.
η_{ch}/η_{dis}	Battery bank charging/discharging efficiency.
$\gamma_{ch.lim}$	Parameter for charging power limit.
$\gamma_{dis.lim}$	Parameter for discharging power limit.
$\lambda_{soc}(t)$	Effective ampere-hour waiting factor.
$\rho_{corr}(t)$	Corrosion layer resistance.
$\xi_{ch/dis}(t)$	Binary variable for charging/discharging switch status.
$A_c(t)$	Effective consumed ampere-hour from battery bank.
$A_c^{'}(t)$	Actual consumed ampere-hour from battery bank.
A_{total}	Total effective ampere-hours lead-acid battery can provide.
$B_{n.c}$	Nominal capacity of a single battery unit in the battery bank.
$BB_{n.c}$	Battery bank nominal capacity.
$BC_{n.c}$	Nominal capacity of a battery cell.
$C_{corr}(t)$	Battery capacity decrement due to corrosion effects.
$C_{deg}(t)$	Battery capacity decrement due to degradation effects.
$C_{rem.b}(t)$	Remaining (rest) capacity of the battery.
DOD	Battery bank depth of discharge.
$f_{acid}(t)$	Factor that represent the effect of acid stratification on lead-acid battery lifetime.
$f_I(t)$	Factor that represent the effect of discharging current on lead-acid battery lifetime.
$f_{SOC}(t)$	Factor that represent the effect of state of charge on lead-acid battery lifetime

$I_b(t)$	Battery current.
I_d	Battery discharging current.
$I_{gas}(t)$	Gassing current in lead-acid battery.
$K_s(t)$	Corrosion speed variable.
$L_f(t)$	Battery bank lifetime losing factor.
$n_{b.ch}(t)$	Influence of the number of ineffective charging.
$P_{ch.dg}(t)$	Battery bank charging power from diesel generator set.
$P_{ch.g}(t)$	Battery bank charging power from the main grid.
$P_{ch.pv}(t)$	Battery bank charging power from PV-array.
$P_{ch}(t)$	Total battery bank charging power.
$P_{dis}(t)$	Battery bank discharging power.
$Q_{b.n}$	Battery bank nominal capacity in ampere-hour.
$R_{cell}(t)$	Battery-cell internal resistance.
$SOC(t)$	Battery bank state of charge.
$SOC_{min/max}$	Lower/Upper limit of battery bank state of charge.
$SOC_{norm}(t)$	Normalized battery bank SOC.
$T_b(t)$	Battery temperature.
$V_b(t)$	Battery-cell voltage.
$V_{b.n}$	Battery bank nominal voltage.
$V_{corr}(t)$	Corrosion voltage of lead-acid battery.
$V_{gas}(t)$	Gassing voltage in lead-acid battery.
$V_{oc}(t)$	Battery-cell open circuit voltage.
Z_0	Number of nominal battery cycles.
$Z_W(t)$	Number of weighted battery cycles.

Optimal Operation

C_p^T/C_q^T	Total cost of the consumed active/reactive power from the MG.
$C_q^{BSS}(t)$	Dispatched reactive power cost from battery-inverter.
$C_q^{dg_i}(t)$	Dispatched reactive power cost from DG_i.
$C_q^{PV}(t)$	Dispatched reactive power cost from PV-inverter.
$C_{b.b}$	Capital cost of a battery bank.
$C_{b.l}(t)$	Cost of battery bank lifetime loss.

$C_{e.g}$	Cost of energy dispatch from the grid.
C_f	Fuel cost.
$C_{n.g}$	Net energy cost of the grid-tie line.
$C_{op.dg}(t)$	Total operation cost of all DGs.
$C_{p.g}/C_{exp}$	Cost of active power imported/exported from/to the main grid.
$C_{q.g}$	Cost of reactive power imported from the main grid.
C_{up_i}/C_{d_i}	DG_i startup/shutdown cost.
k	An EMPC sampling instant.
N_p	Number of time intervals within the prediction horizon.
$\mathbf{U_b}$	Sequence of N_p predicted binary control variables.
$\mathbf{u_b}(t)$	Binary control variables vector.
$\mathbf{U_c}$	Sequence of N_p predicted continues control variables.
$\mathbf{u_c}(t)$	Continuous control variables vector.

Diesel Generator

$\Delta P^X_{inv.loss}(t)$	The power loss in the PV/BSS inverter caused by the reactive power generation.
$\eta_{dg_{i_0}}(t)$	$\mathrm{DG_i}$ alternator efficiency at unity power factor.
$\eta_{dg_{i_r}}(t)$	Reduction in $\mathrm{DG_i}$ alternator efficiency.
$\eta_{dg_i}(t)$	$\mathrm{DG_i}$ alternator efficiency.
$\xi_{dg.i}(t)$	Binary variable for diesel generator status.
$\xi_{up/d.dg_i}(t)$	Binary variables that represent the changes of each diesel generator status.
$f_{con.dg_i}(t)$	Fuel consumption of $\mathrm{DG_i}$ at time t.
$f_{con.dg_{i_0}}(t)$	Fuel consumption of $\mathrm{DG_i}$ working at unity power factor at time t.
N_{dg}	Number of diesel generators.
$P_{dg.l}(t)$	Dispatched active power from DGs set to the load.
$P_{disp.dg_i}(t)$	Total dispatched active power from $\mathrm{DG_i}$ alternator.
$P_{m.dg_i}(t)$	Dispatched mechanical power from the diesel engine of $\mathrm{DG_i}$.
$P_{r.dg_i}$	$\mathrm{DG_i}$ rated power at unity power factor.
$PF_{dg.min_i}$	Lower limit of operating power factor for $\mathrm{DG_i}$.
$PF_{dg_i}(t)$	Operating power factor for $\mathrm{DG_i}$.

$Q_{disp.dg_i}(t)$ Dispatched reactive power from the alternator of DG_i.

S_{dg_i} DG_i rated apparent power.

Grid-Tie Line

$\alpha_g(t)$ Binary variable represents the status of the grid-tie line.

$\xi_{disp}(t)$ Binary variable for power dispatching status from the main grid.

$\xi_{exp}(t)$ Binary variable for power exporting status to the main grid.

Bl_{pr} Blackout period.

Bl_{st} Blackout starting time.

$P_{av.g}(t)$ Available power from grid-tie line.

$P_{disp.g}(t)$ Dispatched active power from main grid.

$P_{exp}(t)$ Exported active power to the main grid.

$P_{g.l}(t)$ Power to load from the main grid.

$P_{g.max}$ Maximum allowed power to be extracted from grid-tie line.

$Q_{disp.g}(t)$ Dispatched reactive power from the main grid.

$S_{g.max}$ Maximum allowed apparent power to be imported/exported from/to the main grid.

Optimal Design

Ω Uncertain variables space.

$\mathbf{A}$ Vector of the adjustment factors of the decision variables.

$C_{a.op.dg}$ Annual operation cost of the diesel generator.

C_g Annual cost of the dispatched energy from the grid.

$C_{m.b}$ Annual maintenance cost of the battery bank.

$C_{m.dg}$ Annual maintenance cost of the diesel generator.

$C_{m.pv}$ Annual maintenance cost of the PV-array.

$CC_{b.b}$ Capital cost of the battery bank.

$CC_{b.inv}$ Capital cost of the battery inverter.

CC_{batt} Capital cost of a single battery unit in the battery bank.

CC_{dg_i} Capital cost of the i^{th} diesel generator rate where $i \in 1, 2, ..., N_{dg}$.

$CC_{pv.inv}$ Capital cost of the PV-inverter.

$CC_{pv.m}$ Capital cost of a single module unit in the PV-array.

CC_{pv} Capital cost of the PV-array.

f_k	The generated probability density function from kernel density estimator.
$f_{G.x}$	Probability density function of solar irradiance.
f_T	Probability density function of ambient temperature.
$h_{dg.lt}$	Maximum number of operation hours of the DG before reaching the end of its life.
$h_{op.dg}$	Annual operation hours of a DG during one year.
L_{inst}	Length of the PV-array installation area.
N_{batt}	Total number of batteries in a battery bank.
N_{batt}^{max}	Maximum number of batteries that can be installed.
N_{dg}	Number of diesel generators.
N_{dg}^{max}	Maximum number of DG that can be installed in the a specified area.
$N_{pv.m}$	Total number of PV-modules in a PV-array.
$N_{pv.m}^{max}$	Maximum number of PV-modules that can be installed in the a specified area.
$N_{rep.x}$	Number of replacement of the component during the MG lifetime, the superscript x can be the battery bank, the diesel generator, the PV-inverter, or the battery-inverter.
$P_{r.dg_i}$	Rated power of the i^{th} DG where $i \in 1, 2, ..., N_{dg}$.
$P_{r.dg_i}^{max}$	Maximum Rate power of the i^{th} DG where $i \in 1, 2, ..., N_{dg}$.
$PV_{inv.size}$	PV-inverter size.
$PV_{inv.size}^{max}$	Maximum size of the PV-inverter.
$r_f^{'}$	Inflation rate.
r_i	Real interest rate.
$r_i^{'}$	Interest rate.
$SG_{d.min}$	Minimum distance between the PV-strings in a PV-array.
W_{inst}	Width of the PV-array installation area.
$\mathbf{u_{max}}$	Vector of maximum values of the decision variable.
$\mathbf{u_{min}}$	Vector of minimum values of the decision variable.
$\mathbf{u}^*$	Adjusted decision variables vector.

Power Electronics

$\eta_{inv}^{BSS}(t)$	Battery inverter efficiency.
$\eta_{inv}^{pv}(t)$	PV-inverter efficiency.
$c_{r.loss}$	Inverter current dependent loss.
c_{self}	Inverter self-losses at standby operation.
$c_{v.loss}$	Inverter output voltage dependent loss.
$P_{disp.inv}^{X}(t)$	Dispatched active power from PV/BSS inverter.
$P_{inv.loss}^{X}(t)$	Power losses in PV/BSS inverter.
$Q_{disp.inv}^{X}(t)$	Dispatched reactive power from PV/BSS inverter.
$S_{b.inv}$	Battery inverter rated apparent power.
$S_{pv.inv}$	PV-inverter rated apparent power.

Microgrid Model

$\xi_{1,\ldots,5}$	Binary variables for controllable switches' status.
$P_{av.l}(t)$	Total available power from the MG to cover the load.
$P_{req.l}(t)$	Required load power to be covered by the MG.
$Q_{av.l}(t)$	Total available reactive power from the MG to cover the load.
$Q_{req.l}(t)$	Required reactive power load to be covered by the MG.

PV-System

β	PV-module inclination angle.
$\overline{G_B}(t)$	Direct beam solar irradiance measured on the horizontal surface.
$\overline{G_D}(t)$	Diffused solar irradiance measured on a horizontal surface.
$\overline{G}(t)$	Global solar irradiance measured on the horizontal surface.
ϕ	The latitude of the installation position of the PV-system.
ρ	Solar irradiance reflection factor.
e	Charge of electron, i.e. 1.602×10^{-19}.
$FF(t)$	Fill factor of a PV-cell.
$FF_0(t)$	Nominal fill factor of a PV-cell.
$FF_{0.stc}$	Nominal fill factor of PV-cell at standard test conditions.
FF_{stc}	Fill factor of PV-cell at standard test conditions.
$G_T(t)$	Total solar irradiance arriving a PV-cell.
$G_B(t)$	Direct beam solar irradiance that arrives the PV-cell without reflection or scattering.

$G_D(t)$	Diffused solar irradiance which is scattered by the clouds.
$G_R(t)$	Reflected solar irradiance by the ground.
$I_0(t)$	The dark current in a PV-cell.
$I_{ph}(t)$	The photo-generated current in a PV-cell.
$I_{sc.c.stc}$	Short circuit current of a PV-cell under standard test conditions.
$I_{sc.c}(t)$	Short circuit current of a PV-cell.
$I_{sc.m.stc}$	Short circuit current of PV-module under standard test conditions.
k_B	Boltzmann's constant, equal to 1.38×10^{-23}.
K_i	Temperature coefficient of the short circuit current of a PV-cell.
K_v	Temperature coefficient of the open circuit voltage of a PV-cell.
n_d	Diode ideality factor.
$N_{c.m}$	Number of PV-cells in PV-module.
N_d	Number of days in a year (i.e 1 to 365 days).
$N_{p.m}$	Number of parallel PV-modules in PV-array.
$N_{s.m}$	Number of series PV-modules in a PV-array.
$NOCT$	Nominal operating PV-cell temperature.
$P_{av.pv}(t)$	Available power from PV-array.
$P_{disp.pv}(t)$	The total dispatched active power from the PV-system.
$P_{max.c.stc}$	Maximum output power of PV-cell under standard test conditions.
$P_{max.c}(t)$	Maximum output power of a PV-cell.
$P_{max.m.stc}$	Maximum output power of PV-module under standard test conditions.
$P_{max.pv}(t)$	Maximum output power of PV-array.
$P_{pv.l}(t)$	Power to load from PV-system.
R_B	Direct beam irradiance factor.
R_p	Parallel resistance of a PV-cell.
R_s	Series resistance of a PV-cell.
$r_s(t)$	Normalized series resistance of a PV-cell.
R_D	Diffuse solar irradiance factor.
$T_a(t)$	Ambient temperature in Celsius.
$T_c(t)$	PV-cell temperature in Celsius.
$T_{a.k}(t)$	Ambient temperature in Kelvin.

$V_{oc.c.stc}$	Open circuit voltage of a PV-cell under standard test conditions.
$V_{oc.c}(t)$	Open circuit voltage of a PV-cell.
$V_{oc.m.stc}$	Open circuit voltage of PV-module under standard test conditions.
$v_{oc}(t)$	Normalized open circuit voltage of PV-cell.
$V_{ph}(t)$	The photo-generated voltage in a PV-cell.
V_t	Thermal voltage of a PV-cell.
w_{ss}	Sunset hour angle on a horizontal surface.
$w_{ss}^{'}$	Sunset hour angle on a tilted surface.

Acronyms

ACC	Annualized capital cost
AMOC	Annual maintenance and operations cost
AR-OPD	Active-reactive optimal power dispatch
ARC	Annual replacement cost
BOS	Balance of system cost
CRF	Capital recovery factor
DG	Diesel generator
EMPC	Economic model predictive controler
GA	Genetic algorithm
GB	Grid blackout
KDE	Kernel density estimation
LCOE	Levelized cost of energy
MCS	Monte Carlo simulation
MG	Microgrid
MILP	Mixed-integer linear programming
MPC	Model predictive controller
OPD	Optimal power dispatch
PDF	Probability density function
PV	Photovoltaic
STC	Standard test conditions
TAPC	Total annual dispatched power cost
TLPS	Total loss of power supply

List of Figures

List of Tables

Chapter 1

Introduction

1.1 Introduction and Motivation

There is no doubt that electrical energy demand has been significantly increased in recent years. This increment can be satisfied by expanding the capacity of the existing electrical power generation system that depends mainly on fossil fuel power stations. However, due to the steady increase in fossil fuel prices and the considerable decrease in the prices of renewable energy systems, such as solar photovoltaics (see Fig. 1.1), it has become imperative to build hybrid energy systems with a substantial environmental and economic benefits [1]. In this sense, a microgrid (MG) concept is a promising approach to facilitate the integration of renewable energy sources with conventional ones to provide a reliable and cost-effective energy source [2].

The MG is defined as "a group of interconnected loads and distributed energy resources with clearly defined electrical boundaries that act as a controllable entity with respect to the grid and can be connected and disconnected from the grid to enable it to operate in both grid-connected or island mode" [1][4]. Based on this definition, a MG can be understood as a local electrical network capable of covering electrical loads independently of the main network. Moreover, the MG contains the necessary energy sources to cover the loads, power conditioning equipment such as power converters, and inverters, as well as an operator to organize the MG opera-

[1]Based on this definition, hybrid energy systems are considered as MGs in this thesis.

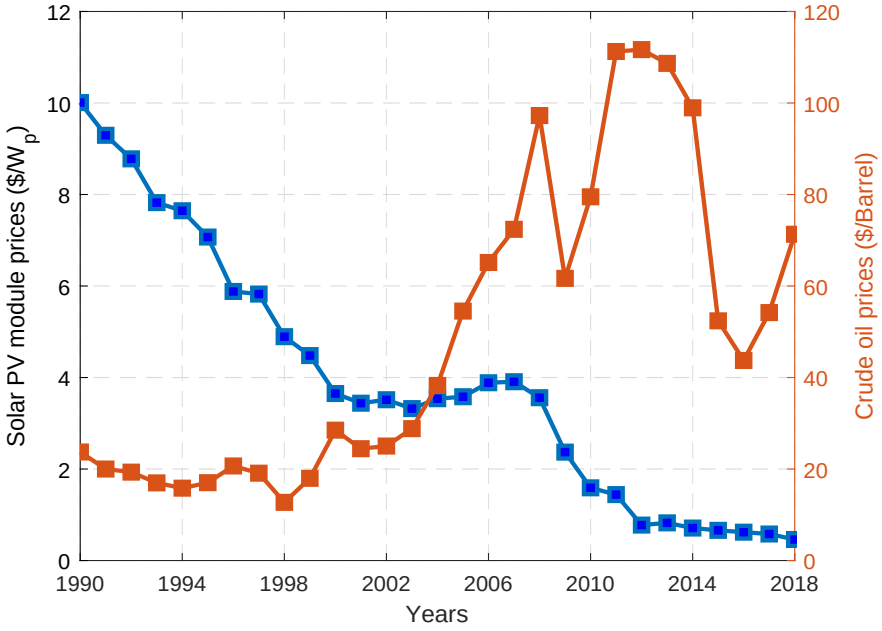

Figure 1.1: Illustration of the decrement in PV module prices and the increment in crude oil prices from 1990 to 2018. [3].

tion, see the MG illustration in Fig. 1.2. Besides, the MG can be used to cover the electrical loads of a single consumer, such as a residential [5] and an industrial [6] MG, or multiple consumers, such as a campus [7] and a community [8] MG.

From another perspective, due to its ability to work in either a grid-connected or an island mode [9], MGs are used to provide a reliable and cost-effective energy source to cover the load during blackout periods. The problem of grid blackout is a major problem in many countries worldwide [10] that has many economic and social impacts [11]. Therefore, many studies have been recently made for finding efficient solutions to develop reliable energy sources for consumers in such situations by utilizing different renewable energy resources [10, 12, 13, 14, 15]. Among these sources, the photovoltaic systems (PV-systems) take notable attention as a clean and cost-effective energy source because of its long lifetime, flexible sizing, and low cost as well as low maintenance and operation costs. Therefore, there is a rapid increase in the installation of solar energy systems globally, as shown in Figure 1.3. In particular, the abundance of solar energy in countries with shortages of electrical power (mostly in Asia and Africa [16]) has made PV-systems one of the best options for providing electrical power in those countries.

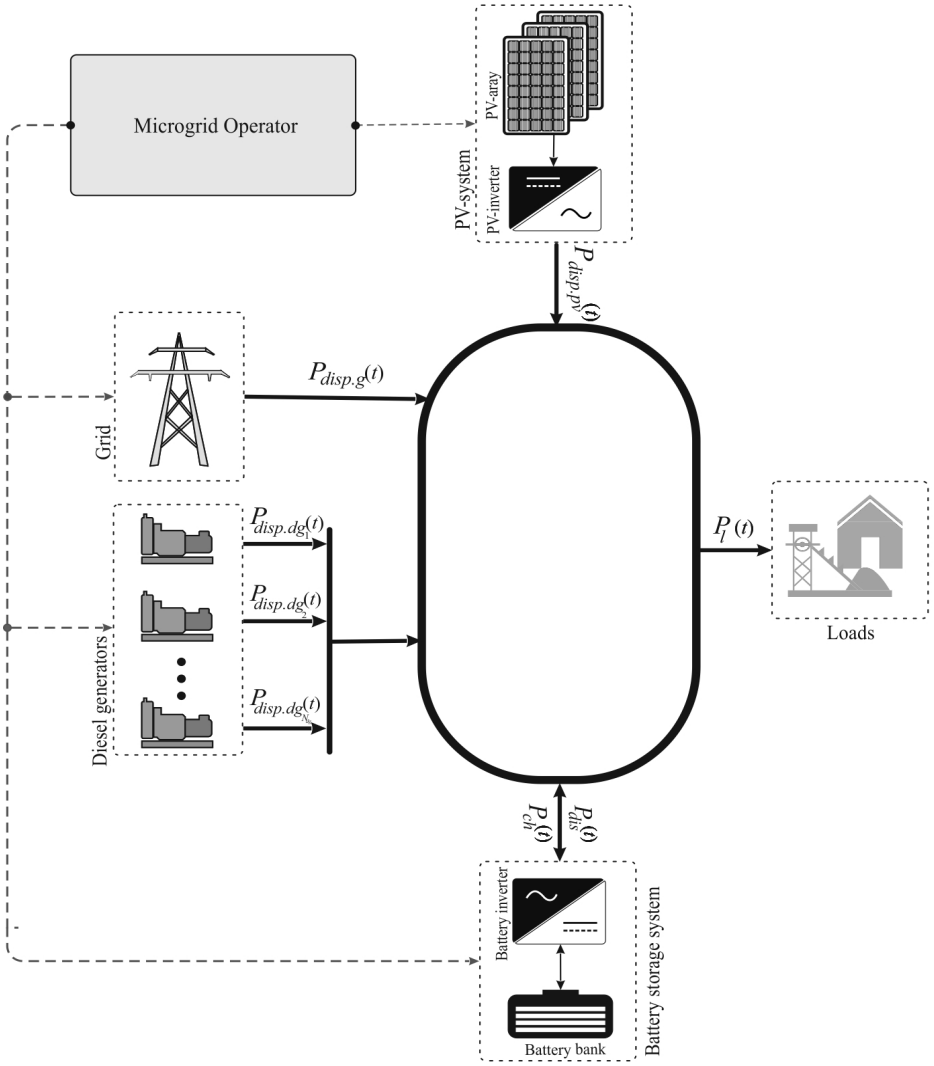

Figure 1.2: Representation of a microgrid.

However, due to the fluctuation of the generated power from the PV-systems, using energy storage system is essential to increase the MG reliability and stability. Electrical energy storage systems have several forms, including pure electrical storage such as superconducting magnetic energy storage and supercapacitor, mechanical systems such as compressed air energy storage and flywheels and electrochemical storage systems such as lead-acid and lithium-ion batteries [17]. Nevertheless, the electrochemical storage systems are mostly used in MGs because of their ability to store the electrical energy for long periods, and their low maintenance and operation costs [18]. However, the main disadvantages of the electrochemical storage systems are their high capital and replacement costs as well as their short lifetime [18]. Accordingly, the battery lifetime is an extremely important factor in determining the

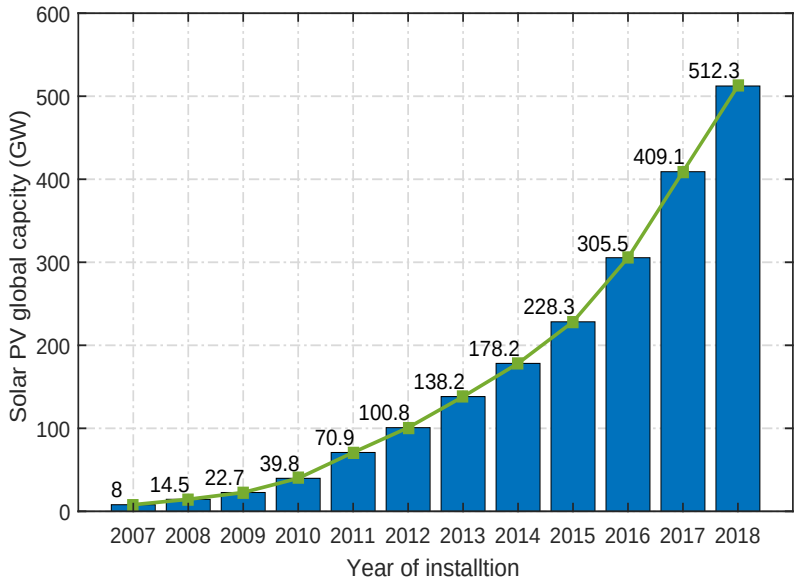

Figure 1.3: Expression of the increment in the installed capacity of PV-systems worldwide[3].

operating conditions and planning of replacement intervals for the batteries.

From another perspective, it is well recognized that optimizing the MG operation is a crucial solution to guarantee a low-cost operation and uninterrupted power supply. However, many technical and economic complexities have to be handled to achieve this goal [9]. Optimizing the MG operation depends on the coordination of the power dispatched from the MG components to cover the load demand with a minimum cost while considering their technical and operational constraints of each component in the MG. Furthermore, the optimal selection of the MG's components and the size of these components increases the MG's practical and economic efficiency in the long run [19]. Consequently, the optimum operation and design of the MG still receive significant attention from energy researchers to ensure a stable and economical electrical source for the consumer. However, optimizing the MG operation and design are complex problems due to the non-linearity and the complexity associated with the MG mathematical model.

1.2 Thesis Contributions

The main aim of this thesis is to develop model-based optimal operation and design algorithms for PV-based MGs, considering the battery lifetime and the problem of

grid blackout. In this study, considerable attention is given to build an accurate model for the MG, considering the practical constraints of each component. Moreover, two different layouts for the MG are used based on the application of the MG. In the residential MG, the DC-layout is employed; whereas, the AC-layout is used for the industrial MG. An operation strategy based on the concept of an economic model predictive controller is proposed to optimize the MGs operation. Also, the reactive power consumption of the load is considered in the industrial MG operation using a newly developed model to calculate the reactive power generation cost. However, it was found the optimal design of the MG is essential to increase the consumed energy from the PV-system and to decrease the cost of the generated power from the MG [20]. Hence, an optimal design algorithm for the MG is developed. In the developed algorithm, an accurate model for the battery lifetime is utilized. Besides, the uncertainty of solar power generation, grid blackout starting time, and grid blackout period are considered to give an accurate estimation for the levelized cost of energy ($LCOE$) and robust design for the MG. The contributions of this thesis can be summarized as follows:

- A comprehensive model for a residential PV-battery MG is developed. In this model, real operational constraints of the system components and the costs of the battery lifetime are taken into account.

- A new operation strategy, based on the economic model predictive controller (EMPC) concept, is proposed to minimize the total operating costs of the PV-battery MG considering the battery lifetime and the grid blackouts problem.

- A considerably accurate model for an industrial PV-battery-diesel MG is developed, taking the real operational constraints of the MG components into account.

- A novel model is introduced to calculate the reactive power generation cost from the diesel generator. Moreover, the cost model of the dispatched reactive power from the PV-system and the battery bank is adapted.

- An EMPC-based active-reactive optimal power dispatch strategy is proposed to minimize the total operating costs of the PV-battery-diesel MG by consid-

ering the cost of battery lifetime loss and reactive power generation cost under grid blackout conditions.

- A comparison between different operation scenarios is made to verify the advantages of the proposed strategies and to illustrate the impacts of considering the costs of the battery lifetime.

- A novel optimal design algorithm is developed to optimize the sizes of the MG components to achieve the lowest cost of the produced energy from the MG over its lifetime, considering the solar radiation, ambient temperature, and grid blackouts uncertainties.

- A new model is implemented to model the uncertainty of grid blackout starting time and blackout period using kernel density distribution.

- An improved method to calculate the $LOCE$ utilizing an accurate estimation of the number of lead-acid battery replacements during the MG lifetime by considering the impact of battery state of charge, discharging current, number of cycles, acid stratification, and sulfate-crystal structure on the battery lifetime.

1.3 Thesis Organization

This thesis is organized as follows:

- **Chapter 2:** This chapter includes a detailed literature review for the previous works that have investigated the optimal operation of the MG, the deterministic, and the stochastics design of the MG as well as the problem of grid blackouts.

- **Chapter 3:** This chapter explores the potential benefits of applying the EMPC to optimize the operation of a residential PV-battery MG to address the grid blackout problem. The proposed control strategy aims to cover the load, meanwhile minimize the total cost of the energy consumed from the grid and the cost of battery lifetime loss.

- **Chapter 4:** In this chapter, an active-reactive optimal power dispatch strategy based on the concept of EMPC is presented. In this operation strategy, the battery lifetime cost, the active-reactive power generation cost, and the grid blackout problem are considered. In addition, a cost model for the dispatched reactive power from the PV-system and battery storage system is developed. Furthermore, a new cost model for reactive power generation from the diesel generator is introduced.

- **Chapter 5:** This chapter introduces a comprehensive method for the optimal design of PV-based MGs, considering the uncertainty of solar radiation, ambient temperature, and grid blackouts. This method aims to minimize the $LCOE$ taking into consideration the limitation of the annual total loss of the power supply ($TLPS$) and the MG operational constraints. In addition, a detailed model for battery lifetime estimation is introduced based on the Physico-chemical mechanism of the lead-acid battery.

- **Chapter 6:** The final chapter gives a brief conclusion of the main contributions of the thesis and presents the main perspectives of the study.

Chapter 2

State of the Art

Nowadays, MG is proposed as a cost-effective and practical solution for many problems in the electrical energy system. Nevertheless, there are still many challenges that must be resolved to find an effective way to design and operate the MGs. In this chapter, a detailed literature review about the recent studies that investigated the problems of MG optimal operation and optimal design will be introduced; moreover, the studies on addressing the grid blackout problem are presented.

2.1 Microgrid Optimal Operation

During the MG operation, many technical and economic complexities have to be handled to provide stable, reliable, and cost-effective electrical energy. To satisfy these requirements, a hierarchical multi-layer structure for the MG control system is used to manage the power flow inside the MG, as shown in Fig. 2.1 [21], namely, operational, supervisory and planning layers. Each layer is characterized by its control variables and the speed of execution. In the operational layer, real-time controllers that are connected to the main components in the MG, take the responsibility to observe and control the voltage and frequency within milliseconds. It is to note that the droop control method is mostly used at the operational layer [22]. The next layer is the supervisory layer, its time frame in the range of seconds to minutes. In this layer, the controller ensures a stable operation between the MG components according to the given setpoints by the planning layer. The highest layer is the plan-

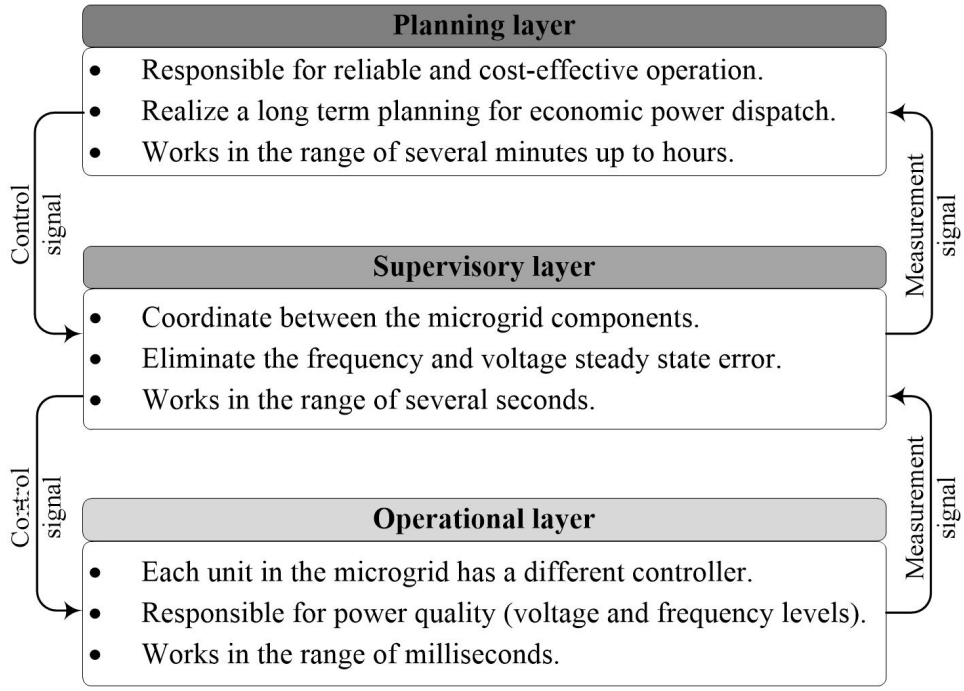

Figure 2.1: Illustration of a hierarchical multi-layer structure for MGs control system.

ning layer, where the controller works in the range of several minutes up to hours. It is responsible for reliable and cost-effective operation for the MG by specifying the amount of the dispatched power from the MG components to cover the load demand with a minimum cost considering their technical and operational constraints. The latter layer is the subject of interest in this thesis.

2.1.1 Optimal Power Dispatch in Microgrids

Optimal power dispatch (OPD) is necessary to increase the economic efficiency of the MG by decreasing the MG operation cost e.g., reducing the fuel consumption cost, decreasing the battery degradation cost and increasing the dispatched power from the renewable energy sources [23]. Therefore, many researchers have proposed various approaches to solve the OPD problem. For instance, an optimal power-sharing scheme was used in [24] to decrease the fuel consumption in a MG with a PV-array, a wind, and a gas turbine. In [25] an intelligent multi-agent management strategy was proposed to minimize the deviation between the forecasted day ahead production from a PV-system and the actual load to increase the dispatched power from the PV-system and increase user satisfaction in PV-based MGs. Be-

sides, a rule-based energy management algorithm was proposed in [26] to maximize the dispatched power from the PV-system in a grid-connected PV-battery MG. The authors in [27] proposed continuous and ON/OFF control methods to reduce the operation cost of a standalone PV-battery-diesel system considering only the cost of diesel generator fuel consumption. An energy management method was proposed in [28] to minimize both the fuel consumption and the lead-acid battery degradation cost in an islanded MG.

For a proper consideration of the dynamic behavior of the MG, a model predictive controller (MPC) was utilized to predict the future behaviour of the process over a finite time horizon and determine the optimal control action with respect to a specified objective function [29]. In [30], an MPC based optimal operation approach for a grid-connected residential MG was presented to minimize the total operation cost of the MG considering electricity market prices and renewable energy output power variation. An optimal power dispatch approach was proposed in [31] to minimize the diesel generator operation cost in a PV-battery-diesel MG using MPC in combination with mixed-integer linear programming (MILP) optimization problem. A rolling horizon based energy management strategy was employed in [32] to minimize the fuel consumption in an isolated MG by optimizing the dispatched power from the renewable energy sources, the battery bank and the diesel generator, but without considering the battery bank lifetime cost and reactive power cost. A two-stage MPC-based control strategy was formulated in [33] to improve the power dispatch, enable a cost-efficient operation, and guarantee reliable power supply in an islanded PV-battery-diesel MG. MPC was also utilized in [34] to provide optimal scheduling for the operation of a grid-connected PV-battery system, which maximizes the economic benefit of the PV plant considering the electricity market prices. A two-layer energy management system using MPC was introduced in [35] to minimize the operational cost of the MG in the upper layer and minimize the power fluctuation by renewable energy resources in the lower layer.

In some exceptional cases, when the cost function in the MPC has a direct reflection on the system's economic performance, it is possible to combine the economic process optimization with the process control and thus the approach is called economic

MPC (EMPC) [36]. The potential of using EMPC in electrical energy management was investigated in [37] to optimize the operation of controllable power generators for reducing the cost of the generated power. For example, the application of EMPC in MG was demonstrated in [38] to minimize the cost of the consumed energy in a community-based PV-battery MG considering the battery lifetime. Moreover, EMPC was used to reduce the fuel consumption of the diesel generator in a hybrid energy system [39]. A nonlinear MPC was utilized in [40] to minimize the operational cost of MGs considering the battery state of charge and temperature limits as well as the operational constraints of the MG components. In [12], an EMPC was proposed to optimize the active power dispatch in a hybrid PV-battery system considering the battery lifetime loss cost. Moreover, it was proved in [12] that considering the cost of battery lifetime loss in the EMPC is highly essential to decrease the total operation cost of the studied system.

In general, a battery storage system is considered as a key solution to improve the performance and reliability of MGs [18]. However, the battery lifetime is an essential factor in determining the operating conditions and planning of replacement intervals for the batteries. For this reason, the battery lifetime has been considered in the introduced MG operation algorithms by several researchers. As an example, the work in [41] proposed a multi-objective optimal operation framework to minimize the power generation cost and maximize the lifetime of the lead-acid battery in a standalone MG. In that research, the effective ampere-hour (Ah) battery aging model was used for battery lifetime estimation. The mentioned model was also used in [42] to formulate the cost of battery lifetime degradation to optimize the battery operation in an islanded MG. In [38], the battery lifetime was considered by adding explicit constraints to the optimization problem in the EMPC algorithm to achieve the desired lifetime degradation limit. An MPC based operation strategy was proposed in [43] to optimize the daily operation of a standalone hybrid PV-wind-diesel-battery system. Moreover, the battery bank aging cost was considered in [43] using an advanced aging model for lead-acid batteries. In another study, the MPC was utilized in [44] to optimize the charge and discharge pattern of the battery bank and maximize the economic benefit of a PV-battery MG. An energy

management strategy for a PV-battery-diesel MG was proposed in [45] to reduce the fuel consumption by the diesel generators considering the battery lifetime. Different types of batteries were used in [45] to reduce diesel generator operation hours, and meanwhile, the battery lifetime was taken into account by controlling the charging and discharging rates. In [46], the practical degradation cost model of a lithium-ion battery lifetime was used in the optimization to minimize the total operation cost of a DC MG. From the studies mentioned above, it can be noticed that different battery technologies and models we utilized to consider the battery lifetime in optimizing the operation of MGs; however, simplified models were preferred to decrease the computation time.

2.1.2 Active-Reactive Optimal Power Dispatch in Microgrids

It is important to note that the reactive power dispatch is an integral part of the AC-power system operation to manage voltage stability and transmission lines losses [47]. In addition, it was demonstrated that the PV and battery inverters could be used for reactive power compensation [48, 49]. Therefore, considerable attention has been paid to optimize both active and reactive power flow in distribution networks to decrease the renewable energy curtailment and increase the system profitability by exporting the reactive power to the upstream network [50].

Because of the increasing importance of MGs, more attention has been paid by the researchers to solve the active-reactive power dispatch (AR-OPD) problem in MGs. For instance, in [51], two operation modes for grid-connected MG were used to solve the AR-OPD problem. One operation strategy works in the grid-connected mode aiming to maximize the revenues based on the energy market prices. The second operation strategy aims to provide a reliable power supply to the customer in the islanded mode. Recently, a day-ahead energy management system was proposed in [52] to solve the AR-OPD problem in a grid-connected MG without considering the reactive power generation cost. In the operational layer of the MG (see Fig. 2.1) AR-OPD problem was heavily investigated to ensure the voltage and frequency stability [53, 54, 55, 56]. For example, in [57, 58], an improved droop control strategy was presented for reactive power sharing in an islanded MG consisting of multiple

distributed generation units connected through power electronic converters. In [59], a two layers control algorithm was proposed to calculate the active and reactive power setpoints of controllable generators in a grid-connected MG considering the voltage and the frequency constraints. It is noted that the economic effects of reactive power sharing were not taken into account in the studies mentioned previously. Several approaches have been developed to calculate the cost of the produced reactive power. The cost of the generated reactive power from a synchronous generator was formulated in [60] based on the opportunity cost concept. Moreover, it was found in [61] that the power losses in PV and battery inverters will increase when they inject reactive power, and this increment cost was used for reactive power pricing. In another work [62], the PV-inverter lifetime reduction due to the reactive power generation was used to estimate the generated reactive power cost. However, to the author's best knowledge, very few previous studies are available that considered the reactive power generation cost in optimizing the MG operation. The economic and technical impact of reactive power generation from a PV-system and a battery bank in a grid-connected MG was discussed in [63]. The results showed that the PV-system and battery storage system could be cost-competitive, comparing the grid and the switched capacitors for reactive power generation. The method in [63] was extended in [64] to provide an analytical approach AR-OPD in a grid-connected PV-system with battery storage and an electric vehicle charging station considering reactive power cost.

2.2 Microgrid Optimal Design

MG design is a long-term planning process. In this process, the optimal size and types of the MG components should be selected in such a way that guaranteed a long-term reliable and cost-effective energy source based on the customer requirements. The optimal design of the MG includes a deep understanding of the operation, lifetime characteristic, and environmental impacts of each component in the MG that highly increased the problem complexity. Moreover, considering the uncertainty of fluctuating renewable energy sources and grid blackouts play an essential role in increasing the optimal design accuracy. To solve the optimal design problem,

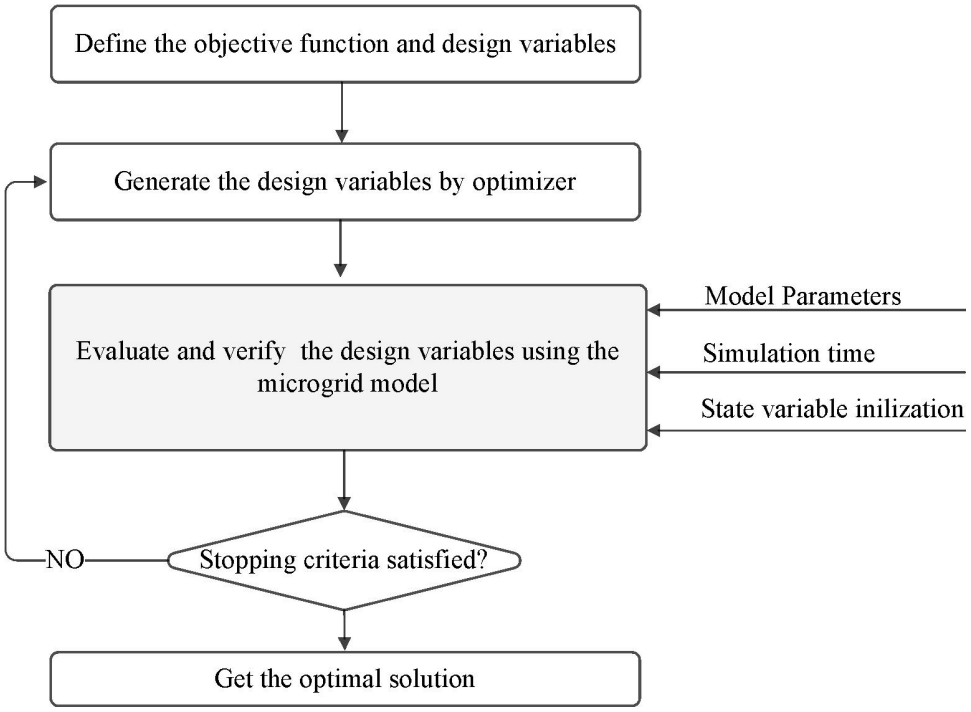

Figure 2.2: Simulation-based optimal design framework.

simulation-based optimization is commonly used to determine the optimal design parameters of the MG [65]. In this method, the simulation is used to evaluate and verify the effect of the design parameters given by the optimizer [66]. As shown in Fig. 2.2, each solution from the optimizer is evaluated based on the MG model; this process is repeated until the iterates converge to the optimal solution. One can classify the solution approach for optimal design problem of the MG into two main categories: 1) deterministic optimal design of MGs, and 2) stochastic optimal design of MGs. The former can calculate the optimal sizes of the MG components, but the solution may not be accurate enough to satisfy the design constraints. The latter provides an optimal solution while satisfying the related technical constraints considering the load, electricity cost, or power sources uncertainty.

2.2.1 Deterministic Optimal Design of Microgrid

The deterministic optimal design does not take into account the uncertainties in the MG model parameters. Therefore, it is based on the assumption that the forecasted values are accurate enough to give a quick and reasonable solution.

Several studies have appeared in recent years to handle the problem of MG optimal

sizing with different aims and design variables. For grid-connected MGs, different approaches were proposed to decrease the consumed power cost by increasing the dependency on renewable energy sources. As an example, the work in [67] proposed an optimal sizing approach for a grid-connected PV-battery system considering different electricity pricing tariffs to decrease the annual operation cost of the system. In [68], an optimal sizing method for a grid-connected PV-battery system is suggested to minimize the consumer electricity bill. A techno-economic optimal approach was introduced in [69] to minimize the total net present value of a PV-battery system for a smart household considering the annual cost of electricity consumption.

From a different perspective, various approaches were stated to optimize the size of off-grid MGs to decrease the levelized cost of energy and increase system reliability. For instance, in [70], an optimal design approach was presented to determine the optimal size of a PV-wind-battery system to minimize the annual capital cost while considering a specified total loss of power supply ($TLPS$) value. An optimal design method is introduced in [71] to minimize the operation cost of a MG with a hybrid DC-AC structure. In [72], a household PV-battery system was optimized, taking the effect of the load increment on the system reliability into account. In [73], an optimal sizing approach for a standalone residential MG was introduced to minimize the operation cost, greenhouse gas emissions, and critical dump energy. An optimization algorithm based on iterative simulation was proposed in [74] to optimize the PV-array and battery sizes in a standalone PV system, where a detailed dynamic model of the lead-acid battery was utilized to simulate the battery performance. However, most of the previous studies [67]-[74] did not consider the battery lifetime degradation effect.

Due to high capital cost and short lifetime of a battery storage system (BSS), compared to other components in a MG, more and more attention has been drawn to optimizing its size by utilizing different approaches for battery lifetime estimation. The work in [75] proposed a multi-objective optimization approach to minimize the $TLPS$ and the cost of the generated energy, where the life loss cost of the lead-acid battery was considered based on the weighted Ah counting method. In [5], an optimal sizing method for a residential MG was proposed, where a linear bat-

tery capacity degradation model was used to estimate the lead-acid battery lifetime degradation by considering only the discharged power effect. A two-stage approach was introduced in [76] to determine the battery size, the battery depth of charge, and the battery lifetime by counting the battery operation cycles. Recently, a bi-level optimization model was introduced in [77] to optimize the capacity of the components in an isolated MG. In the developed model, the battery lifetime was estimated by considering the total cumulative transfer energy based on the number of charge/discharge cycles. The work in [78] proposed a simplified method to optimize the size of a grid-connected PV-battery system to minimize the total cost, and meanwhile, the battery lifetime was considered by using a generalized lifetime estimation model for both lithium-ion and lead-acid battery. In addition, the optimal sizing of different battery technologies was investigated in [79] to reduce the total expansion cost of a grid-tied MG, considering the influence of the battery depth of discharge and the number of charge/discharge cycles. A linear optimization approach was used in [80] to optimize the battery size and select the battery technology (lead-acid or lithium-ion) in a PV-battery residential MG while minimizing the battery bank degradation cost. In [81], an optimal design method for an off-grid PV-battery system was introduced to determine the PV-system and the battery bank capacity. Moreover, an electrochemical model was used in [81] to estimate the lithium-ion battery lifetime. A simplified optimization approach was proposed in [82] to optimize lithium-ion battery size in a household PV-battery system, where the discharged power effect on the battery lifetime was considered.

From the above discussions, it can be noticed that lithium-ion and lead-acid batteries are dominant battery technologies used in MG applications. However, due to its low cost, high safety, and high recyclability rate, lead-acid battery is the most commonly used electrochemical energy storage in various fields [83, 84]. Furthermore, the lead-acid battery is an effective solution for a wide range of applications such as backup power supplies and hybrid PV-systems especially in developing countries [85], which is in line with this thesis aim at developing an optimization method to find the optimal size of PV-systems working in the area suffering from daily and long periods of grid blackouts.

2.2.2 Stochastic Optimal Design of Microgrid

Deterministic design approaches highly depend on the given input parameters of the model as any deviation due to uncertainty could lead to a suboptimal solution [86]. Therefore, several studies have been conducted to incorporate the uncertainty of renewable power generation in the MG optimal design problem considering different stochastic parameters and models as well as solutions strategies [87, 88]. For instance, a chance-constrained programming approach was utilized in [89] to design a standalone wind-PV-battery system considering the non-Gaussian stochastic model for the produced power by the wind turbine and the PV-system. In [90], Monte Carlo simulation (MCS) and practical swarm algorithm were used to find the optimal size of a wind-PV-battery system while considering the wind speed, solar irradiance and load demand uncertainty. Also, the optimal size of a PV-wind-battery system was investigated in [91]; meanwhile, MCS was utilized to handle the uncertainty of wind and PV-system production without considering the seasonal variation in the developed stochastic model. A concept of design space was applied in [92] to optimize the size of a PV-battery system incorporating the uncertainty of the generated power from the PV-array, taking into consideration the desired confidence level. Besides, the design space approach was used in [93] for sizing an islanded wind-battery system by considering the wind speed uncertainty. Chance constrained programming method was used in [94] to address the uncertainties in renewable resources to optimize a PV-wind-battery system. Recently, a scenario reduction method is proposed to simplify the impact of the uncertainty in the load profile and the renewable energy output on MG optimal design problem [95].

Special attention was given to optimize the energy storage system in order to increase MG reliability and decrease the impact of the uncertainty. As an example, the work in [96] used Markov chain method with MCS to calculate the optimal size of the energy storage system in a MG to minimize the power mismatch between the generated power from the renewables and load considering wind speed uncertainty. Moreover, a stochastic optimization problem was formulated in [97] to find the optimal size of a battery storage system in an islanded MG considering the wind speed and the load growth factor uncertainty. In [98], the stochastic optimization problem

was transformed into a deterministic one using the point estimated method with Cholesky decomposition to optimize the energy storage size considering the intermittent power generation from the wind turbines. In [99], a stochastic programming technique was used to optimize energy storage system size in a grid-connected MG to enhance its reliability under wind speed uncertainties. A detailed lead-acid battery lifetime estimation model was combined with MCS in [100] to optimize the size of a standalone PV-wind-diesel-battery system considering the wind speed, solar irradiance, and load uncertainty. It is worth to mention that the grid blackout uncertainty was not considered in the studies mentioned previously.

2.3 Grid Blackout Problem

2.3.1 Problem Description

The rapid growth in electrical loads requires a steady increase in the power generated to cover the loads as well as a constant upgrade to the distribution network. However, in many developing countries, it is not always possible to expand the generation system for economic, technical, or political reasons, resulting in a shortage of energy supplies to cover the beneficiaries' loads [101, 102]. In this case, the power system operator disconnects the loads from the network to maintain the restrictions of power system operation such as voltage and frequency limits. To manage this problem in the long run, electrical distribution companies classify the distribution networks to several zones and distribute the available energy according to a specific schedule. This situation is still present in many countries throughout the world [103, 104, 105, 106, 107, 108], and cause a significant economic loss to the customers [109, 110]. Therefore, many efforts have been made to develop reliable energy sources to supplement the shortage during the period of blackouts.

2.3.2 Solution Approaches for the Grid Blackout Problem

According to [111], using an adequate design, operation, and integration of distributed energy resources make it possible to cover the loads in case of planned or unplanned blackouts. The results obtained in [103] demonstrated the capability of

a diesel generator as an economical solution to solve the problem of long periods of grid blackouts. However, the continuous decreasing price of PV-modules and the expected increase in fuel prices makes hybrid PV-diesel systems more economical than using pure diesel systems. This concept was extended in [112] where the integration of distributed diesel generators with the public grid was proposed as a replacement of the primary grid during the blackout periods. A supervisory control method was used to guarantee the power supply quality of the primary grid, where the fuel consumption of the diesel generators is decreased by installing a PV-system. On the other hand, energy storage has been widely used as a backup system to cover electrical loads during blackout periods. The work in [113] presented an analytical approach to evaluate the performance of an electrical energy storage system during the blackout periods and determined the size of the storage to achieve a specified reliability level. A grid-interactive PV uninterruptible power supply system was implemented in [107] using a combination of a battery and a diesel generator to solve the problem of frequent blackouts and voltage instability in India. In [105], a diesel-battery system was proposed as a solution to compensate planned and unplanned grid blackouts and meanwhile minimize the operation costs by developing a power management system.

In [104], it was shown that the optimal design of a hybrid PV-battery system could make it more beneficial than a diesel-based system for residential loads in the areas suffering from planned grid blackouts. In another work [114], the authors proposed a real-time demand-side management approach for a PV-battery system to control the operational time of the loads. The work in [115] showed the techno-economic feasibility of using a hybrid PV-battery system as a backup power supply to meet residential loads, considering the seasonal variation of load profiles. Customer damage cost function due to the occurrence of blackouts was formulated in [116]; the formulated function was incorporated to find the optimal size of the battery in a grid-connected PV-battery system. An optimal design method for a grid-connected MG was discussed in [19, 117] to decrease the power interruption cost. An optimal design method was introduced in [118] to optimize the size of a grid-connected PV-battery-diesel MG that proposed an alternative to using a diesel generator to cover

the load during as frequent grid outages. In [14] a new optimal design method for residential MGs is proposed to minimize the levelized cost of energy while satisfying the required annual total loss of power supply percentage, where battery lifetime and long term daily grid blackout are considered. However, due to the presence of several factors that affect the grid blackout starting and its duration, it was better to take into account their uncertainty effect. Nevertheless, the impact of grid blackouts uncertainty in the MG optimal design problem was considered in very few studies. For instance, in [119], the battery and the diesel generator sizing problem was investigated considering the uncertainty of renewable energy outputs and grid blackouts; however, a simplified stochastic model with linear objective function and constraints were used to formulate the optimization problem. Recently, a simulation-based design method for the battery in a grid-connected PV-battery system for emergence usage was introduced in [120] considering only the yearly grid blackout uncertainty. Besides, in [121] the influence of battery price and customer damage cost on the optimal size of a PV-battery system was explored considering the number of yearly blackouts and its duration uncertainty. It is worth to mention that a parametric probability density function was used to describes the uncertainty of grid blackout in the studies mentioned previously.

From another perspective, the work in [122] proposed two operation frameworks for a PV-battery MG considering grid blackouts. The first one used a receding horizon based optimal dispatch algorithm to minimize the total power cost in the grid-connected mode, while the second one used a rule-based algorithm to cover the load during the blackout periods. Moreover, a master-slave control strategy was proposed in [106] to reduce the fuel consumption of a PV-diesel-battery system for non-residential loads to deal with grid scheduled blackouts, i.e., power supply from the grid is switched off daily for a certain period. The work in [123] provide a load scheduling approach for a PV-battery-diesel MG considering grid blackout problem. The developed approach aimed to reduce fuel consumption and increase the contribution of solar energy in covering the loads. In [124] a predictive energy management approach was developed for a PV-battery MG to minimize the PV power curtailment and increase the energy supply reliability, where a periodic blackout

from the primary grid was addressed without considering the battery lifetime. In [12], an EMPC was proposed to optimize the active power dispatch in a hybrid PV-battery system considering the battery lifetime loss cost and grid blackout problem. It was proved in [12] that considering the cost of battery lifetime loss in the EMPC is highly essential to decrease the total operation cost of the studied system. This work was extended in [15] to optimize the performance of a MG considering the AR-OPD problem for the industrial load.

2.4 Challenges

From the discussions above, it can be seen that many studies have been carried out on the optimal operation and design of PV-based MGs, which aim to decrease the operating, investment, and the fuel consumption costs of the MG, as well as the curtailment of the PV power generation. However, the main drawbacks of previous studies can be summarized as follows

- The majority of the previous studies relied on the standard DC/AC layout in MG modeling. This led to disregard many practical operational constraints of the MG without taking into account the nature of the connected loads.

- Most of the previous studies were focused on the intermittent behavior of renewable energy sources or the loads as the main problem to be solved. But the problem of the discontinuous power supply from the primary grid is rarely considered, although it is still a common issue in many developing countries in the world.

- Most improvements have been achieved by minimizing the total operation cost of MGs considering the cost of active power only with or without taking the battery lifetime cost into account. Nonetheless, it is possible to further improve the MG operation by considering the cost of active and reactive power, as well as the battery lifetime simultaneously.

- A large number of the previous studies that focused on calculating the size of the MGs considered that the battery life is constant, although it is affected

by the size and operational conditions of the battery, which may lead to a significant error in the calculation of the levelized cost of energy.

- Great attention has been given to consider renewable energy, load, and price uncertainties in the MGs design problem. However, less attention has been paid to consider the grid blackout uncertainty effect in the optimal design problem.

- Mainly, a parametric probability density function was used to describe the uncertainty of the grid blackout. However, due to the existence of several reasons that lead to planned or unplanned blackouts, parametric probability density function cannot characterize the stochastic behavior of the grid blackout accurately.

In this thesis, the previous drawbacks have been comprehensively investigated to build improved operation and design methods for grid-connected MGs, considering the battery lifetime and grid blackout problem.

Chapter 3

Optimal Operation of Residential Microgrids

This chapter explores the potential benefits of applying the economic model predictive control (EMPC) to optimize the operation of a residential PV-battery MG to address the grid blackout problem. The proposed control strategy aims to cover the load, meanwhile minimize the total cost of the consumed energy and the cost of battery lifetime loss. For this, a detailed model for the PV-array and solar irradiance are presented. A battery operating model is described and a weighted Ah model is used to predict the battery lifetime loss. Besides, a model for grid-tie line status is introduced. Moreover, a comparison between different operation strategies for the MG considering the seasonal variation in the load and the PV power generation is made.

3.1 Switching Model of Residential PV-Battery Microgrids

It was proved in [125, 126] that the PV-battery MG is an appropriate economical solution to meet the energy demands of a residential household located in an area rich in solar energy. Moreover, it was found in [127] that the DC-coupled MG is more applicable for residential MG because of its simple structure, low system cost, safety, and ease of maintenance. In this thesis, the DC-coupled architecture of PV-

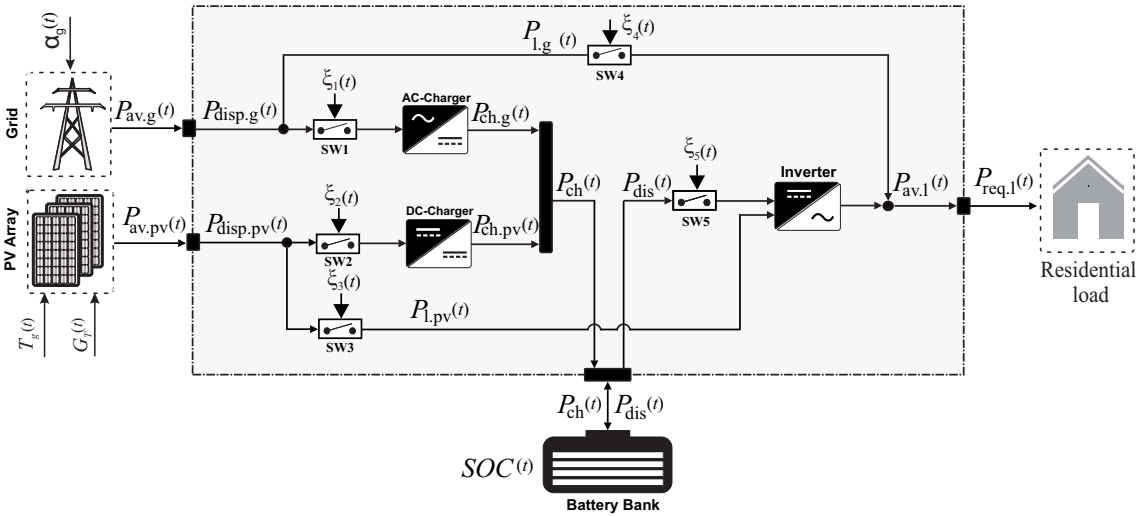

Figure 3.1: Schematic diagram of the studied PV-battery MG.

battery MG [127] is modified by adding controllable switches ($SW_{1,\ldots,5}$) to hold the operational constraints in the MG, as shown in Fig. 3.1. The MG consists of a PV-array, a battery bank, an AC charger to charge the battery bank from the grid, a DC charger to charge the battery bank from the PV-array, a DC/AC inverter to supply AC power to the load from the battery bank and the PV-array, a grid-tie line, and a residential load. The mathematical model of the major components of the MG and their operational constraints are modelled in the following sections.

3.2 PV-System Model

The PV-system is mainly composed of a PV-array to convert the solar energy into an electrical energy and a power electronic device to enhance the quality of the PV-array output power. However, multiple factors affect the performance of the PV-array, such as the installation location, the tilt angle, the azimuth angle, the solar radiation, and the ambient temperature. In the following subsections, a detailed and accurate models for the PV-array operation and the solar irradiance components are explained to emulate the PV-system performance.

3.2.1 PV-Array

The PV-cell is the nucleus of the PV-array that converts the energy of the solar irradiance to electrical energy. Nevertheless, for practical use, the PV-cells are

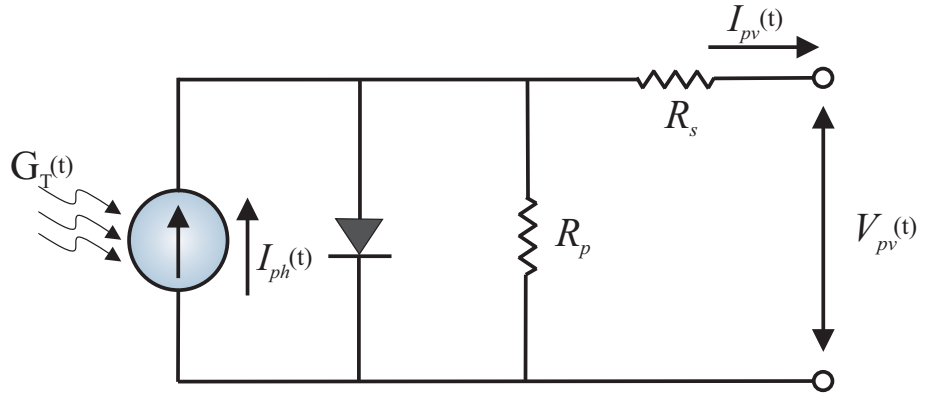

Figure 3.2: The equivalent electrical circuit of a PV-cell.

combined to form the PV-modules, which can be connected either in series or in parallel to form a PV-array with the desired voltage and current.

In this thesis, the single diode equivalent circuit model of the PV-cell shown in Fig. 3.2 is used to predict the behaviour of the PV-cell. This model depends on the PV-cell electrical characteristic and the local weather data to simulate the PV-cell performance with significant accuracy [128, 129]. According to this model, the relation between the generated current from the PV-cell $I_{pv}(t)$ and its voltage $V_{pv}(t)$ can be defined with a sufficient accuracy by [130, 131]

$$I_{pv}(t) = I_{ph}(t) - I_0\left(exp\left(\frac{V_{pv}(t) + I_{pv}(t)R_s}{V_t}\right) - 1\right) - \frac{V_{pv}(t) + I_{pv}(t)R_s}{R_p}, \quad (3.1)$$

where $I_{ph}(t)$ is the photo-generated current that generated because of the photo-voltaic effect [132], I_0 is the dark current, which is generated without the influence of the solar irradiance, R_s and R_p are the series resistance and the parallel resistance of the PV-cell, respectively, and V_t is the PV-cell thermal voltage. Nonetheless, Eq. (3.1) cannot be used directly to obtain the output power prediction of the PV-cell. This is because there are some parameters such as $I_{ph}(t)$ and I_0 cannot be measured directly. Therefore, it is vital to use a model that depends on the data from the PV-module manufactures and the meteorological centers measurements.

A practical model is developed by [130] and adapted in [12] is used in this thesis to calculate the maximum generated power by the PV-cell $P_{max.c}(t)$ which takes into consideration the PV-module specifications, the received solar irradiance as well as the ambient temperature as follows

$$P_{max.c}(t) = V_{oc.c}(t)I_{sc.c}(t)FF(t) \quad (3.2)$$

where the values of both of the open circuit voltage $V_{oc.c}(t)$ and the short circuit current $I_{sc.c}(t)$ of the PV-cell depend on the received solar irradiance $G_T(t)$ and the temperature $T_c(t)$ of the PV-cell. The instantaneous value of $V_{oc.c}(t)$ and $I_{sc.c}(t)$ are given by

$$V_{oc.c}(t) = V_{oc.c.stc} + K_v(T_c(t) - 25), \tag{3.3}$$

$$I_{sc.c}(t) = (I_{sc.c.stc} + K_i(T_c(t) - 25)), \frac{G_T(t)}{1000} \tag{3.4}$$

where

$$T_c(t) = T_a(t) + \frac{(NOCT - 20)}{800} G_T(t), \tag{3.5}$$

and the subscript *stc* indicates that the parameter value is calculated under standred test conditions. The fill factor $FF(t)$ in Eq. (3.2) is the ratio of the maximum power that can be produced by the PV-cell to the product of the open-circuit voltage and short-circuit current of the PV-cell. The formula from [130] is used to calculate the fill factor by

$$FF(t) = \frac{P_{max.c}(t)}{V_{oc.c}(t) I_{sc.c}(t)} = FF_0(t)(1 - r_s(t)), \tag{3.6}$$

where $FF_0(t)$ is the nominal fill factor of the PV-cell and given by

$$FF_0(t) = \frac{v_{oc}(t) - ln(v_{oc}(t) + 0.72)}{v_{oc}(t) + 1}, \tag{3.7}$$

as well as $r_s(t)$ and $v_{oc}(t)$ are the normalized series resistance and the open-circuit voltage for the PV-cell, respectively, which are calculated by

$$r_s(t) = R_s \frac{I_{sc.c}(t)}{V_{oc.c}(t)}, \tag{3.8}$$

$$v_{oc}(t) = \frac{V_{oc.c}(t)}{V_t(t)}, \tag{3.9}$$

where

$$V_t(t) = \frac{n_d k_B T_{a.k}(t)}{e}. \tag{3.10}$$

The value of the series resistance of the PV-cell R_s depends on the material of the PV-cell, which is affected by the PV-cell operating conditions. However, this effect could be insignificant and negligible [133, 134, 135]. According to [130] the R_s value can be calculated using the available data in the PV-module datasheet [136] by

$$R_s = \Big(1 - \frac{FF_{stc}}{FF_{0.stc}}\Big)\frac{V_{oc.c.stc}}{I_{sc.c.stc}}, \tag{3.11}$$

where FF_{stc} and $FF_{0.stc}$ can be calculated by Eq. (3.6) - (3.7) and Eq. (3.9) - (3.10), respectively, using $P_{max.c.stc}$, $I_{sc.c.stc}$, $V_{oc.c.stc}$ and $T_{a.k.stc}$ values of the PV-cell. Note that the available data in the datasheet normally are for the PV-module and not for the PV-cells, which are connected in series inside the PV-module. Therefore, the PV-cell parameters are calculated by

$$P_{max.c.stc} = \frac{P_{max.m.stc}}{N_{c.m}}, \tag{3.12}$$

$$V_{oc.c.stc} = \frac{V_{oc.m.stc}}{N_{c.m}}, \tag{3.13}$$

$$I_{sc.c.stc} = I_{sc.m.stc}, \tag{3.14}$$

where $N_{c.m}$ is the number of PV-cells in side the PV-module. Based on the maximum output of the PV-cell, the output of the whole PV-array can be calculated as follows

$$P_{av.pv}(t) = N_{s.m}N_{p.m}N_{c.m}P_{max.c}(t) \tag{3.15}$$

where $N_{s.m}$ and $N_{p.m}$ are the number of PV-modules connected in series and parallel, respectively.

3.2.2 Solar Irradiance on a Tilted PV-Module

The PV-module is mostly installed with a tilted angle β to achieve a higher annual yield. In this thesis, the isotropic model is used to calculate the total solar irradiance $G_T(t)$ received by a tilted PV-module, as follows [137]

$$G_T(t) = G_B(t, \beta) + G_D(t, \beta) + G_R(t, \beta), \tag{3.16}$$

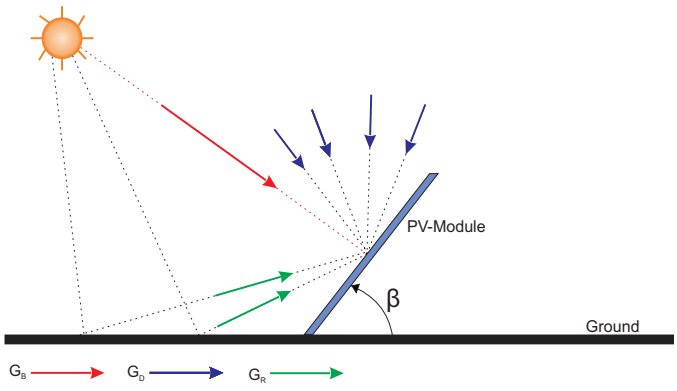

Figure 3.3: Components of solar irradiance falling on a tilted PV-module.

where $G_B(t,\beta)$, $G_D(t,\beta)$ and $G_R(t,\beta)$ are the beam, diffused and reflected solar irradiance, respectively, arriving onto a PV-module with the inclination angle β, as shown in Fig. 3.3. These components are explained as follow

Beam irradiance Is the solar irradiance, which does not undergo either scattering or absorption during its journey from the sun to the PV-module, it is called the beam or the direct irradiance. It can be calculated using the measured solar irradiance on a horizontal surface by [138]

$$G_B(t,\beta) = R_B \overline{G}_B(t), \tag{3.17}$$

where $\overline{G}_B(t)$ is the beam irradiance measured on a horizontal surface at ground level, and R_B is the ratio of the beam irradiance arriving on a tilted surface to that arriving on a horizontal surface. For a PV-module installed in the northern hemisphere (all locations on Earth that is north of the equator), R_B is expressed as [139]

$$R_B = \frac{\cos(\phi-\beta)\cos\delta\sin\omega'_{ss} + \left(\frac{\pi}{180}\omega'_{ss}\sin(\phi-\beta)\sin\delta\right)}{\cos\phi\cos\delta\sin\omega_{ss} + \left(\frac{\pi}{180}\omega_{ss}\sin\phi\sin\delta\right)}. \tag{3.18}$$

Meanwhile, for surfaces in the southern hemisphere, R_B is calculated as [139]

$$R_B = \frac{\cos(\phi+\beta)\cos\delta\sin\omega'_{ss} + \left(\frac{\pi}{180}\omega'_{ss}\sin(\phi+\beta)\sin\delta\right)}{\cos\phi\cos\delta\sin\omega_{ss} + \left(\frac{\pi}{180}\omega_{ss}\sin\phi\sin\delta\right)}, \tag{3.19}$$

where ϕ is the latitude of the installation position of the PV-system, ω_{ss} and ω'_{ss} are the sunset hour angle for a horizontal and a tilted surface, respectively, and δ is the sun declination angle.

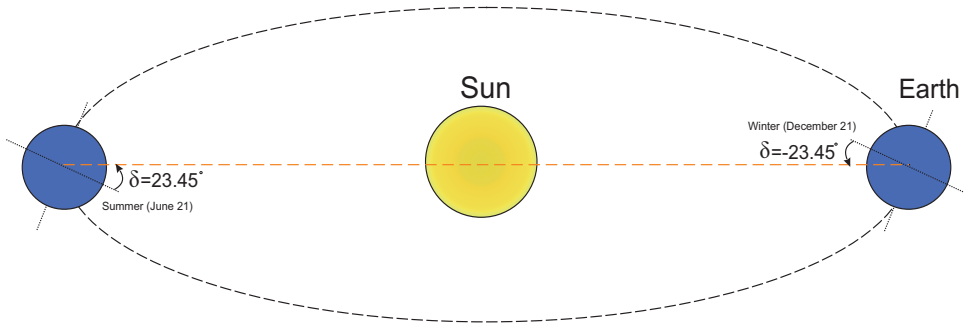

Figure 3.4: Graphical illustration of the solar declination angle.

In general, the sun hour angle represents its angular displacement east or west of the meridian, which is changing by 15 degree per hour due to earth rotation on its axis. The sun hour angle at sunset for a horizontal surface is given by [140]

$$w_{ss} = cos^{-1}\left(-tan\,\phi\,tan\,\delta\right). \tag{3.20}$$

Meanwhile, the hour angle at sunset for a tilted surface is calculated as [139]

$$w_{ss}^{'} = \min\left[cos^{-1}\left(-tan\,\phi\,tan\,\delta\right), cos^{-1}\left(-tan\left(\phi-\beta\right)tan\,\delta\right)\right]. \tag{3.21}$$

Moreover, the sun declination angle is an angle between a line joining the centers of the sun and the earth and its projection on the equatorial plane (a plane passing through the equator of the earth), see Fig. 3.4. The solar declination angle changes mainly due to the rotation of the earth in its orbit around the sun. Its values is in the range of -23.45^{o} to $+23.45^{o}$ throughout a year period. The declination angle at each day can be calculated by [138]

$$\delta = 23.45^{\circ} sin\left[360^{\circ}\frac{284+N_d}{365}\right], \tag{3.22}$$

where N_d is the number of the day in the year (i.e 1 to 365 days).

Diffuse irradiance It is the solar irradiance that does not directly reach a PV-module, but was subjected to diffusion during its journey from the sun to the PV-module due to the clouds or dust in the air. The diffuse irradiance on a tilted surface can be expressed as [141]

$$G_D(t,\beta) = R_D\overline{G_D}(t) \tag{3.23}$$

Table 3.1: Guide values for reflection factor.

Option	Value
Asphalt	0.1 - 0.15
Green forest	0.1 - 0.2
Wet ground	0.1 - 0.2
Dry ground	0.15 - 0.3
Grass-covered ground	0.2 - 0.3
Concrete	0.2 - 0.35
Desert sand	0.3 - 0.4
Old snow	0.5 - 0.75
Newly fallen snow	0.75 - 0.9

where R_D is the ratio of the diffuse irradiance arriving on a tilted surface to that arriving on a horizontal plane, which is calculated as

$$R_D = \frac{1 + \cos\beta}{2}, \tag{3.24}$$

and $\overline{G}_D(t)$ is the diffuse irradiance measured on a horizontal surface at ground level.
Reflected irradiance Is the reflected irradiance by the ground and radiated back to the PV-module, which is given by

$$G_R(t, \beta) = \overline{G}(t)\rho\frac{1 - \cos\beta}{2} \tag{3.25}$$

where $\overline{G}(t)$ is the global solar irradiance measured on a horizontal surface at ground level, and ρ is the diffuse reflection factor from the ground. Table 3.1 shows the different value of ρ which is determined by the type of the considered surface [141].

3.3 Battery Bank Model

The battery bank is important to increase the dispatched power from the PV-array in a MG. Moreover, it is necessary to reduce the fluctuations of the generated solar power and to provide a continuous power supply to the load during the blackout periods or at low solar irradiance time. The key physical property of the battery bank is the state of charge (SOC) [142]. However, during the battery operation,

important practical constraints should be considered. In this thesis, a controllable switches are employed to handle the battery operational constraints, see Fig. 3.1. Moreover, a simplified but accurate weighted ampere-hour (Ah)[1] model is used to predict the battery lifetime loss while considering the SOC effect [75]. The battery bank operational model and cost of battery lifetime loss calculation are explained in the following subsection.

3.3.1 Battery Bank Operational Model

The SOC of the battery bank increases due to charging from the grid or the PV-array, and decreases due to discharging to cover the load demand. In this study, the charging and discharging processes are controlled by the proposed EMPC through controllable switches, see Fig. 3.1. The change of SOC of the battery bank is expressed by

$$SOC(t+\Delta t) = SOC(t) + \eta_{ch} P_{ch}(t)\Delta t - \frac{P_{dis}(t)\xi_5(t)}{\eta_{dis}}\Delta t, \tag{3.26}$$

where the charging power $P_{ch}(t)$ consists of the charging power from the grid $P_{ch.g}(t)$ and the charging power from the PV-system $P_{ch.pv}(t)$. Therefore, $P_{ch}(t)$ can be calculated by

$$P_{ch}(t) = P_{ch.g}(t)\xi_1(t) + P_{ch.pv}(t)\xi_2(t), \tag{3.27}$$

where $\xi_i(t)$ with $i \in 1, 2, \ldots 5$ is a binary variable that represents the status of one of the controllable switch shown in Fig. 3.1. To prevent overcharging or deep discharging of the battery bank, the SOC should be limited according to the capability of the battery bank [143], i.e.,

$$SOC_{min} \leq SOC(t) \leq SOC_{max}, \tag{3.28}$$

where SOC_{min} and SOC_{max} are the lower and upper limit of the battery SOC, respectively. The SOC_{min} is related to the depth of charge of the battery bank by

$$SOC_{min} = (1 - DOD)SOC_{max}, \tag{3.29}$$

[1] Ah is the consumed current from the battery in one hour.

and SOC_{max} is given by

$$SOC_{max} = V_{b.n} Q_{b.n}, \tag{3.30}$$

where $V_{b.n}$ is the battery bank nominal voltage and $Q_{b.n}$ is the battery bank nominal capacity in Ah.

To avoid battery overheating, the maximum charging power should be limited [144]. According to [143], the charging power should be constrained by

$$P_{ch} \leq \gamma_{ch.lim} V_{b.n} Q_{b.n} \tag{3.31}$$

where $\gamma_{ch.lim}$ is a parameter for the limit of the charging power, which is typically between 0.1 and 0.2 to enable an optimum charge. Note that the charging and discharging processes of the battery bank cannot simultaneously take place. In addition, the battery bank cannot be charged by different chargers (i.e., grid charger or PV-array charger) at the same time [145]. To satisfy these conditions, the following constraint should be held

$$\xi_1(t) + \xi_2(t) + \xi_5(t) \leq 1. \tag{3.32}$$

Based on Eq. (3.32), only one of the controllable switches can be ON, i.e., the battery bank will not simultaneously be charged and discharged. In addition, the battery bank will not be charged from the grid and the PV-array at the same time. Due to the synchronization issue of the AC power (matching the frequency, phase angle, and voltage amplitude), the DC/AC inverter and the grid cannot simultaneously supply power to the load. Thus, the following constraints should also be added

$$\xi_3(t) + \xi_4(t) \leq 1, \tag{3.33a}$$

$$\xi_5(t) + \xi_4(t) \leq 1. \tag{3.33b}$$

By the constraint in Eq. (3.33a), the load will not simultaneously be covered from the grid and the PV-system. Similarly, the load will not simultaneously be covered from the grid and the battery bank because of the constraint in Eq. (3.33b).

3.3.2 Cost of Battery Lifetime Loss

Battery manufacturers usually give the expected lifetime of the battery based on well-defined standard tests [146]. Consequently, the battery lifetime is expressed by the number of operation cycles measured by discharging the battery with constant power to a certain depth of discharge and charging it to its maximum value with a certain charging algorithm [147]. However, in practical operations, the battery does not work under the so-called standard operating conditions, and thus its lifetime varies according to the real operating environment [148]. The weighted Ah battery aging model takes into account the real-time variations to estimate the battery lifetime [146, 149]. It is assumed that the battery lifetime is ended when the battery Ah throughput reached its maximum value based on its rated value [150]. Moreover, the impact of the consumed Ah on the battery life depends on the battery operation condition at discharge time. Based on the data from manufacturers of deep-cycle lead-acid batteries, the total Ah throughput of the lead-acid battery can be calculated by [75, 41]

$$A_{total} = \varepsilon \times Q_{b.n}. \tag{3.34}$$

Here ε is a parameter used to calculate the total Ah throughput over the battery lifetime based on its nominal capacity, which is equal to 490 [41] for lead-acid batteries. Accordingly, the battery lifetime loss factor $L_f(t)$ is defined as the ratio of the weighted consumed Ah to the total Ah throughput of the battery [41, 151] , which can be expressed as

$$L_f(t) = \frac{A_c(t)}{A_{total}}, \tag{3.35}$$

where $A_c(t)$ is the weighted consumed Ah, which is calculated by

$$A_c(t) = \lambda_{soc}(t) A_c^{'}(t), \tag{3.36}$$

and $A_c^{'}(t)$ is the actual consumed Ah from the battery and $\lambda_{soc}(t)$ is a weighting factor that graphically related to the battery $SOC(t)$ [41, 151], as seen in Fig. 3.5. For simplicity, this relationship is expressed mathematically as

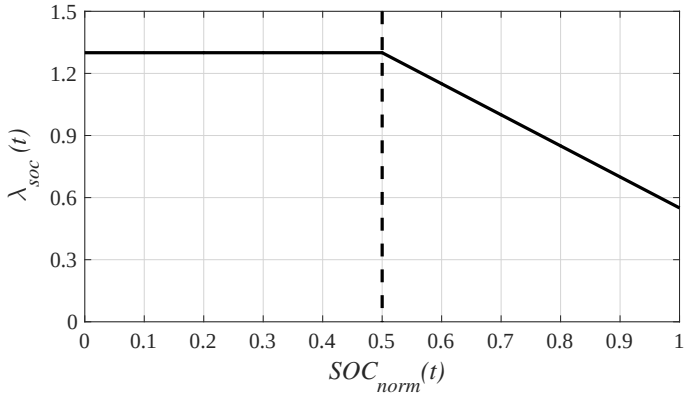

Figure 3.5: The relation between $SOC_{norm}(t)$ and $\lambda_{soc}(t)$.

$$\lambda_{soc}(t) = \begin{cases} a & 0 \leq SOC_{norm}(t) < 0.5 \\ bSOC_{norm}(t) + c & 0.5 \leq SOC_{norm}(t) \leq 1, \end{cases} \tag{3.37}$$

where $SOC_{norm}(t)$ is equal to $SOC(t)/SOC_{max}$, and the parameters a=1.3, b=-1.5, c=2.05 are calculated based on the battery manufacturer datasheet [41]. From Eq. (3.37), it can be determined that discharging 1 Ah from the battery bank at $SOC_{norm}(t) \leq 0.5$ is approximately equivalent to remove 1.3 Ah from the total Ah throughput of the battery. If $SOC_{norm}(t) = 1$ discharging 1 Ah from the battery bank is equivalent to removing 0.55 Ah from the total Ah throughput of the battery. According to this analysis, discharging at higher SOC_{norm} value will be more beneficial for lead-acid batteries.

Using the calculated $L_f(t)$ in Eq. (3.35), the cost of the lifetime loss of the battery bank can be calculated by

$$C_{b.l}(t) = L_f(t)C_{b.b}, \tag{3.38}$$

where $C_{b.b}$ is the initial cost of the battery bank.

3.4 Grid-Tie Line

In this thesis, the MG described in section 3.1 is considered as being connected to an electrical grid that is suffering from long periods of a grid blackout. It is assumed that the blackout starting time BL_{st} and the blackout period BL_{pr} are specified from the power distribution company and known to the user, as shown in Fig. 3.6.

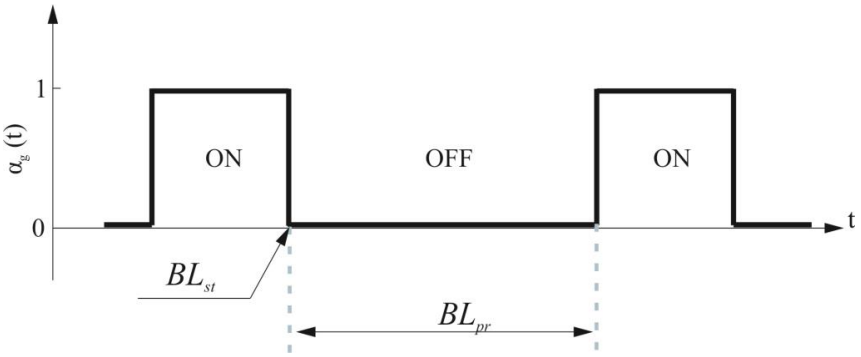

Figure 3.6: Illustration of the grid-tie line status.

This problem exists in many countries because there is no enough energy to cover all the connected loads to the main grid [103, 104, 105, 106, 107]. Therefore, the electrical power distribution company distributes the available power based on a predefined schedule. In this study, the available power from the MG is represented as

$$P_{av.g}(t) = \alpha_g(t) P_{g.max}, \tag{3.39}$$

where

$$\alpha_g(t) = \begin{cases} 0, & \text{if blackout occured} \\ 1, & \text{otherwise.} \end{cases} \tag{3.40}$$

Here $\alpha_g(t)$ represents the status of the grid-tie line, i.e. when $\alpha_g(t) = 1$, the grid power is available (the grid is ON) and when $\alpha_g(t) = 0$, the grid power is unavailable (the grid is OFF), see Fig. 3.6. It is to note that the maximum dispatched active power from the main grid is restricted by the grid-tie line capacity in the grid-connected mode as follows

$$P_{disp.g}(t) \leq \alpha_g(t) P_{g.max}, \tag{3.41}$$

where $P_{disp.g}(t)$ is the total dispatched power from the grid and $P_{g.max}$ is the maximum allowed active power to be dispatched from the main grid.

3.5 Predictive OPD of Residential Microgrids

This section introduces the optimal power dispatch (OPD) methodology utilized to manage the power flow through the PV-battery MG. The OPD aims to compensate

the grid blackout problem depicted in Fig. 3.6 considering the battery lifetime and the MG operational constraints. In this context, the economic model predictive controller (EMPC) is used to optimize the operation of the PV-battery MG to achieve the following major goals

- Provide a reliable energy source to cover the load, and meanwhile, minimizing the dispatched energy from the grid when it is available.
- Manage the battery bank *SOC* to guarantee the availability of enough energy to cover the load during blackout periods.
- Minimize the cost of the lifetime loss of the battery bank.

3.5.1 Implementation of EMPC-Based OPD

In this thesis, the dynamic behaviour of the battery is considered. Therefore, the operation of the PV-battery for multiple time steps should be taken into account to optimize the MG operation. Accordingly, model predictive control (MPC) [152, 153] has been widely used for optimal operation of renewable energy hybrid systems, because it can explicitly handle system dynamics, data forecasting, and operational constraints. What distinguishes the MPC from other control methodologies can be listed below [154]

- The explicit usage of the system model to predict the future system behaviour.
- The computation of the control variables is done by solving an optimization problem considering the system constraints.
- MPC works based on a receding horizon fashion, i.e. the control variables are calculated over a specified prediction horizon, and only the first optimal control values are sent to the system.

The economic model predictive controller (EMPC) differs from the standard MPC in that the controller provides its actions to improve the economic performance of the process, rather than tracking a predefine setpoint [155, 156]. The operation strategy by EMPC is similar to the conventional MPC [29]. In general, control actions of MPC are obtained by solving a dynamic optimization problem over a

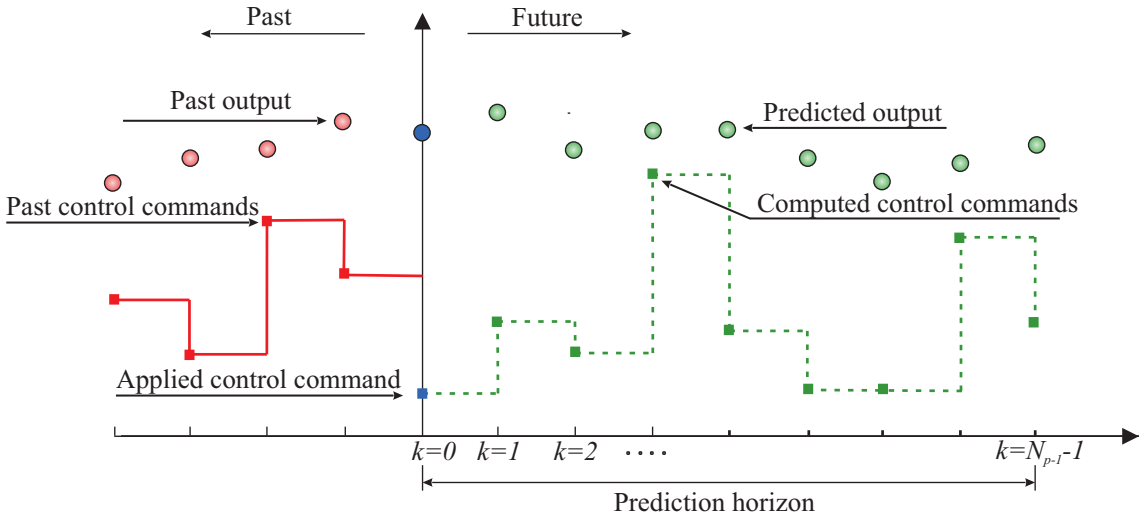

Figure 3.7: Representation of receding horizon working concept.

specified prediction horizon N_p. MPC is performed based on a so-called receding horizon strategy (see Fig. 3.7), i.e. at each time step, new measurements are taken, new predictions for the system behaviour over N_p are made, and control commands are computed [153]. Once the optimal control profiles for the prediction horizon are available, only the values of the control variables for the first time step are applied as the inputs to the system. The optimization problem of the proposed EMPC is defined to achieve the stated goals in section 3.5 as follows

$$\min_{\mathbf{U}_c(t),\mathbf{U}_b(t)} J = F_1 + F_2 \tag{3.42}$$

where

$$F_1 = \sum_{k=0}^{N_p-1} C_{e.g} P_{disp.g}(t+k|t), \tag{3.43}$$

and

$$F_2 = \sum_{k=0}^{N_p-1} C_{b.b} L_f(t+k|t). \tag{3.44}$$

Considering the following constraints

$$P_{av.l}(t+k|t) = P_{req.l}(t+k|t), \qquad \forall k = 0, ..., N_p - 1, \tag{3.45}$$

$$SOC_{min} \leq SOC(t+k|t) \leq SOC_{max}, \qquad \forall k = 0, ..., N_p - 1, \tag{3.46}$$

$$P_{ch}(t+k|t) \leq \gamma_{ch.lim} V_{b.n} Q_{b.n}, \qquad \forall k = 0, ..., N_p - 1, \tag{3.47}$$

$$P_{disp.pv}(t+k|t) \leq P_{av.pv}(t+k|t), \qquad \forall k = 0, ..., N_p - 1, \tag{3.48}$$

$$P_{disp.g}(t+k|t) \leq \alpha_g(t+k|t)P_{g.max}, \qquad \forall k = 0, ..., N_p - 1, \tag{3.49}$$

$$\xi_1(t+k|t) + \xi_2(t+k|t) + \xi_5(t+k|t) \leq 1, \qquad \forall k = 0, ..., N_p - 1, \tag{3.50}$$

$$\begin{cases} \xi_3(t+k|t) + \xi_4(t+k|t) \leq 1 \\ \xi_5(t+k|t) + \xi_4(t+k|t) \leq 1 \end{cases} \qquad \forall k = 0, ..., N_p - 1. \tag{3.51}$$

The objective function in Eq. (3.42) aims to minimize the cost of the dispatched power from the grid-tie line F_1, and meanwhile to minimize the cost of battery lifetime loss. Moreover the decision variables vectors, $\mathbf{U}_c(t) = [\mathbf{u}_c(t), ..., \mathbf{u}_c(t+N_p-1|t)]$ and $\mathbf{U}_b(t) = [\mathbf{u}_b(t), ..., \mathbf{u}_b(t+N_p-1|t)]$ are a sequence of N_p predicted continuous and binary control variables of the PV-battery MG, respectively, where $\mathbf{u}_c(t)$ and $\mathbf{u}_b(t)$ are expressed as follows

$$\mathbf{u}_c(t) = [P_{ch.g}(t), P_{ch.pv}(t), P_{dis}(t), P_{pv.l}(t)], \tag{3.52}$$

$$\mathbf{u}_b(t) = [\xi_1(t), \xi_2(t), \xi_3(t), \xi_4(t), \xi_5(t)]. \tag{3.53}$$

In addition to the constraints of the battery bank described in section 3.3, new constraints are added to the optimization problem, such as Eq. (3.45) to ensure the required load $P_{req.l}(t)$ coverage from the MG, Eq. (3.48) to prevent dispatching power higher than the available power from the PV-array, and Eq. (3.49) to prevent dispatching power higher than the allowed power amount from the grid, where

$$P_{av.l}(t) = P_{g.l}(t)\xi_4(t) + P_{pv.l}(t)\xi_3(t) + P_{dis}(t)\xi_5(t) \tag{3.54}$$

$$P_{disp.pv}(t) = P_{ch.pv}(t)\xi_2(t) + P_{pv.l}(t)\xi_3(t) \tag{3.55}$$

$$P_{disp.g}(t) = P_{ch.g}(t)\xi_1(t) + P_{g.l}(t)\xi_4(t). \tag{3.56}$$

The work flow of proposed EMPC is illustrated schematically in Fig. 3.8. At each time step, the EMPC reads the current value of the $SOC(t)$ and the forecasted load, grid-tie line status, and PV-array power. Then, it determines the optimal values for the control variables $\mathbf{u}_c(t)$ and $\mathbf{u}_b(t)$ over the prediction horizon N_p by solving the above-defined optimization problem using the optimizer in the EMPC. The control variables computed for the first time step are applied to the MG model. After that, the prediction horizon moves to the next time step and the whole procedure is

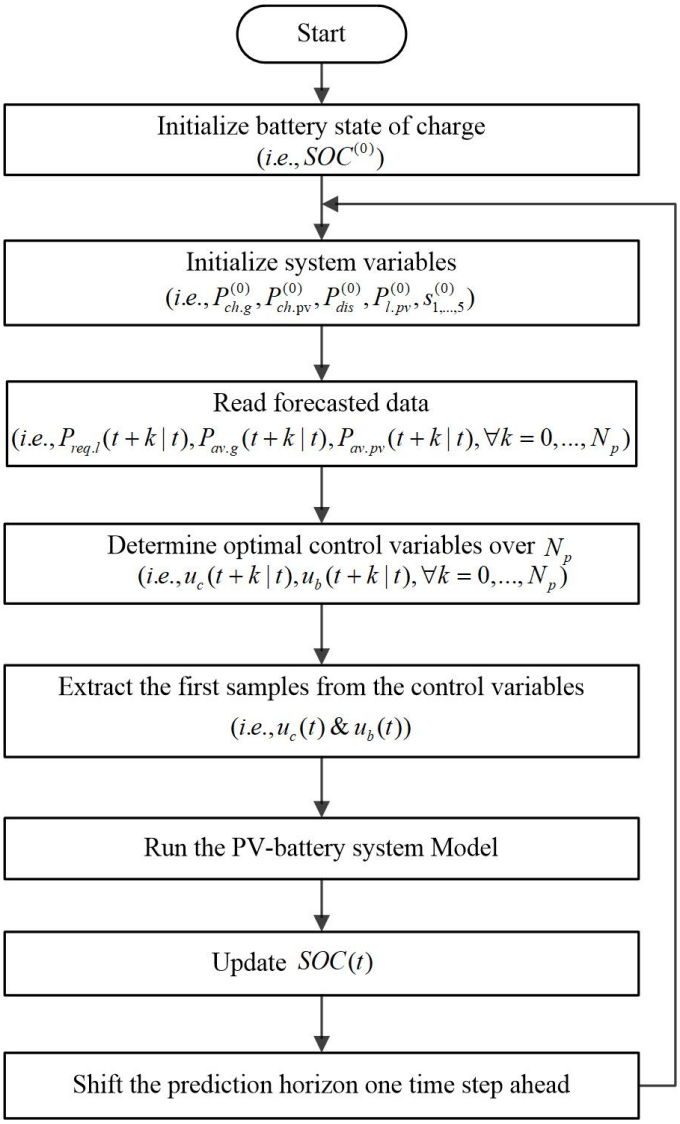

Figure 3.8: Flowchart of the proposed EMPC working concept in the residential MG.

repeated. Note that in this study, it is assumed that the values of the solar power generation, the demand and the available power from the grid in the predictive horizon are perfectly forecasted.

3.5.2 The Optimization Algorithm of EMPC

The optimization problem formulated in Eqs. (3.42) - (3.51) leads to a mixed-integer nonlinear programming (MINLP) problem consisting of four continuous and five binary control variables which are time-dependent during the prediction horizon (i.e, $9 \times N_p$ in total), as shown Eqs. (3.52) - (3.53). In addition, the existence of the nonlinear cost function and nonlinear constraints leads to a complex MINLP

Table 3.2: Options of the GA tool in MATLAB to solve OPD problem.

Option	Value
Population size	1500
Elite count	100
Crossover function	Intermediate
Crossover fraction	0.8
Mutation function	Gaussian
Selection function	Stochastic uniform
Creation function	Uniform
Scaling function	Rank based
Function tolerance	1e−3
Constraint tolerance	1e−4
Use parallel	true

problem. Genetic algorithm (GA) is an effective stochastic optimization algorithm developed by Holland [157] and Goldberg [158] inspired by the natural selection process which mimics the biological evolution. GA is different from traditional optimization algorithms in that they work with many candidate solutions known as a population rather than just one solution. At each step, GA modifies a population of candidate solutions by performing the selection, crossover and mutation processes to produce new children for the next generation [159]. Over successive generations, the population will be closer to an optimal solution. The explained process stops when the best solution in each generation changes by a small amount in comparison to the subsequent best solution. It is worth to mention that GA has no restrictions regarding the model of the system or the type of decision variables [160]. Because of these features, in this study, GA is employed to solve the MINLP problem described in Eqs. (3.42) - (3.51), by using the GA tool in MATLAB [161]. Meanwhile, parallel computing is used to speed up the calculations. The parameters used for the GA tool in MATLAB are given in Table 3.2. Note that the sampling time for the EMPC is set to be 1 h.

3.6 A Case Study

To illustrate the potential of the proposed OPD method to optimize the operation of the PV-battery MG shown in Fig. 3.1, a case study is adapted from [143] with the

Table 3.3: Type, size and capability of the system components of the residential MG.

Component	Size/Capability
PV-module	(250 Wp)x12= 3 kWp
DC/AC Inverter	3 kW
AC charger	2.88 kW
DC charger	2.88 kW
Battery bank	(12 V-200 Ah)x4= 9.6 kWh

Table 3.4: The battery bank parameters in the residential MG.

Parameter	DOD (-)	η_{ch} (%)	η_{dis} (%)	$V_{b.n}$ (V)	$Q_{b.n}$ (Ah)	$\gamma_{ch.lim}$ -
Value	0.7	95	95	48	200	0.2

Table 3.5: The PV-module parameters.

Parameter	$P_{max.m.stc}$ (W)	$V_{oc.m.stc}$ (V)	$I_{oc.m.stc}$ (A)	$NOCT$ °C	K_v (%/°C)	K_i (%/°C)	$N_{c.m}$ -	n -
Value	250	37.6	8.92	46	-0.32	0.05	60	1

components sizes listed in Table 3.3. The parameters of the battery bank are listed in Table 3.4, while the PV-module specifications in Table 3.5 [136]. The number of parallel and series-connected modules is taken to be 3 and 4, respectively. The price of the lead-acid batteries is set to 213 \$/kWh [162] which gives $C_{b.b} = 2044.8$ \$. To show the effects of the seasonal variations of the load profile and the PV-system output, two days from each season of a year are selected. The solar irradiance and temperature data are taken from [163] and shown in Fig. 3.9 (a) and (b), respectively. According to [143], two daily blackouts are considered, where the first blackout starts at 6 o'clock and the second one starts at 14 o'clock. Meanwhile, the blackout duration considered to be 8 hours. Moreover, the maximum allowed power to be extracted from the grid is 5 kW, and the cost of the consumed power from the grid is $C_{e.g} = 0.15$ \$/kWh.

The output of each PV-module is generated using the PV-array model described in section 3.2 and shown in Fig. 3.9 (c). It is to note that the PV-module is working

under practical operating conditions. Therefore, the actual output power from the PV-module is less than its rated power stated in Table 3.5, which is calculated according to the standard test conditions (STC) [164]. The available power from the grid, the load profile [165], and the available power from the PV-array are shown in Fig. 3.10 (a), (b) and (c) (dashed-blue), respectively.

To demonstrate the benefits of using the proposed EMPC-based control strategy that is introduced in section 3.5, the following three different operation scenarios are used to operate the PV-battery MG considering the grid blackout problem:

- **Scenario A:** The backup operation strategy [104], i.e., the MG is used only to cover the load during the blackout periods, but without using EMPC.
- **Scenario B:** The EMPC-based operation strategy but without considering the cost of the battery lifetime, i.e., $F2$ in Eq. (3.42) is not included.
- **Scenario C:** The EMPC-based operation strategy with considering the cost of the battery lifetime, i.e, $F2$ in Eq. (3.42) is included, which is the proposed strategy.

The computation is carried out on a desktop with Intel Core I7 CPU 3.4 GHz and 8 GB RAM. The initial values, denoted by $^{(0)}$, chosen for all computations are as follows : $P_{ch.g}^{(0)} = P_{ch.pv}^{(0)} = P_{dis}^{(0)} = P_{pv.l}^{(0)} = s_{1,\dots,5}^{(0)} = 0$ and $SOC^{(0)} = 0.75 \times SOC_{max}$.

The comparison results are shown in Tables 3.6 - 3.8 and Figs. 3.10 - 3.12. The results of each operation scenario are discussed below in detail.

- **Scenario A:** In this scenario, the PV-battery MG is working according to the backup operation strategy [104], i.e., the grid (when it is available) is responsible for covering the load and charging the battery bank. The PV-array with or without the battery bank will cover the load during the blackout periods only. If there is extra power from the PV-array after covering the load, it will be used to charge the battery bank.

  The results are given in Tables 3.6 - 3.8 (Scenario A) and Fig. 3.10. It can be observed from the results that the MG highly depends on the grid to cover the load and to charge the battery bank. As an example, during the day hours in Summer (e.g., time steps 102-110 in Fig. 3.10), although the available power

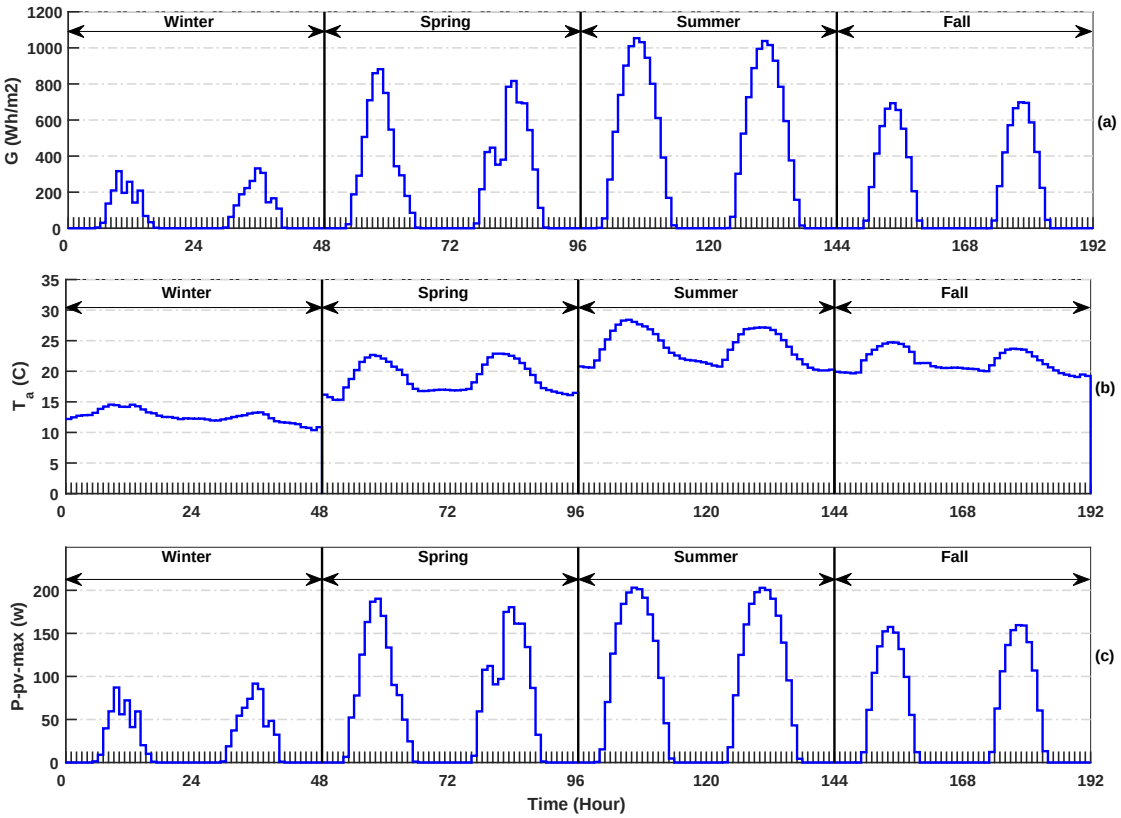

Figure 3.9: PV-array model performance. (a) Global solar irradiance at ground level. (b) Ambient temperature. (c) The maximum generated power by the PV-module.

from the PV-array is enough to cover the load and charge the battery bank, the MG dispatches the required energy from the grid. This increases the total dispatched energy from the grid and decreases the dispatched energy from the PV-array, as shown in Tables 3.6 and 3.7, receptively.

In contrast, comparing Fig. 3.10 (f) with Fig. 3.11 (f) and Fig. 3.12 (f), it can be clearly seen that the SOC level of the battery bank is the highest in Fig. 3.10 (f), because of the high value of the charging power from the grid, as shown in Fig. 3.10 (d). Therefore, the value of the consumed weighted Ah from the battery bank will be decreased, which will reduce the lifetime loss of the battery bank.

As a result, the cost of the dispatched energy from the grid $F1$ is highly increased, and the total cost of battery bank lifetime loss $F2$ is decreased. Consequently, the total operating costs of the PV-battery MG J is increased, as shown in Table 3.8.

- **Scenario B:** Here, we use the same input data as in scenario A, but EMPC is used to optimize the PV-battery MG operation, without considering the cost of the battery lifetime. The results are given in Tables 3.6 - 3.8 (scenario B) and Fig. 3.11.

  Due to considering the cost of the dispatched energy from the grid in the optimization problem of the EMPC, a huge reduction in the total dispatched energy from the grid is gained, in comparison to Scenario A, as shown in Table 3.6. This effect decreases the total costs of the dispatched energy from the grid in comparison to Scenario A, as seen in Table 3.8. The reason behind this is that the EMPC forces the MG to dispatch power from the PV-array even if the grid is available during the day hours, as shown in Figs. 3.11 (a) - (c).
  On the other hand, reducing the dispatched energy from the grid decreases the total charging power as well. Therefore, the SOC level of the battery bank is lowered, as seen in Fig. 3.11 (f).
  From Table 3.8, it can be clearly seen that the cost of the dispatched energy from the grid $F1$ is decreased and the total cost of the battery bank lifetime loss $F2$ is increased, in comparison to Scenario A. As a result, the total operation costs of the MG J is decreased except in winter where the cost of the lifetime loss of the battery bank is highly increased due to the lack of generated power from the PV-array, as seen in Fig. 3.11 (c) (dashed-blue).

- **Scenario C:** In this scenario, with the same input data as in Scenario B, but the EMPC is used to optimize the PV-battery MG operation considering the cost of the battery lifetime. This means that both the cost of the dispatched energy from the grid and the battery lifetime loss are considered in the optimization problem of the EMPC. The results are given in Tables 3.6-3.8 (Scenario C) and Fig. 3.12.

  The aim of this scenario is to see the impacts of considering the battery lifetime cost. Comparing Figs. 3.12 (d), (f) with Figs. 3.11 (d), (f), it is clearly seen that the total charging power scenario C is increased to raise the battery bank SOC level. This increment leads to increase in the dispatched power from the PV-array as seen in Table. 3.7. Meanwhile, the dispatched

Table 3.6: Dispatched energy from the grid in kWh in two days at each scenario in the residential MG.

Seasons	Scenario A	Scenario B	Scenario C
Winter	26.1	21.35	21.7
Spring	22.01	12.22	13.07
Summer	33.31	23.24	22.65
Fall	21.65	11.29	13.02

Table 3.7: Dispatched energy from the PV-array in kWh in two days at each scenario in the residential MG.

Seasons	Scenario A	Scenario B	Scenario C
Winter	5.77	7.38	9.79
Spring	6.29	14.05	15.15
Summer	10.18	19.4	20.59
Fall	5.12	11.73	13.53

Table 3.8: Cost of the dispatched energy for each scenario in the residential MG.

	Scenario A			**Scenario B**			**Scenario C**		
Seasons	$F1(\$)$	$F2(\$)$	$J(\$)$	$F1(\$)$	$F2(\$)$	$J(\$)$	$F1(\$)$	$F2(\$)$	$J(\$)$
Winter	3.91	5.02	**8.93**	3.2	6.42	**9.62**	3.26	5.1	**8.36**
Spring	3.3	3.51	**6.81**	1.84	4.46	**6.3**	1.96	3.66	**5.62**
Summer	4.99	5.65	**10.64**	3.48	5.92	**9.4**	3.39	5.56	**8.95**
Fall	3.25	3.51	**6.86**	1.69	4.42	**6.11**	1.95	3.53	**5.48**

energy from the grid is slightly increased.

As a result, the cost of the dispatched energy from the grid is slightly increased in comparison to Scenario A, the cost of battery lifetime loss is highly decreased in comparison to Scenario B, and the total operation cost of the MG is decreased in all seasons comparing to Scenario A and B, as shown in Table 3.8.

From the above discussion, it can be concluded that the total dispatched energy from the grid can be considerably reduced, and the dispatched energy from the PV-array can highly be increased by using the EMPC-based operation strategy for the PV-battery MG which increases the economic and environmental benefits of installation of the PV-array. Nevertheless, considering the battery lifetime with the EMPC is necessary to decrease the cost of battery lifetime loss while reducing the cost of consumed energy by the load.

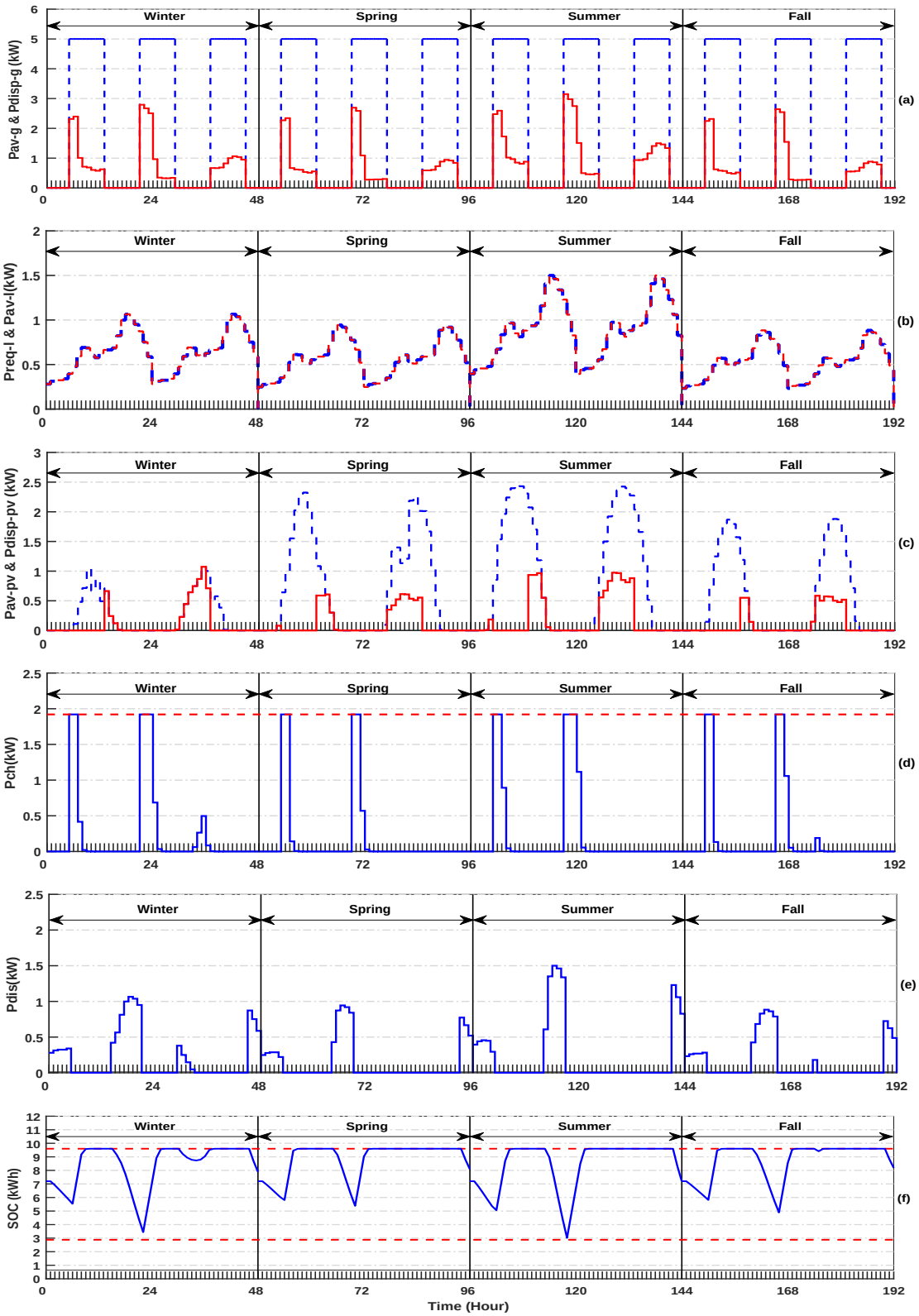

Figure 3.10: MG operation in arbitrary two days for each season for Scenario A. (a) Available power (dashed-blue) and power dispatch (solid-red) from the grid. (b) Required load power (dashed-blue) and available power to cover load (solid-red). (c) Available power (dashed-blue) and power dispatch (solid-red) from PV-array. (d) Charging power of battery bank (solid-blue) and the charging power limit (dashed-red). (e) Discharging power of battery bank. (f) Battery bank SOC (solid-blue) and SOC upper and lower limits (dashed-red).

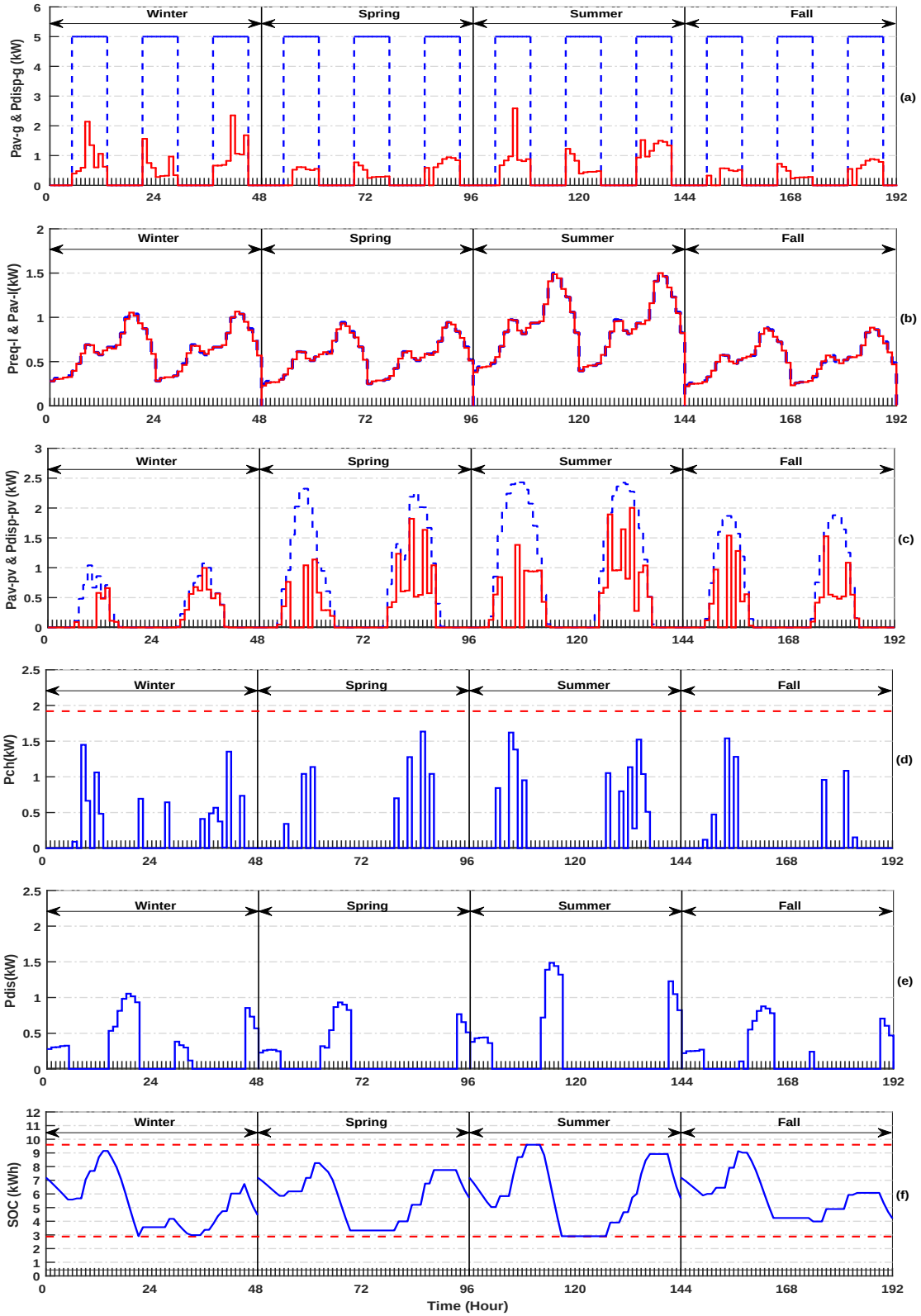

Figure 3.11: MG operation in arbitrary two days for each season for Scenario B. (a) Available power (dashed-blue) and power dispatch (solid-red) from the grid. (b) Required load power (dashed-blue) and available power to cover load (solid-red). (c) Available power (dashed-blue) and power dispatch (solid-red) from PV-array. (d) Charging power of battery bank (solid-blue) and the charging power limit (dashed-red). (e) Discharging power of battery bank. (f) Battery bank SOC (solid-blue) and SOC upper and lower limits (dashed-red).

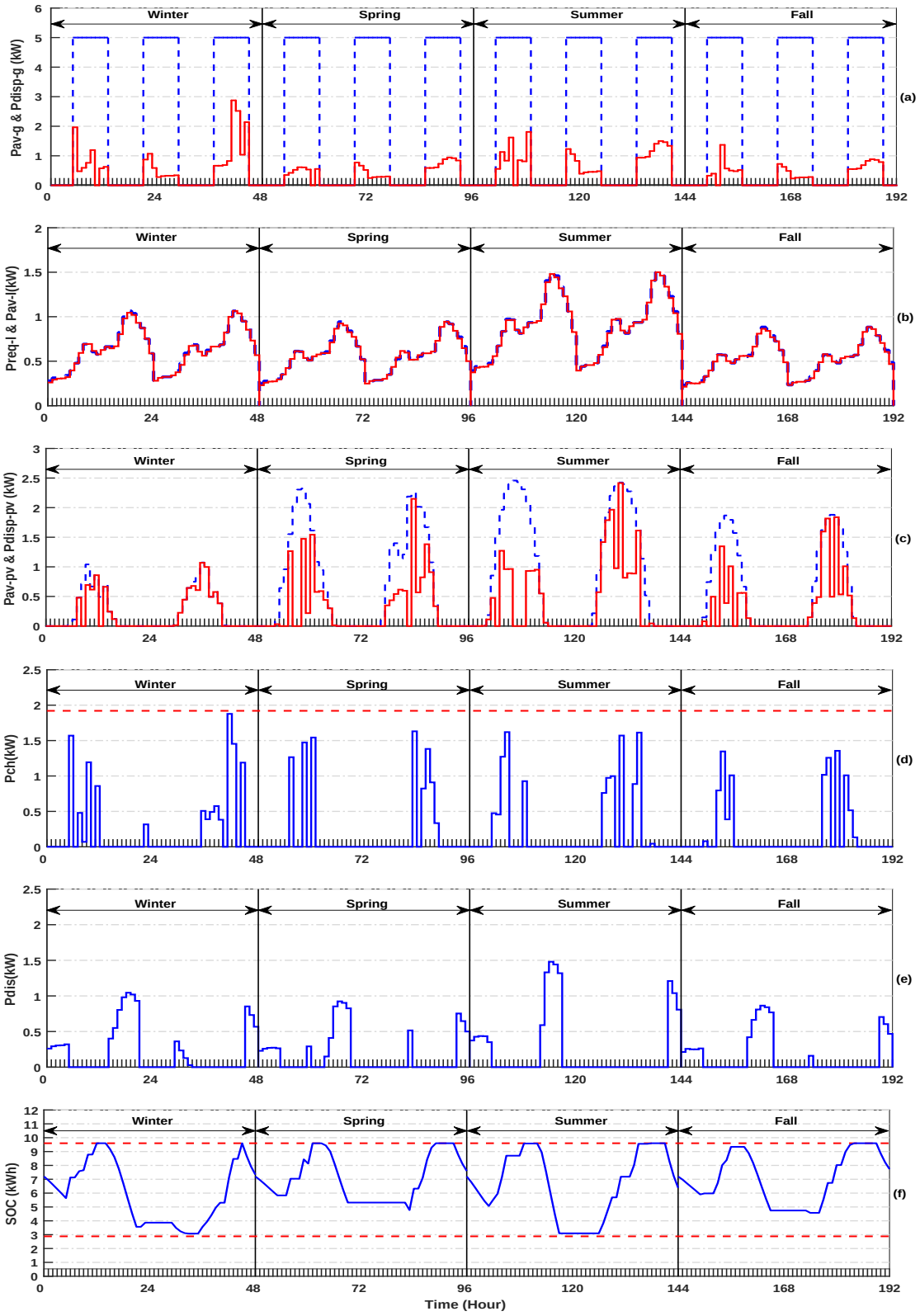

Figure 3.12: MG operation in arbitrary two days for each season for Scenario C. (a) Available power (dashed-blue) and power dispatch (solid-red) from the grid. (b) Required load power (dashed-blue) and available power to cover load (solid-red). (c) Available power (dashed-blue) and power dispatch (solid-red) from PV-array. (d) Charging power of battery bank (solid-blue) and the charging power limit (dashed-red). (e) Discharging power of battery bank. (f) Battery bank SOC (solid-blue) and SOC upper and lower limits (dashed-red).

3.7 Conclusions

In this chapter, a new comprehensive model for a residential PV-battery MG is developed to address the grid blackout problem. The model considers the real operational constraints of the MG as well as the costs of the battery lifetime. Controllable switches are added to control the on/off power flows through the MG. The inclusion of the controllable switches leads to a complex MINLP problem which is solved by using genetic algorithm. A new OPD strategy based on economic model predictive control (EMPC) is developed to minimize the total cost of the energy dispatched from the grid and the cost of battery lifetime loss under grid blackouts. To verify the effectiveness of the proposed OPD approach, a compersion between a traditional backup operation strategy and the EMPC-based OPD strategy is made. The results show that the proposed approach leads to a significant reduction of the cost of the total energy consumed from the grid while decreasing the curtailment of the generated power from the PV-array and maximizing the battery lifetime.

Chapter 4

Optimal Operation of Industrial Microgrid

A particular property of the industrial loads is that they have low power factors. Therefore, the reactive power consumption of the load cannot be neglected. This chapter presents an active-reactive optimal power dispatch (AR-OPD) operation strategy based on the concept of an economic model predictive controller (EMPC). In this operation strategy, the battery lifetime cost, the active-reactive power generation cost, and the grid blackout problem are considered. The diesel generator, the battery-inverter, and the PV-inverter models are added to the developed MG model in chapter 3. Besides, a cost model for the dispatched reactive power from the PV-system and battery storage system is developed. Furthermore, a new cost model for reactive power generation from the diesel generator is introduced. The applicability of the proposed EMPC framework is demonstrated using a real case study to manage the power dispatch in the MG in a cost-effective and reliable manner for both grid-connected and islanded mode.

4.1 Modelling of Industrial Microgrids Considering Reactive Power Dispatch

The MG to be studied is shown in Fig. 4.1. It consists of a PV-system, a battery storage system (BSS), multiple diesel generators (DGs), grid-tie line, controllable

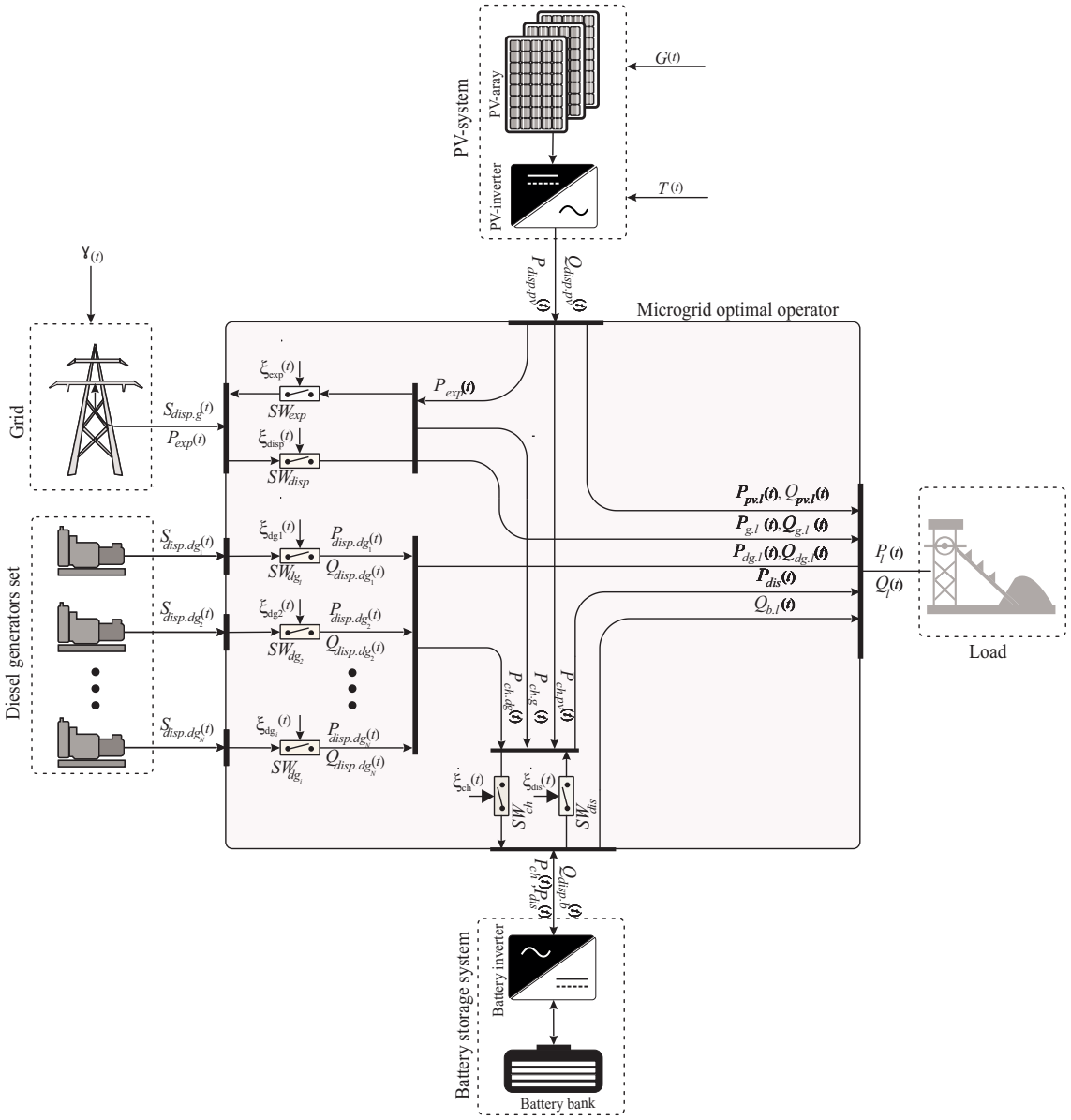

Figure 4.1: The proposed PV-battery-diesel microgrid schematic diagram.

switches as well as given active-reactive load profiles. The PV-system includes a PV-array and an on-grid PV-inverter. The BSS consists of a battery bank with lead-acid batteries and a battery-inverter. SW_{ch} and SW_{dis} are ON/off switches used to manage the charging and discharging processes. Similarly, SW_{disp} and SW_{exp} are used to maintain active-reactive power import/export constraints from/to the grid. Moreover, $SW_{dg.i}$ are used to manage the DGs' status.

The MG components are modelled considering all their technical and operational constraints. The same PV-array model explained in section 3.2 is used in this chapter to calculate the generated active power from the PV-array. Similarly, the battery bank model in section 3.3 is used here to simulate the battery bank operation. The

PV-inverter, the battery inverter, the diesel generator, and the status of grid-tie line models are explained as follows.

4.1.1 PV and Battery Inverters

The PV-inverter is used to convert the DC-power generated from the PV-array to AC-power used to cover the load, charge the battery bank, or export it to the main grid. Meanwhile, the battery inverter introduced here is a bi-directional inverter, i.e., it converts the AC-power to DC-power to charge the battery bank. In the opposite way, it converts the DC-power to AC-power to cover the load. Nevertheless, the power inversion process in both inverters leads to loss of power inside the inverter, e.g., in the form of heat, which reduces the inverter efficiency $\eta^X_{inv}(t)$. Based on the dispatched power from the inverter $P^X_{disp.inv}(t)$ its efficiency can be calculated by

$$\eta^X_{inv}(t) = \frac{P^X_{disp.inv}(t)}{P^X_{disp.inv}(t) + P^X_{inv.loss}(t)} \tag{4.1}$$

where $P^X_{inv.loss}(t)$ is the inverter power loss, and the superscript X can be PV or BSS (the calculation of the exact value of $P^X_{inv.loss}(t)$ will be discussed in detail in subsection 4.2.4). It is to note that each of the PV and the battery inverter has its technical constraints that should be satisfied during the MG operation.

PV-Inverter Operation Constraints The dispatched active power from the PV-Inverter should be limited by the maximum generated power from the PV-array and the PV-inverter efficiency as follows

$$P^{PV}_{disp.inv}(t) \leq \eta^{PV}_{inv} P_{av.pv}(t), \tag{4.2}$$

where

$$P^{PV}_{disp.inv}(t) = P_{pv.l}(t) + P_{ch.pv}(t) + P_{exp}(t). \tag{4.3}$$

Moreover, the PV-inverter capability to produce both active and reactive power is limited by its rated apparent power [64]

$$\sqrt{(P^{PV}_{disp.inv}(t))^2 + (Q^{PV}_{disp.inv}(t))^2} \leq S_{pv.inv}, \tag{4.4}$$

where $S_{pv.inv}$ is the rated capacity of the PV-inverter and $Q^{PV}_{disp.inv}(t)$ is the reactive power dispatched from the PV-inverter.

Battery Inverter Operation Constraints The dispatched active power from the battery inverter is limited by the maximum allowable discharging power [166] and the available energy in the battery, i.e.,

$$P_{dis}(t) \leq \min\left(\gamma_{dis.lim} SOC_{max}, \frac{SOC(t) - SOC_{min}(t)}{\Delta t}\right). \tag{4.5}$$

where $\gamma_{dis.lim}$ is a parameter for discharging power limit. Besides, the battery inverter can produce reactive power during the charging or discharging processes [6] commensurate with its rated capacity. Therefore, the following constraints should be added

$$\sqrt{\xi_{ch}(t)(P_{ch}(t))^2 + \left(Q^{BSS}_{disp.inv}(t)\right)^2} \leq S_{b.inv} \tag{4.6}$$

$$\sqrt{\xi_{dis}(t)(P_{dis}(t))^2 + \left(Q^{BSS}_{disp.inv}(t)\right)^2} \leq S_{b.inv}, \tag{4.7}$$

where $S_{b.inv}$ is the rated capacity of the battery inverter, $Q^{BSS}_{disp.inv}(t)$ is the dispatched reactive power from the battery inverter, and $\xi_{ch}(t)$ and $\xi_{dis}(t)$ are binary control variables used to prevent simultaneous charging and discharging during the battery bank operation. This is held by adding the following constraint

$$\xi_{ch}(t) + \xi_{dis}(t) \leq 1. \tag{4.8}$$

It is worth to mention that in this study, the charging power from each source is specified individually by the MG controller. Therefore, the total charging power of the MG is described by

$$P_{ch}(t) = P_{ch.pv}(t) + P_{ch.dg}(t) + P_{ch.g}(t). \tag{4.9}$$

where $P_{ch.pv}(t)$, $P_{ch.dg}(t)$ and $P_{ch.g}(t)$ are the charging power from the PV-system, DGs and the grid-tie line, respectively.

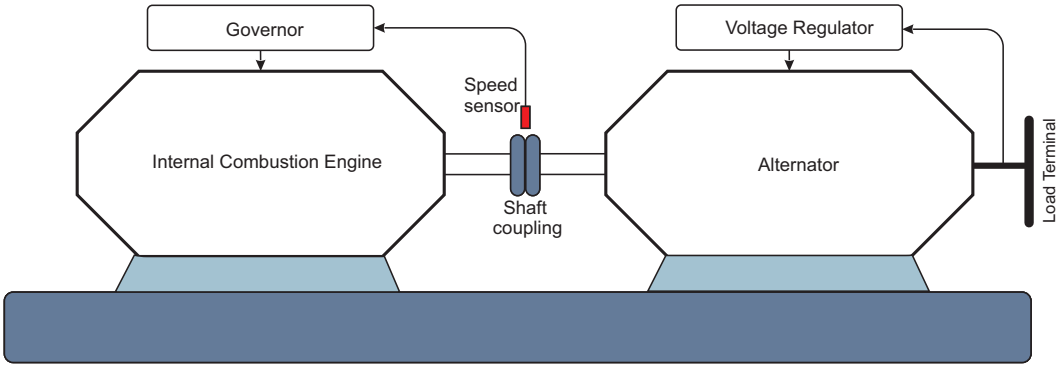

Figure 4.2: Diesel generator block diagram.

4.1.2 Diesel Generator

Basically, the DG consists of two main parts, as shown in Fig. 4.2. The first part is an internal combustion engine integrated with a governer that controls the fuel supply of the engine to maintain the shaft speed as required. The second part is an alternator incorporated with a voltage regulator to maintain the output terminal voltage [167]. In a DG, the diesel engine is responsible for producing mechanical power and the alternator converts it to electrical power. However, part of the converted power in the alternator is lost due to stray, friction, copper, and core losses [168], see Fig. 4.3. Accordingly, the relation between the dispatched electrical power from each alternator $P_{disp.dg_i}(t)$ with $i \in \{1, 2, ..., N_{dg}\}$ and the generated mechanical power can be expressed as

$$P_{disp.dg_i}(t) = \eta_{dg_i}(t) P_{m.dg_i}(t), \tag{4.10}$$

where $\eta_{dg_i}(t)$ is the alternator efficiency whose value depends on the dispatched power from the diesel generator (the calculation of the exact value of $\eta_{dg_i}(t)$ will be discussed in details in subsection 4.2.3).

On the other hand, knowing the changing in the operating status of the DG is important to accurately calculate its operating cost. To describe the changing in the DG status, either it started up on or shut down, the following equations are introduced

$$\xi_{up.dg_i}(t) = \xi_{dg_i}(t)(1 - \xi_{dg_i}(t-1)), \ \forall i = 1, 2, ..., N_{dg} \tag{4.11}$$

$$\xi_{d.dg_i}(t) = \xi_{dg_i}(t-1)(1 - \xi_{dg_i}(t)), \ \forall i = 1, 2, ..., N_{dg}, \tag{4.12}$$

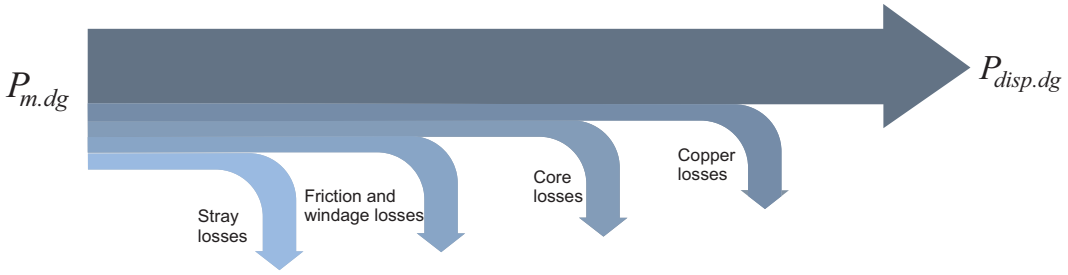

Figure 4.3: The power flow diagram of an alternator. [168]

where $\xi_{dg_i}(t)$ is a binary variable represents the status of the i^{th} DG as well as $\xi_{up.dg_i}(t)$ and $\xi_{d.dg_i}(t)$ are auxiliary binary variables that represent the changes at each diesel generator status. If $\xi_{up.dg_i}(t) = 1$, it means that the i^{th} diesel generator is started up at this time step, otherwise no change is occurred. If $\xi_{d.dg_i}(t) = 1$, it means that the i^{th} diesel generator is shut down at this time step, otherwise no change is occurred.

DG Operation Constraints The total dispatched power from each DG is limited by the manufacturer specifications to prevent overheating and additional mechanical stress. Therefore,

$$\sqrt{(P_{disp.dg_i}(t))^2 + (Q_{disp.dg_i}(t))^2} \leq S_{dg_i.max} \tag{4.13}$$

where $P_{disp.dg_i}(t)$ and $Q_{disp.dg_i}(t)$ are the dispatched active and reactive power from each DG, respectively, and $S_{dg_i.max}$ is the DG rated apparent power. Besides, the power factor of the dispatched power have to be within the specified range, i.e.

$$PF_{dg.min_i} \leq PF_{dg_i}(t) \leq 1, \tag{4.14}$$

where $PF_{dg.min_i}$ is the minimum allowed value of the DG power factor and $PF_{dg_i}(t)$ is the DG operating power factor at time t, which is given as

$$PF_{dg_i}(t) = \frac{P_{disp.dg_i}(t)}{\sqrt{P^2_{disp.dg_i}(t) + Q^2_{disp.dg_i}(t)}} \forall i = 1, 2, ..., N_{dg}. \tag{4.15}$$

Since the frequent operation of the DG at a low load increases the risk of DG engine failure due to the wet stacking problem [169], the following constraint needs to be added

$$P_{disp.dg_i}(t) \geq 0.3 \times P_{r.dg_i}, \qquad \forall i = 1, 2, ..., N_{dg}, \tag{4.16}$$

where $P_{r.dg_i}$ is the rated power of the DG.

4.1.3 Grid-Tie Line

The introduced grid-tie line model in chapter 3 is adapted here to include the reactive power effect. The maximum dispatched active and reactive power from the main grid as well as the maximum exported active power is restricted by the grid-tie line capacity in the grid-connected mode as follows

$$\xi_{disp}(t) \times \sqrt{P^2_{disp.g}(t) + Q^2_{disp.g}(t)} \leq \alpha_g(t) S_{g.max} \tag{4.17}$$

and

$$\xi_{exp}(t) \times P_{exp}(t) \leq \alpha_g(t) S_{g.max} \tag{4.18}$$

where $P_{disp.g}(t)$ and $Q_{disp.g}(t)$ are the dispatched active and reactive power from the main grid, respectively, $P_{exp}(t)$ is the exported active power to the main grid, $S_{g.max}$ is the maximum allowed apparent power to be imported/exported from/to the main grid, and $\alpha_g(t)$ is used to represent the status of the grid-tie line, i.e.,

$$\alpha_g(t) = \begin{cases} 0, & \text{if blackout occured} \\ 1, & \text{otherwise.} \end{cases} \tag{4.19}$$

Moreover, the following constraint is added to prevent simultaneous dispatching from and exporting power to the main grid

$$\xi_{disp}(t) + \xi_{exp}(t) \leq 1, \tag{4.20}$$

where $\xi_{disp}(t)$ and $\xi_{exp}(t)$ are binary variables that represent the status of SW_{disp} and SW_{exp} switches, respectively. It is to note that exporting reactive power to the main grid is not considered in this study.

4.2 Operation Cost of Industrial Microgrids

For an accurate calculation of the industrial MG operation cost, the cost of the active-reactive dispatched power from all available sources is considered. Moreover, the cost of battery lifetime loss due to dispatching active power from the BSS is

calculated using the introduced model subsection 3.3.2. In the following subsections, the net energy cost of the grid-tie line, as well as the operation cost of the DGs, the PV-inverter and the battery inverter will be explained in details.

4.2.1 The Net Energy Cost of the Grid-Tie Line

In this study, it is assumed that the MG can import active and reactive power from the main grid; meanwhile, it is allowed to export only active power. Therefore, the net energy cost from the grid-tie line is expressed by

$$C_{n.g}(t) = C_{p.g}P_{disp.g}(t) + C_{q.g}Q_{disp.g}(t) - C_{exp}P_{exp}(t), \tag{4.21}$$

where $C_{n.g}$ is the net energy cost of the grid-tie line, $C_{p.g}$ and $C_{q.g}$ are the cost of the dispatched active power and reactive power from the main grid, respectively, and C_{exp} is the cost of exported active power to the main grid.

4.2.2 Diesel Generator Operation Cost

The main operating cost of the DG is the diesel engine fuel consumption due to active-reactive power consumption from the alternator. Moreover, in this study, the startup and shutdown costs of each DG are counted in the problem formulation. Therefore, the total operation cost of the DG set $C_{op.dg}$ is formulated as follows

$$C_{op.dg}(t) = \sum_{i=1}^{N_{dg}} (C_f f_{con.dg_i}(t) + C_{up_i}\xi_{up.dg_i}(t) + C_{d_i}\xi_{d.dg_i}(t))), \tag{4.22}$$

where $f_{con.dg_i}$ is the hourly fuel consumption of DG_i, C_f is the fuel cost in $\$/l$, C_{up_i} and C_{d_i} are the startup and shutdown costs, respectively. In this study, the startup cost is considered equal to the fuel consumption cost of the DG during 10 minutes of operation at 25% from its rated capacity. Meanwhile, the shutdown cost is considered equal to the fuel consumption cost of the DG during 6 minutes of operation at no load [33], i.e.,

$$C_{up_i} = C_f \frac{f_{con.dg_i}(0.25 \times P_{r.dg_i})}{6}, \tag{4.23}$$

$$C_{d_i} = C_f \frac{f_{con.dg_i}(0)}{10}. \tag{4.24}$$

The consumed fuel by each DG can be calculated using the following third order equation

$$f_{con.dg_i}(t) = \xi_{dg_i} \times (a_{k_i} P^3_{m.dg_i}(t) + a_{k_i} P^2_{m.dg_i}(t) + a_{k_i} P_{m.dg_i}(t) + a_{k_i}), \tag{4.25}$$

where the equation coefficients a_k with $k \in \{1, 2, 3, 4\}$ are fitted to the fuel consumption curve given from the diesel engine data-sheet [170, 171], and $P_{m.dg_i}$ is the dispatched mechanical power from the diesel engine of DG_i, which is related to the alternator efficiency and the dispatched electrical power from the DG as

$$P_{m.dg_i}(t) = \frac{P_{disp.dg_i}(t)}{\eta_{dg_i}(t)}. \tag{4.26}$$

4.2.3 Cost of Reactive Power from Diesel Generators

The DG generates reactive power to maintain its terminal voltage within the specified limits based on the load requirements. However, generating reactive power increases the current flow inside the alternator of the DG [168]. Since the copper losses inside the alternator increases by increasing the current flow [168], the alternator efficiency is going to be decreased.

Based on the manufacturer's datasheet, the alternator efficiency at unity power factor $\eta_{dg_{i_0}}(t)$ can be expressed by a third-order polynomial function

$$\eta_{dg_{i_0}}(t) = b_{k_i} P^3_{disp.dg_i}(t) + b_{k_i} P^2_{disp.dg_i}(t) + b_{k_i} P_{disp.dg_i}(t) + b_{k_i}, \tag{4.27}$$

where the equation coefficients b_k with $k \in \{1, 2, 3, 4\}$, are fitted to the efficiency curve given in [172] at unity power factor for DG_i. However, by a close look at the alternator efficiency curve (see Fig. 4.4), it can be noticed that the alternator efficiency is reduced by decreasing the operating power factor of the DG that will be decreased by increasing the reactive power consumption. In addition, the efficiency reduction $\eta_{dg_{i_r}}(t)$ can be approximated by a linear relationship with the operating

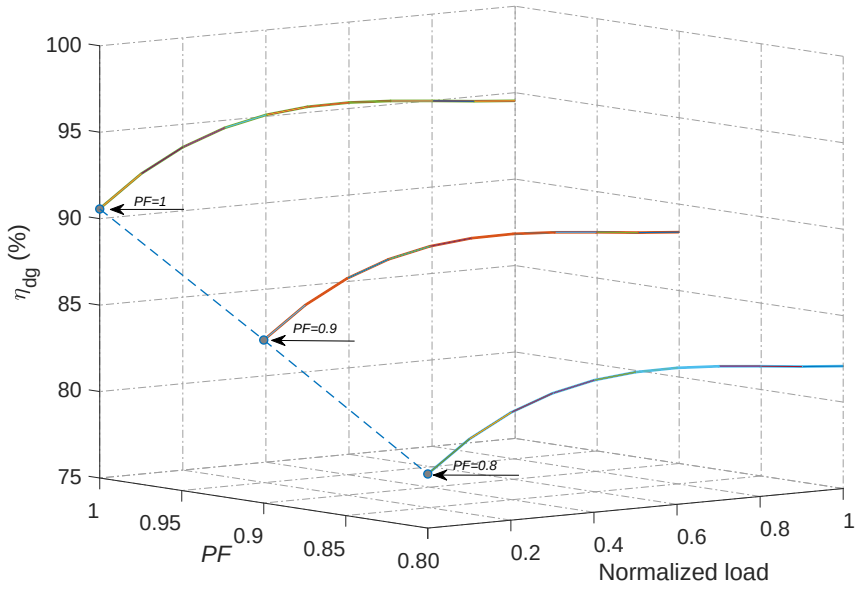

Figure 4.4: Diesel generator alternator efficiency curve [172].

power factor, which can be formulated as

$$\eta_{dg_{i_r}}(t) = c_{k_i} PF(t) + c_{k_i}, \tag{4.28}$$

where the equation coefficients c_k with $k \in \{1, 2\}$, are extracted from the efficiency reduction curve given in the alternator data-sheet [172]. Based on this, the actual alternator efficiency $\eta_{dg_i}(t)$ at a specified power factor is formulated as

$$\eta_{dg_i}(t) = \eta_{dg_{i_0}}(t) - \eta_{dg_{i_r}}(t). \tag{4.29}$$

Now $\eta_{dg_i}(t)$ can be used to calculate the generated mechanical power from the diesel engine (see, Eq. (4.26)) and its fuel consumption (see, Eq. (4.25)) at the operating power factor of the DG. Consequently, to calculate the generated reactive power cost, the difference between the diesel engine fuel consumption at the unity power factor and the actual operating power factor is used as follows

$$C_q^{dg_i}(t) = C_f \left(f_{con.dg_i}\Big(\eta_{dg_i}(t), P_{m.dg_i}(t)\Big) - f_{con.dg_{i_0}}\Big(\eta_{dg_{i_0}}(t), P_{m.dg_i}(t)\Big) \right), \tag{4.30}$$

where $f_{con.dg_{i_0}}(t)$ is the diesel engine fuel consumption at the unity power factor.

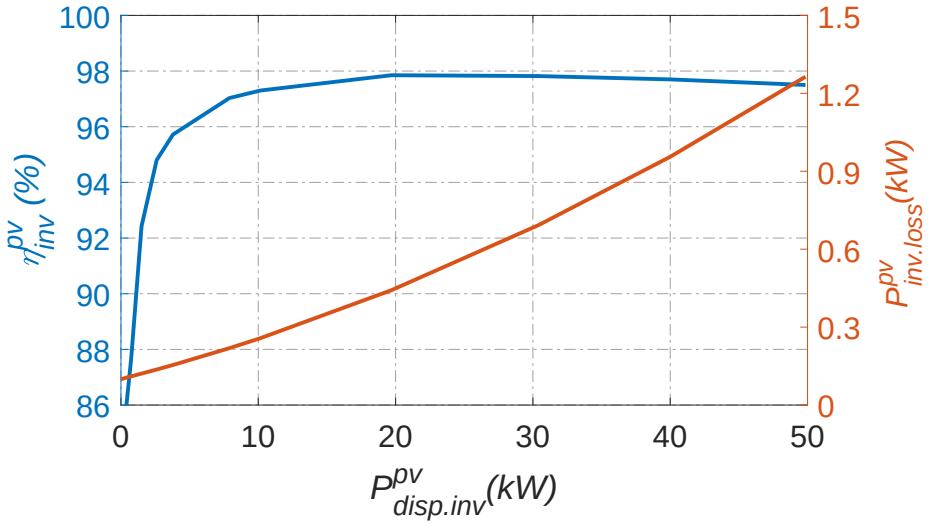

Figure 4.5: Efficiency and power loss curves of a 50 kVA PV-inverter [173].

4.2.4 Cost of Reactive Power from Inverter-Based Sources

The PV and the battery inverters are used to convert the DC-power generated from the PV-array or battery bank to AC-power with very low cost. However, the inversion process leads to loss of power inside the inverter, e.g., in the form of heat. Based on an experimental results, it was shown in [61] that the power loss in the inverter $P^{X}_{inv.loss}(t)$ depends on the dispatched active and reactive power and can be approximated by

$$P^{X}_{inv.loss}(t) = c_{self} + c_{v.loss}\sqrt{(P^{X}_{disp.inv}(t))^2 + (Q^{X}_{disp.inv}(t))^2} + c_{r.loss}((P^{X}_{disp.inv}(t))^2 + (Q^{X}_{disp.inv}(t))^2), \tag{4.31}$$

where c_{self} is the inverter self-loss at the standby operation, $c_{v.loss}$ is the output voltage dependent loss, and $c_{r.loss}$ is the current dependent loss, where the superscript X can be PV or BSS. Eq. (4.31) can be driven using the efficiency curve of the inverter (which is available in the manufacturer datasheet) by reformulating Eq. (4.1) as follows

$$P^{X}_{inv.loss} = P^{X}_{disp.inv}\frac{(1-\eta^{X}_{inv})}{\eta^{X}_{inv}}. \tag{4.32}$$

As an example, the $P^{pv}_{inv.loss}$ of a 50 kVA PV-inverter is illustrated in Fig. 4.5 (orange curve) which is calculated using Eq. (4.32) and the inverter efficiency (blue curve).

The MG compensates the lost power according to the available energy at each time step, which increases the operation cost of the MG. The cost of the dispatched reactive power depends on the additional power loss caused by the reactive power generation $\Delta P^X_{inv.loss}(t)$ and the cost of the active power utilized to cover it. Using Eq. (4.31), $\Delta P^X_{inv.loss}(t)$ can be calculated by

$$\Delta P^X_{inv.loss}(t) = \begin{cases} P^X_{inv.loss}(t) - P^X_{inv.loss_0}(t), & \text{if} \\ & P^X_{disp.inv}(t) \neq 0 \;\&\; Q^X_{disp.inv}(t) \neq 0 \\ c_{self} + c_{v.loss} Q^X_{disp.inv}(t) + c_{r.loss}(Q^X_{disp.inv}(t))^2, & \text{if} \\ & P^X_{disp.inv}(t) = 0 \;\&\; Q^X_{disp.inv}(t) \neq 0 \end{cases}, \tag{4.33}$$

where $P^X_{inv.loss_0}(t)$ is the power loss in the inverter considering only the dispatched active power, see Eq. (4.31).

In the PV-inverter, $P^{PV}_{inv.loss}(t)$ will be covered by the PV-system without additional cost in case that the available power from the PV-array is enough to cover it. Otherwise, $P^{PV}_{inv.loss}(t)$ will be covered by the same power used to cover the load, and the average cost of the dispatched power from the MG will be used to calculate the cost of the dispatched reactive power from the PV-inverter $C^{PV}_q(t)$ as follows

$$C^{PV}_q(t) = \begin{cases} 0, & \text{if} \quad P_{av.pv}(t) \geq P^{PV}_{inv.loss}(t) \\ \dfrac{C_{p.g} P_{disp.g}(t) + C_{op.dg}(t) + C_{b.l}(t)}{P_{req.l} + P^{pv}_{inv.loss}(t)} \Delta P^{pv}_{inv.loss}(t), & otherwise. \end{cases} \tag{4.34}$$

where $C_{p.g} P_{disp.g}$ is the cost of the dispatched power from the grid, $C_{op.dg}$ is the operation cost of the DG set and $C_{b.l}$ is the cost of the dispatched power from the BSS.

In the battery-inverter, $P^{BSS}_{inv.loss}(t)$ will be covered from the battery bank in the case that the available energy in the battery bank is enough to cover it. In this case, the battery lifetime loss cost (see section 3.3.2) will be used to calculate the cost of the dispatched reactive power from the battery-inverter $C^{BSS}_q(t)$. Otherwise, $P^{BSS}_{inv.loss}(t)$ will be covered by the same power used to cover the load, and the average cost of

the dispatched power from the MG will be used to calculate $C_q^{BSS}(t)$ as follows

$$C_q^{BSS}(t) = \begin{cases} C_{b.l}(t), & \text{if} \quad \dfrac{E_{av.BSS}(t)}{\Delta t} \geq P_{inv.loss}^{BSS}(t) \\ \dfrac{C_{p.g}P_{disp.g}(t) + C_{op.dg}(t)}{P_{req.l}(t) + P_{inv.loss}^{BSS}(t)} \Delta P_{inv.loss}^{BSS}(t), & otherwise. \end{cases} \tag{4.35}$$

where $E_{av.BSS}(t) = (SOC(t) - SOC_{min}(t))$ is the available energy in the BSS at time t.

4.3 Predictive AR-OPD of Industrial Microgrids

The proposed AR-OPD method is built based on the EMPC concept to provide the profiles of the optimal control variables by solving the formulated optimization problem over a specified time horizon. The EMPC is responsible for determining the dispatched active and reactive power set-points for each power source in the MG to cover the load with minimum cost. Therefore, the objective function of the optimization problem is formulated to achieve the following goals

- Covering the active and reactive power demand in the islanded or in the grid connected mode with a minimum cost.
- Reducing the fuel consumption of the DGs.
- Decreasing the cost of battery bank lifetime loss.
- Utilizing the generated energy from the PV-array as much as possible.

Therefore, the objective function of the EMPC is formulated as shown in Eq. (4.36) to minimize the net energy cost of the grid-tie line F_1, the reactive power cost from the PV and battery inverters F_2, the DG total operation cost F_3, and the cost of battery lifetime loss F_4. It is to note that the reactive power cost from the DG is included in F_3. Meanwhile, all operation constraints of the MG will be held at the whole prediction horizon, as stated in Eqs. (4.37) - (4.52).

$$\min_{\mathbf{U}_c(t),\mathbf{U}_b(t)} J = F_1 + F_2 + F_3 + F_4 \tag{4.36}$$

where

$$F_1 = \sum_{k=0}^{N_p-1} C_{e.g} P_{disp.g}(t+k|t) + C_{q.g} Q_{disp.g}(t+k|t) - C_{exp} P_{exp}(t+k|t)$$
$$F_2 = \sum_{k=0}^{N_p-1} C_q^{BSS}(t+k|t) + C_q^{PV}(t+k|t)$$
$$F_3 = \sum_{k=0}^{N_p-1} C_{op.dg}(t+k|t)$$
$$F_4 = \sum_{k=0}^{N_p-1} C_{b.init} L_f(t+k|t).$$

subject to,

$$P_{av.l}(t+k|t) = P_{req.l}(t+k|t), \qquad \forall k = 0, ..., N_p - 1, \tag{4.37}$$

$$Q_{av.l}(t+k|t) = Q_{req.l}(t+k|t), \qquad \forall k = 0, ..., N_p - 1, \tag{4.38}$$

$$P_{disp.pv}^{PV}(t+k|t) \leq \eta_{inv}^{PV}(t+k|t) P_{av.pv}(t+k|t), \qquad \forall k = 0, ..., N_p - 1, \tag{4.39}$$

$$\sqrt{(P_{disp.pv}(t+k|t))^2 + (Q_{disp.inv}^{PV}(t+k|t))^2} \leq S_{pv.inv}, \qquad \forall k = 0, ..., N_p - 1, \tag{4.40}$$

$$P_{disp.dg_i}(t+k|t) \geq 0.3\, P_{r.dg_i}, \qquad \forall k = 0, ..., N_p - 1, \tag{4.41}$$

$$PF_{dg.min_i} \leq PF_{dg_i}(t+k|t) \leq 1, \qquad \forall k = 0, ..., N_p - 1, \tag{4.42}$$

$$\sqrt{(P_{disp.dg_i}(t+k|t))^2 + (Q_{disp.dg_i}(t+k|t))^2} \leq S_{dg_i}, \qquad \forall k = 0, ..., N_p - 1, \tag{4.43}$$

$$\xi_{exp}(t+k|t) P_{exp}(t+k|t) \leq \alpha_g(t+k|t) S_{g.max}, \qquad \forall k = 0, ..., N_p - 1, \tag{4.44}$$

$$\xi_{disp}(t+k|t)\sqrt{P^2_{disp.g}(t+k|t)+Q^2_{disp.g}(t+k|t)} \leq \alpha_g(t+k|t)S_{g.max}, \quad \forall k=0,...,N_p-1, \tag{4.45}$$

$$\xi_{disp}(t+k|t)+\xi_{exp}(t+k|t) \leq 1, \quad \forall k=0,...,N_p-1, \tag{4.46}$$

$$\xi_{ch}(t+k|t)+\xi_{dis}(t+k|t) \leq 1, \quad \forall k=0,...,N_p-1, \tag{4.47}$$

$$P_{ch}(t+k|t) \leq \gamma_{ch.lim}V_{b.n}Q_{b.n}, \quad \forall k=0,...,N_p-1, \tag{4.48}$$

$$P_{dis}(t+k|t) \leq \gamma_{dis.lim}V_{b.n}Q_{b.n}, \quad \forall k=0,...,N_p-1, \tag{4.49}$$

$$\sqrt{\xi_{ch}(t+k|t)(P_{ch}(t+k|t))^2+\left(Q^{BSS}_{disp.inv}(t+k|t)\right)^2} \leq S_{b.inv}, \quad \forall k=0,...,N_p-1, \tag{4.50}$$

$$\sqrt{\xi_{dis}(t+k|t)(P_{dis}(t+k|t))^2+\left(Q^{BSS}_{disp.inv}(t+k|t)\right)^2} \leq S_{b.inv}, \quad \forall k=0,...,N_p-1, \tag{4.51}$$

$$SOC_{min} \leq SOC(t+k|t) \leq SOC_{max}, \quad \forall k=0,...,N_p-1. \tag{4.52}$$

In Eq. (4.36) , the control variables of the optimization problem are determined to specify all the dispatched active and reactive power set-points for each power source in the MG. Moreover, binary control variables are introduced to specify the status of the controllable switches in the MG model, see Fig. 4.1. Therefore, the control variables of the optimization problem are divided into continuous $\mathbf{u}_c(t)$ and binary $\mathbf{u}_b(t)$, hence

$$\begin{aligned}\mathbf{u}_c(t) = [&P_{g.l}(t+k|t), P_{ch.g}(t+k|t), P_{exp}(t+k|t), Q_{g.l}(t+k|t),\\ &P_{disp.dg_i}(t+k|t), Q_{disp.dg_i}(t+k|t), P_{ch.dg}(t+k|t), P_{pv.l}(t+k|t),\\ &Q_{disp.pv}(t+k|t), P_{ch.pv}(t+k|t), P_{dis}(t+k|t), Q_{disp.b}(t+k|t)],\end{aligned} \tag{4.53}$$

and

$$\mathbf{u}_b(t+k|t) = [\xi_{exp}(t+k|t), \xi_{disp}(t+k|t), \xi_{ch}(t+k|t), \xi_{dis}(t+k|t), \xi_{dg_i}(t+k|t)]. \tag{4.54}$$

According to the calculated control variables the total dispatched active power from the PV-system $P_{disp.pv}(t)$, the total dispatched active power from the DG set $\sum_{i=1}^{N_{dg}} P_{disp.dg_i}(t)$, the total dispatched active power from the grid $P_{disp.g}(t)$ as well as the available active power $P_{av.l}(t)$ and the available reactive power $Q_{av.l}(t)$ to cover the load, are calculated, respectively, by

$$P_{disp.pv}(t) = P_{pv.l}(t) + P_{ch.pv}(t) + P_{exp}(t), \tag{4.55}$$

$$\sum_{i=1}^{N_{dg}} P_{disp.dg_i}(t) = P_{dg.l}(t) + P_{ch.dg}(t), \tag{4.56}$$

$$P_{disp.g}(t) = P_{g.l}(t) + P_{ch.g}(t), \tag{4.57}$$

$$P_{av.l}(t) = P_{pv.l}(t) + P_{g.l}(t) + P_{dg.l}(t) + P_{dis}(t), \tag{4.58}$$

$$Q_{av.l}(t) = Q^{PV}_{disp.inv}(t) + Q_{disp.g}(t) + \sum_{i=1}^{N_{dg}} Q_{disp.dg_i}(t) + Q^{BSS}_{disp.inv}(t). \tag{4.59}$$

The workflow of the proposed EMPC is illustrated schematically in Fig. 4.6. At each time step, the EMPC updates the battery bank SOC, the DGs status, hourly solar irradiance, ambient temperature, active power, and reactive power load. Then, the optimal values of the control variables are calculated for the whole time horizon using a genetic algorithm (GA) to minimize the stated objective function in Eq. (4.36). However, only the first optimal control values (at $k = 0$) are applied to the MG model. Consequently, the predictive horizon moves to the next time step and the whole procedure is repeated.

The formulated optimization problem of the EMPC is solved using the GA function in MATLAB utilizing the function parameters shown in Table 4.1. It is noted that the sampling time is chosen to be $k = 1$ h, and the prediction horizon length is $N_p = 24$ h.

4.4 A Case study

To demonstrate the effectiveness of the proposed AR-OPD framework for optimizing both active and reactive power dispatch in the MG shown in Fig. 4.1, a real case study from [12] is adapted and simulated using real temperature and solar irradiance

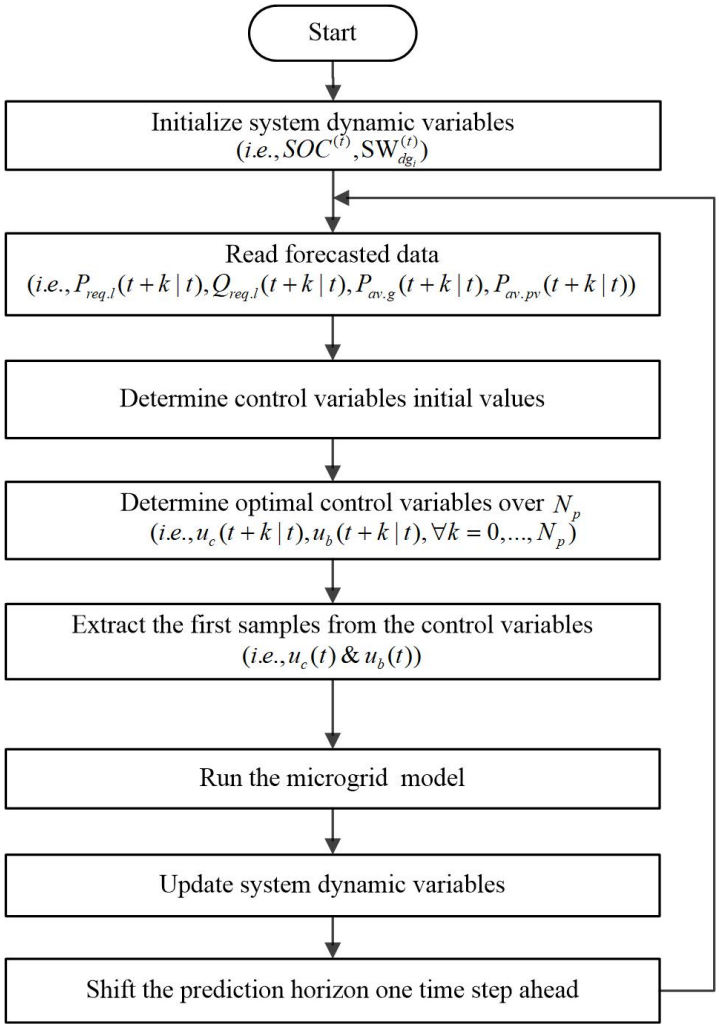

Figure 4.6: Flowchart of the proposed EMPC working concept in the industrial MG.

profiles [163]. Moreover, to emphasize the adaptivity of the proposed control strategy to different environmental conditions, optimizing the MG operation in two days from each season of a year are considered.

The technical and economic parameters of the main components in the MG are given in Table 4.2, while the detailed parameters of the battery bank and the PV-panel are listed in Table 4.3 and 4.4, respectively.

The efficiency curves of the battery-inverter and the PV-inverter are taken from the corresponding datasheet in [173] and [174], respectively. Besides, the efficiency curves of the diesel engines are obtained from [170] and [171], while the efficiency curves of the alternators are taken from [172].

The grid blackouts period and its rhythm are taken from [12]. The blackouts start at 6 o'clock and 14 o'clock daily; meanwhile, the blackout duration considered to be

Table 4.1: Parameters of the GA tool in MATLAB to solve AR-OPD problem.

Option	Value
Population size	900
Elite count	100
Maximum generations	3000
Crossover function	Intermediate
Crossover fraction	0.92
Mutation function	Gaussian
Selection function	Stochastic uniform
Creation function	Uniform
Scaling function	Rank based
Function tolerance	1e−3
Constraint tolerance	1e−2
Use parallel	true

8 hours. The active and reactive load profiles are obtained from [6] and shown in Fig. 4.7 (a). The output of the PV-system is generated using the PV-array model described in section 3.2 and shown in Fig. 4.7 (b) (dashed-blue).
Several scenarios are used to demonstrate the benefit of using the proposed AR-OPD operation strategy. The following four different operation scenarios to operate the PV-battery-diesel MG under the grid blackout are considered:

- **Scenario A**: The proposed AR-OPD operation strategy in section 4.3 is used to operate the MG **with** considering the battery lifetime loss cost and the reactive power cost. Nevertheless, importing reactive power from the main grid is **prevented**.
- **Scenario B**: The proposed AR-OPD operation strategy in section 4.3 is used to operate the MG **without** considering the battery lifetime loss cost and the reactive power cost. Nevertheless, importing reactive power from the main grid is **prevented**.
- **Scenario C**: The proposed AR-OPD operation strategy in section 4.3 is used to operate the MG **without** considering the battery lifetime loss cost and the reactive power cost. Here, importing reactive power from the main grid is **allowed**.

Table 4.2: Technical and economic parameters of the main components in the industrial MG.

Load	
Maximum load	500 kVA
Load power factor	0.8
PV-system	
PV-array size	700 kWp
PV-inverter size and type	Sunny tripower core1/50 kVA
PV-inverter power factor	from 0 to 1
Number of PV-inverters	10
Battery storage system	
Total energy capacity	960 kWh
Battery-inverter size and type	Sunny tripower storage-60/75 kVA
Number of battery-inverters	7
Battery-inverter power factor	from 0 to 1
Charging limiter	0.2
Discharging limiter	1
Ah throughput parameter	390
Diesel generator$_1$	
DG_1 type and S_{dg}	Cummins QSL9/300 kVA [175].
Diesel engine size and type	Cummins QSL9-G5/310 kWm [170].
Alternator size and type	Stamford UCI274H/300 kVA [172].
Minimum power factor for DG_1	0.8
DG lower limit	$0.3 \times P_{r.dg_1}$
Fuel cost	1.3 \$/l
Diesel generator$_2$	
DG_2 type and S_{dg}	Cummins QSB7/200 kVA [175].
Diesel engine size and type	Cummins QSB7-G5/213 kWm [171].
Alternator size and type	Stamford HC4D/200 kVA [172].
Minimum power factor	0.8
DG lower limit	$0.3 \times P_{r.dg_2}$
Fuel cost	1.3 \$/l
Grid	
Grid maximum importing/exporting power capability	500 kVa
Active power buying tariff	0.15\$/kWh
Reactive power buying tariff	0.0375\$/kVAR
Active power selling tariff	0.1\$/kWh

Table 4.3: The battery bank parameters in the industrial MG.

Parameter	DOD (-)	η_{ch} (%)	η_{dis} (%)	$V_{b.n}$ (V)	$BB_{n.c}$ (Ah)	γ_{ch} -
Value	0.5	95	95	48	40000	0.2

Table 4.4: The PV-module parameters.

Parameter	$P_{max.m.stc}$ (W)	$V_{oc.m.stc}$ (V)	$I_{oc.m.stc}$ (A)	$NOCT$ °C	K_v (%/°C)	K_i (%/°C)	$N_{c.m}$ -	n -
Value	250	37.6	8.92	46	-0.32	0.05	60	1

- **Scenario D**: The rule-based operation strategy [176] is used to operate the proposed MG considering only the active power dispatch.

All computations were undertaken under the MATLAB 8.2 environment, running on a desktop with an Intel Core I7-3.4 GHz CPU and 8 GB RAM. The results are shown in Tables 4.5 - 4.7 and Figs. 4.7 - 4.11. The results of each operation scenario are discussed below in detail.

- **Scenario A**: It can be noticed from Tables 4.5 - 4.7 that the total cost of the active and reactive power is the lowest in this scenario. This cost reduction is due to considering the cost of battery lifetime and reactive power in the optimization problem of the EMPC. Compared to other scenarios, the MG controller increases the battery SOC level to reduce the value of the weighted factor of the dispatched current from the battery (see, Eq. (3.36)) to decrease the battery lifetime loss, as seen in Fig. 4.7 (e), Fig. 4.8 (e), and Fig. 4.9 (e). On the other hand, it can be seen from Fig. 4.10 that importing reactive power from the main grid is prevented and the controller depends on the local power sources to cover the load, while considering the reactive power generation cost. As explained in subsections 4.2.3 and 4.2.4, generating reactive power increases the power losses in the DG as well as in the battery and the PV inverters. However, the MG compensates the lost power according to the available energy at each time step. To decrease the cost of reactive power compensation, the EMPC increases reactive power dispatching from the PV-inverter, especially in the day time, as seen in Fig. 4.10 at time steps 100-115. Besides, the EMPC forces the DG to work at a high power factor to decrease the power loss, as

seen in Fig. 4.10 (c). Therefore, the total cost of the dispatched reactive power from the MG is the lowest in this scenario, as shown in Table 4.6

Due to considering the startup and shutdown costs in the objective function, the number of startup and shutdown switches is reduced by decreasing the frequency of running and stopping the same DG, as seen in Fig.4.7 (d).

- **Scenario B**: Here, the same input data as in scenario A is used, but EMPC is utilized to optimize the MG operation without considering the cost of the battery lifetime. The results are shown in Tables 4.5 - 4.7 (scenario B) and Fig. 4.8.

  Since the battery lifetime cost is not considered in this scenario, the EMPC increases the discharged power from the BSS to decrease the dispatched power from the main grid in the grid-connected mode or from the DG in the blackout periods. However, this operation strategy increases the battery lifetime cost significantly, which increases the total power cost compared with scenario A, as seen in Table 4.5. To understand the effect of SOC level on the battery lifetime cost, one can compare the SOC in Fig. 4.7 (e) with that in Fig. 4.8 (e). It can be seen that the SOC in scenario A is higher than the SOC in scenario B, and discharging is activated only at high SOC levels, which decrease its effect on the lifetime cost.

  Also, in this scenario, importing reactive power from the main grid is still forbidden, moreover the reactive power generation cost from the local sources is neglected. Therefore, the amount of the dispatched reactive power from the PV and battery inverter is nearly equal. Moreover, from Fig. 4.11, it can be seen that the operation power factors of the DGs are low in comparison to that in scenario A.

  From Table 4.5, it can be seen that the total cost of the dispatched active power is increased due to the increment in the cost of battery lifetime loss. In addition, the cost of reactive power is increased, as shown in Table 4.6, due to increasing the dispatched reactive power from the BSS and the DGs.

- **Scenario C**: This scenario is similar to scenario B; however, importing reactive power from the main grid is allowed. From Table 4.5, we can notice

that the cost of active power is nearly not affected. Meanwhile, the cost of reactive power is highly increased compared with its cost in scenarios A and B, as shown in Table 4.6. This demonstrates that generating reactive power locally is more cost-effective than importing it from the main grid.

- **Scenario D**: In this scenario, the conventional rule-based operation strategy is applied to operate the MG by considering only the active power dispatch. Here, the PV-system is used to meet the load requirement as the first priority. If the generated energy from the PV-system is more than the needed load, the excess energy will be stored in the BSS. In case the PV-system cannot meet the load, the BSS will work with the PV-system to meet the load while considering the SOC constraints of the battery bank. However, if the BSS is not able to meet the deficit energy, the PV-inverter will work with the grid-tie line to cover the load in grid-connected mode. Otherwise, the PV-inverter will work with the DG to cover the load in the islanded mode.
  The explained operation strategy is illustrated in Fig. 4.9, it can be seen that the controller depends mainly on the BSS and the PV-system to cover the load. Therefore, the battery lifetime cost is highly increased, and the cost of dispatched power from the main grid and from the DG is decreased. As a result, the total cost of the dispatched power is highly increased compared with that in scenario A, see Table 4.7.

From the above discussion, we can see that the proposed AR-OPD operation strategy is able to operate the PV-battery-diesel MG optimally to cover both the active and the reactive power demand. In addition, it is demonstrated that considering the battery lifetime cost is necessary to minimize the total operation cost of the MG. Moreover, considering the reactive power cost has a high impact on optimizing the power flow in the MG. Furthermore, the results show that the PV-inverter is able to generate reactive power with very low cost in comparison to the battery-inverter and the DG.

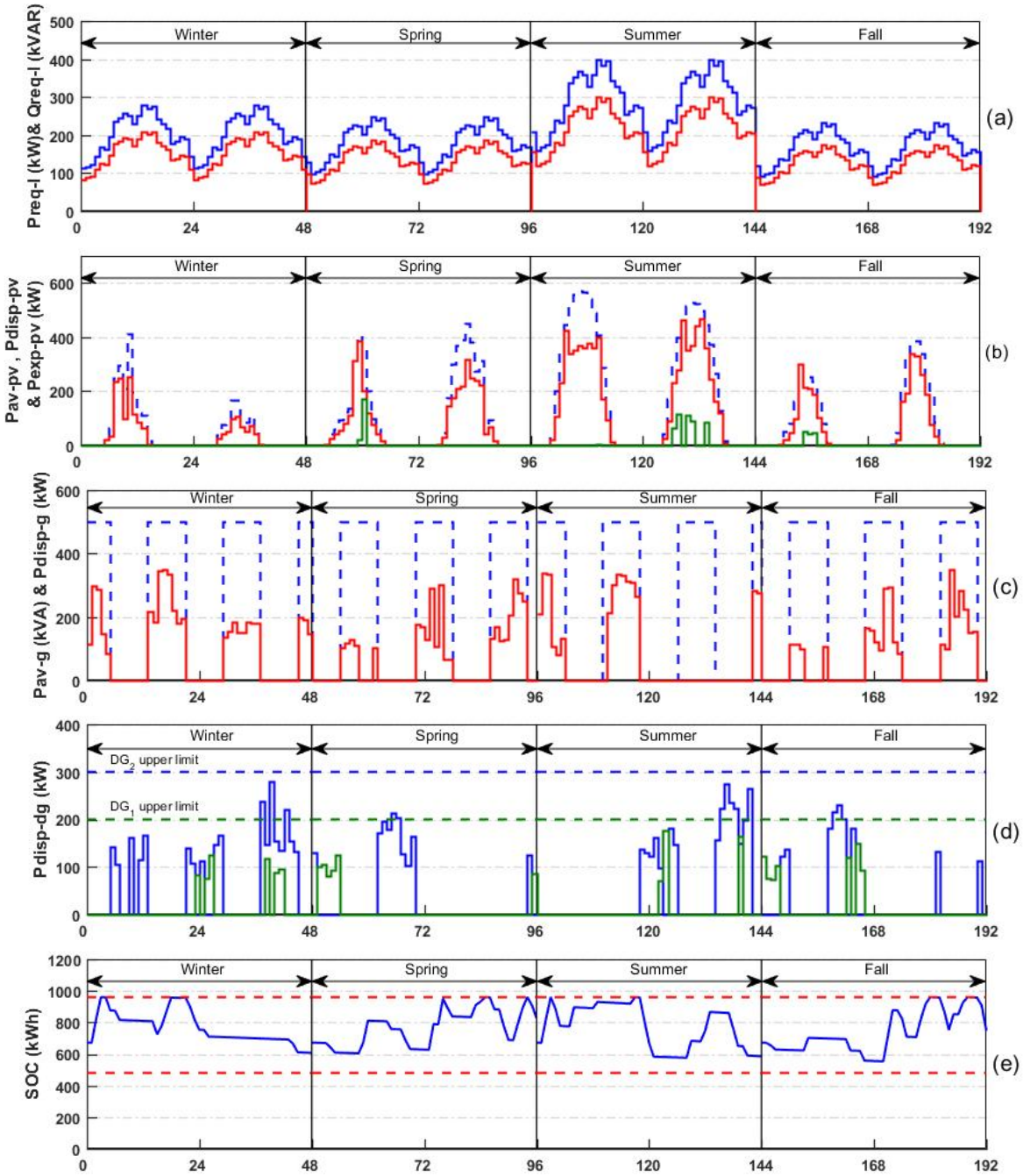

Figure 4.7: Active power dispatch in arbitrary two days for each season for scenario A. (a) Required load active power (solid-blue) and reactive power (solid-red). (b) Available power (dashed-blue), locally dispatched power (solid-red) and exported power (solid-green) from the PV-system. (c) Available power (dashed-blue) and power dispatch (solid-red) from the grid. (d) Total dispatched power from DG_1 (solid-blue) and DG_2 (solid-green). (e) Battery bank SOC (solid-blue) and SOC upper and lower limits (dashed-red).

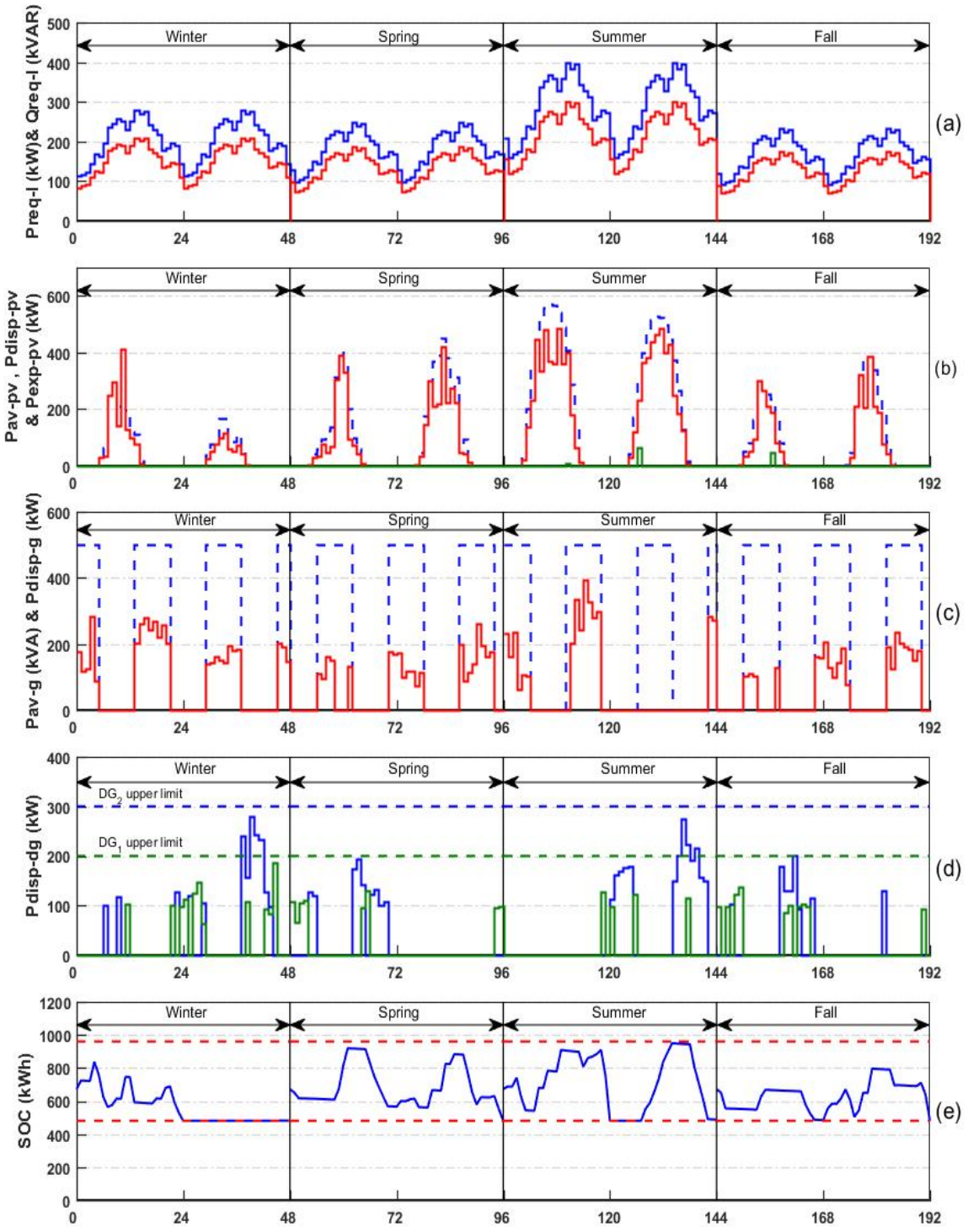

Figure 4.8: Active power dispatch in arbitrary two days for each season for scenario B. (a) Required load active power (solid-blue) and reactive power (solid-red). (b) Available power (dashed-blue), locally dispatched power (solid-red) and exported power (solid-green) from the PV-system. (c) Available power (dashed-blue) and power dispatch (solid-red) from the grid. (d) Total dispatched power from DG_1 (solid-blue) and DG_2 (solid-green). (e) Battery bank *SOC* (solid-blue) and *SOC* upper and lower limits (dashed-red).

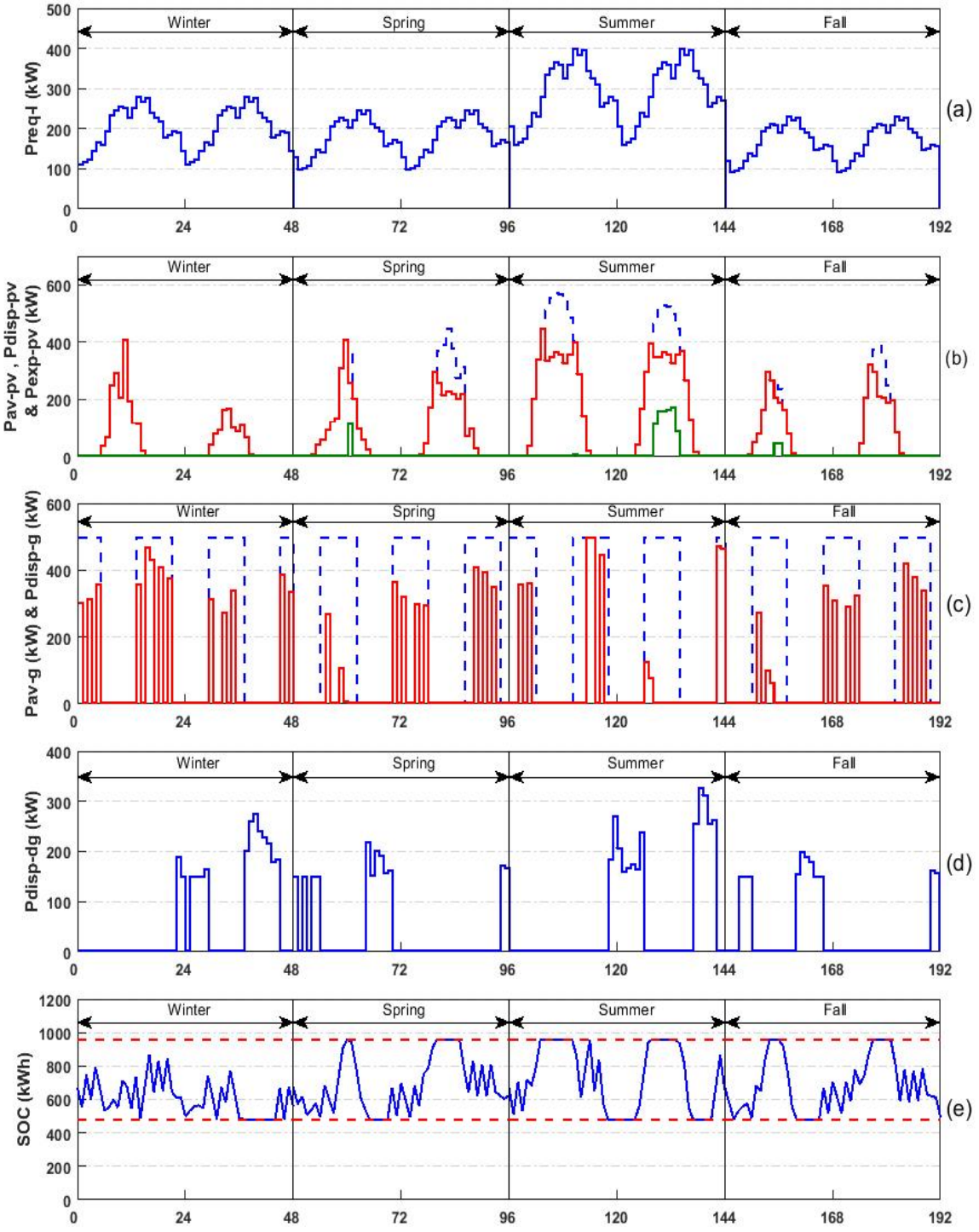

Figure 4.9: Active power dispatch in arbitrary two days for each season for scenario D. (a) Required load active power (solid-blue) and reactive power (solid-red). (b) Available power (dashed-blue), locally dispatched power (solid-red) and exported power (solid-green) from the PV-system. (c) Available power (dashed-blue) and power dispatch (solid-red) from the grid. (d) Total dispatched power from DG_1 (solid-blue) and DG_2 (solid-green). (e) Battery bank SOC (solid-blue) and SOC upper and lower limits (dashed-red).

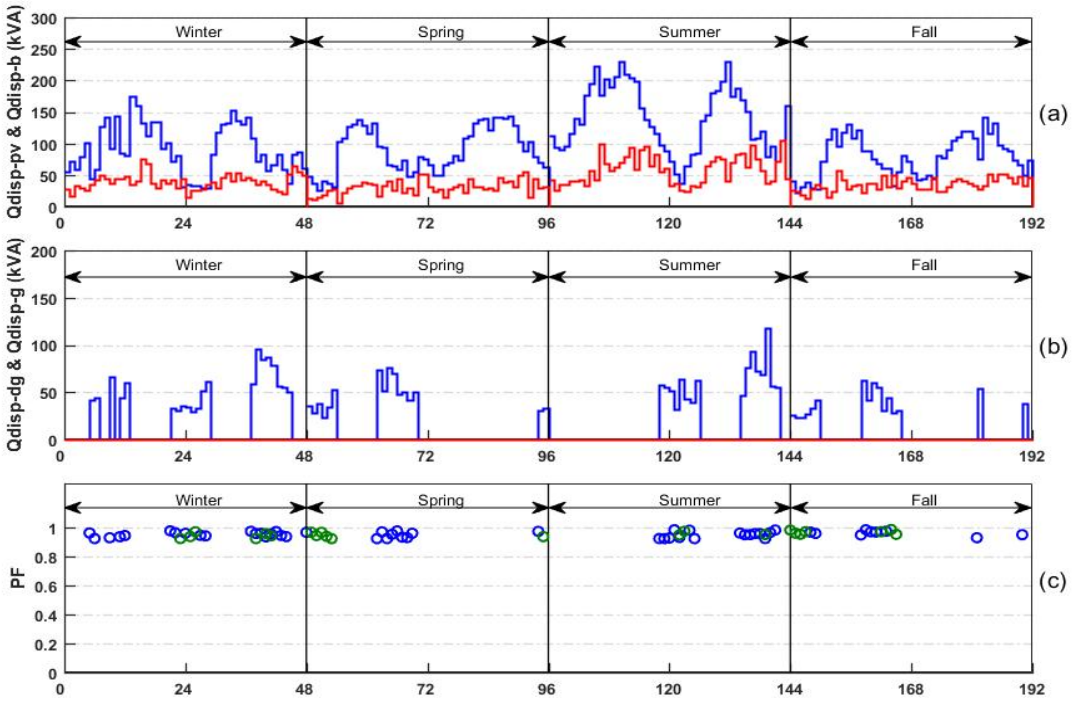

Figure 4.10: Reactive power dispatch in arbitrary two days for each season for scenario A. (a) Dispatched reactive power from the PV-system (solid-blue) and from the battery bank (solid-red). (b) Total dispatched reactive power from DG_1 and DG_2 and the dispatched reactive power from the min grid (solid-red). operating power factor for DG_1 (blue-circle) and for DG_2 (green-circle).

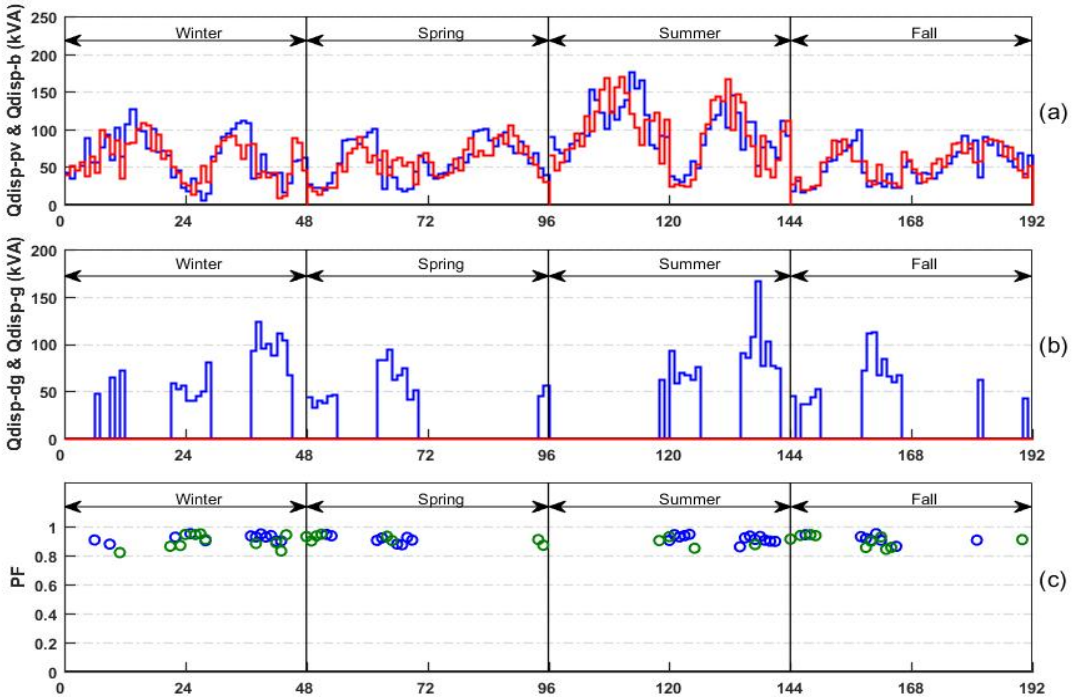

Figure 4.11: Reactive power dispatch in arbitrary two days for each season for scenario B. (a) Dispatched reactive power from the PV-system (solid-blue) and from the battery bank (solid-red). (b) Total dispatched reactive power from DG_1 and DG_2 (solid-blue) and the dispatched reactive power from the min grid (solid-red). operating power factor for DG_1 (blue-circle) and for DG_2 (green-circle).

Table 4.5: Cost of the dispatched active power at scenarios A-C in the industrial MG.

	Scenario A				**Scenario B**				**Scenario C**			
Seasons	$C_{op.dg}(\$)$	$C_{p.g}(\$)$	$C_{b.l}(\$)$	$C_p^T(\$)$	$C_{op.dg}(\$)$	$C_{p.g}(\$)$	$C_{b.l}(\$)$	$C_p^T(\$)$	$C_{op.dg}(\$)$	$C_{p.g}(\$)$	$C_{b.l}(\$)$	$C_p^T(\$)$
Winter	1249.07	723	220.75	2193	1227.43	684.61	446.39	2239.39	1350	646.29	272	2169.56
Spring	814.6	507.25	300.65	1622	782.08	454.33	446.38	1682.8	752.89	448.54	527.89	1739.33
Summer	1105.78	538.88	336.81	1981.48	1011.17	524.92	525.64	2061.73	1107.28	570.66	471.19	2149.12
Fall	853.46	491.27	292.05	1636.79	846.31	455.67	433.01	1735	944.58	395.5	365.66	1705.75

Table 4.6: Cost of the dispatched reactive power at scenarios A-C in the industrial MG.

	Scenario A					**Scenario B**					**Scenario C**				
Seasons	$C_{q.g}(\$)$	$C_q^{BSS}(\$)$	$C_q^{dg}(\$)$	$C_q^{PV}(\$)$	$C_q^T(\$)$	$C_{q.g}(\$)$	$C_q^{BSS}(\$)$	$C_q^{dg}(\$)$	$C_q^{PV}(\$)$	$C_q^T(\$)$	$C_{q.g}(\$)$	$C_q^{BSS}(\$)$	$C_q^{dg}(\$)$	$C_q^{PV}(\$)$	$C_q^T(\$)$
Winter	0	21.05	10.59	4.33	**41.82**	0	24.6	8.38	7.19	**44.8**	51.31	27.22	9.96	5.21	**93.71**
Spring	0	17.64	8.8	2.92	**18**	0	27.04	6.82	4.48	**21.66**	34.41	21.56	9.84	2.67	**68.49**
Summer	0	25.51	8.94	3.71	**18.74**	0	34.71	7.73	6.29	**22.26**	42.87	30.68	6.84	8.95	**42.25**
Fall	0	19.9	10.06	2.07	**30.01**	0	30.25	8.65	5.08	**37.19**	33.48	23.57	10.52	3.62	**37.71**

Table 4.7: Cost of the dispatched energy for scenarios A and D in the industrial MG.

	Scenario A				Scenario D			
Seasons	$C_{op.dg}(\$)$	$C_{p.g}(\$)$	$C_{b.l}(\$)$	$C_p^T(\$)$	$C_{op.dg}(\$)$	$C_{p.g}(\$)$	$C_{b.l}(\$)$	$C_p^T(\$)$
Winter	1249.07	723	220.75	2193	1058.8	702.02	1291.8	3052.5
Spring	814.6	507.25	300.65	1622	813.78	412.41	1137.6	2363.8
Summer	1105.78	538.88	336.81	1981.48	1117.7	408.84	866.80	2393.3
Fall	853.46	491.27	292.05	1636.79	719.79	420.25	1153.1	2293.1

4.5 Conclusions

In this chapter, an AR-OPD approach is introduced to optimize both the active and the reactive power dispatch in a PV-battery-diesel MG under grid blackout condition. In this study, the active-reactive power generation cost and the battery lifetime are taken into account. A detailed model for a PV-battery-diesel MG with both active-reactive power economical and technical constraints are developed. Moreover, a novel model is introduced to calculate the reactive power generation cost from the DG. It is demonstrated by a real case study that considering the battery lifetime cost is necessary to minimize the total operation cost of the MG. Besides, considering the reactive power cost has a high impact on the optimal power flow in the MG. Moreover, it is approved that generating reactive power locally is more cost-effective than importing it from the main grid. Furthermore, the results show that the PV-inverter is able to generate reactive power with very low cost compared with the battery-inverter. Finally, the results show that the proposed operation strategy leads to a significant reduction (up to 31 %) in the total operation cost of the MG in comparison to the conventional rule-based operation strategy.

Chapter 5

Optimal Design of PV-based Microgrids Under Uncertainty

The optimal design of a MG is challenging since multiple components, and complicated operating conditions have to be taken into account. In this chapter, a comprehensive method for the optimal design of both the residential and industrial MGs that were studied in chapter 3 and 4 is proposed to determine the optimal size of the MG components under the considerable uncertainties. The proposed method aims to minimize the levelized cost of energy ($LCOE$), where the limitation of the annual total loss of the power supply ($TLPS$) and the operational constraints are addressed. However, neglecting the uncertainties of the input parameters could lead to an unreliable design for the MG. Therefore, the uncertainties of solar irradiance, ambient temperature, blackouts starting time, and blackouts duration are modeled and considered in the optimization problem. Chance constrained optimization (CCOPT) with Monte-Carlo simulation approaches are utilized to formulate and solve the stochastic optimal design problem. Due to the high capital cost and short lifetime of the battery bank, compared to other components in the MG, especial attention is given in this chapter to estimate the battery bank lifetime accurately. For that, a comprehensive model for the lead-acid battery is utilized to simulate the battery operation and aging, based on the physio-chemical processes of the battery.

5.1 Problem Formulation

Optimal design of a MG means finding the optimal sizes of its components to reach the lowest price for the produced energy from the MG over its lifetime. However,

due to the diversity of energy sources within the MG and the difference in the methods of operating each of them, it is difficult to find a reliable solution to the optimal design problem. Moreover, the existence of integer decision variables in the design problem leads to a mixed-integer nonlinear programming (MINLP) problem. Also, incorporating input parameters uncertainties adds stochastic terms to the optimization problem. Therefore, the optimal design problem of the MG can be, in general, defined as a stochastic MINLP optimization problem.

Since there exist random parameters in the optimization problem, it will be uncertain to satisfy the problem constraints. Chance constrained optimization (CCOPT) methods have been recognized as comparative approaches for solving constrained optimization problems under uncertainty. The CCOPT was introduced in [177] as an efficient solution method for financial planning problems. Due to its effectiveness, it has been used in various fields, such as optimal power flow [178, 179, 180], water management [181], chemical engineering [182], robust control [183], robotics [184] and many others. In CCOPT, the inequality constraints in the stochastic optimization problem will be satisfied with a predefined probability value to ensure a specific level of reliability.

In this study, the proposed optimal design method aims to minimize the $LCOE$, considering the limitation of the annual $TLPS$ taking into account the uncertainty of the input parameters. Therefore, a chance constraint $Pr\{TLPS(\mathbf{x}, \mathbf{u}, \boldsymbol{\zeta}) \leq TLPS_{max}\} \geq \alpha_{rel}$ is used to satisfy the limitation of the $TLPS$ by a predefined probability level α_{rel}. Based on that the optimal design problem of the MG can be, in general, defined as a chance constrained MINLP optimization problem expressed as follows:

$$\begin{aligned} & \min_{\mathbf{u}} E[J(\mathbf{x}, \mathbf{u}, \boldsymbol{\zeta})] \\ s.t. & \\ & \mathbf{u}_{min} \leq \mathbf{u} \leq \mathbf{u}_{max} \\ & Pr\{TLPS(\mathbf{x}, \mathbf{u}, \boldsymbol{\zeta}) \leq TLPS_{max}\} \geq \alpha_{rel} \\ & \boldsymbol{\zeta} \in \Omega. \end{aligned} \tag{5.1}$$

In Eq. (5.1), $E[f(\mathbf{x}, \mathbf{u}, \boldsymbol{\zeta})]$ is the objective function to be minimized which is the expected value of the levelized cost of energy, $\mathbf{x}$ is the vector of the state variables that comprise the dispatched power from the MG components, $\mathbf{u}$ is the vector of the decision variables, $\boldsymbol{\zeta}$ is the vector of random variables (i.e. uncertainty) which includes the solar radiation, ambient temperature, the blackout starting time and the blackouts period as well as $\mathbf{u}_{min/max}$ are the lower/upper limits of the decision variables. The chance constraint is expressed in which $\Pr\{ \bullet \}$ is the probability operator and α_{rel} is the pre-defined probability level. As an example, if $\alpha_{rel} = 0.95$ this means that in the presence of uncertainty $\boldsymbol{\zeta}$ the maximum allowed $TLPS$ constraint is to be satisfied by 95%.

In this study, the decision variables are adjusted before their evaluation to make them compatible with the real sizes of the MG components as follows

$$\mathbf{u}^* = \mathbf{A} \odot \mathbf{u} \tag{5.2}$$

where $\odot$ denotes component-wise multiplication, $\mathbf{A}$ is the vector of adjustment factors , and $\mathbf{u}^*$ is the adjusted decision variables vector (more details will be given in subsection 5.6.1).

5.2 Modeling the Uncertain Parameters

Several studies have been conducted to investigate the effect of the input parameters uncertainty on the MG optimal design problem [86]. However, most of the previous studies take into account the uncertainty of the generated power from the renewable energy sources [92, 91, 89] and the power consumption by the load [90, 95]. Moreover, it was shown in [12] that the power generation from the PV-system depends on the solar irradiance and the ambient temperature; therefore, considering the uncertainty for both is essential for reliable calculation of the generated power from the PV-system [185]. In this chapter, in addition to the uncertainty of the generated power from the PV-system, more importantly, the uncertainty of the grid blackout is taken into account in the optimization problem. Moreover, for appropriate consideration of the load consumption variation, the deviation in the load consumption in workdays and weekends as well as the seasonal variation in the load profiles are

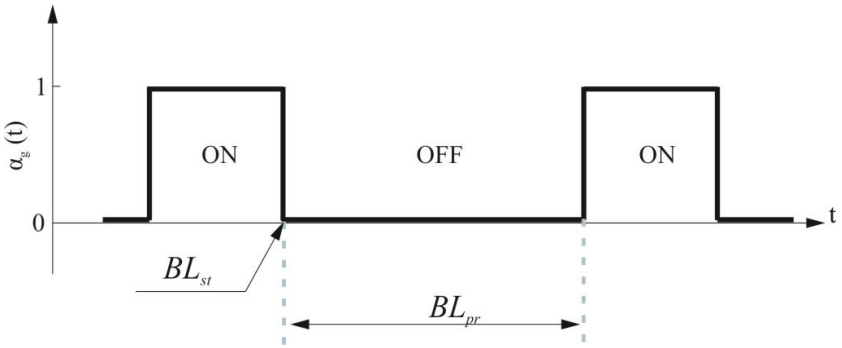

Figure 5.1: Illustration of the grid-tie line status variable α_g.

considered.

To include the input parameters uncertainty in the optimal design problem, a stochastic model has to be built. In general, there are two methods to model the uncertainties of random parameters using probability density function (PDF), namely the parametric and the non-parametric techniques [186]. The parametric PDF involves standard distribution functions, e.g., Gaussian, Beta and Binomial, that are able to describe the stochastic behavior of the data accurately and their parameters can be calculated from the data sets. The non-parametric techniques are used in case the parametric distributions cannot characterize the stochastic behavior of the data accurately.

5.2.1 Blackouts Uncertainty Model

For an accurate stochastic representation of the main grid blackouts, the uncertainty of the blackout starting time Bl_{st} and the blackout period Bl_{pr} are investigated, see Fig. 5.1. The model of the grid-tie line status α_g (which was introduced in section 3.4) is reformulated to include the blackout uncertainty as follows

$$\alpha_g(Bl_{st}, Bl_{pr}) = \begin{cases} 0, & Bl_{st} \leq t \leq Bl_{st} + Bl_{pr} \\ 1, & otherwise, \end{cases} \tag{5.3}$$

where Bl_{st} and Bl_{pr} are stochastic parameters. Different models were utilized to model blackout uncertainties, such as normal probability distribution [187], bell-shaped distribution [188], Poisson distribution [121], and Weibull distribution [113] . However, due to the existence of several reasons that lead to planned or unplanned

blackouts, it is hard to find a general parametric PDF that describes the uncertainty of blackout parameters. Therefore, the method of kernel density estimator (KDE) is used in this study to estimate the uncertainty of Bl_{st} and Bl_{pr}. KDE or Parzen's window is a non-parametric density estimator that can formulate its shape from the data itself [189]. KDE builds for similar data samples their own probability density curve; then these curves are smoothed and combined in one curve that represents the PDF for all samples [190, 191]. As an example, a histogram of random samples is shown in Fig. 5.3(a), to build a PDF representing these samples by KDE, each pin in the histogram is replaced by Gaussian PDF, as shown in Fig. 5.3(b) (orange curves). After that, the Gaussian PDFs are summed together to build the kernel estimate, see Fig. 5.3(b) (blue curve). The general formula of the kernel density estimator f_k for any real values of x is given by [189]

$$f_k(x) = \frac{1}{nh} \sum_{i=1}^{n} K\Big(\frac{x - X_i}{h}\Big), \tag{5.4}$$

where n is the samples number, h denotes the bandwidth that controls the smoothness of the KDE probability density curve, K is a smooth function called the kernel function [189], $X_1, X_2, ..., X_n$ are the random samples. It is noteworthy to mention that the value of the bandwidth parameter is important to shape the KDE. Choosing a high value for the bandwidth leads to a smooth KDE that may hide some characteristics of the distribution. Meanwhile, a small bandwidth value may over-estimate some characteristics of the distribution. In this study, the **ksdensity** function in MATLAB [192] is utilized to generate the PDFs of the blackout starting time and blackout period. In **ksdensity** the optimal value of the bandwidth is calculated based on the method proposed in [190].

The way of calculating the PDFs of the blackout starting time and the blackout period from a historical data is summarized in Fig. 5.4 and explained by the following steps

- Step 1: The status of the grid-tie line was observed and recorded for three months in an area suffering from long periods of daily blackouts [193].

- Step 2: The daily status of the grid-tie line is extracted.

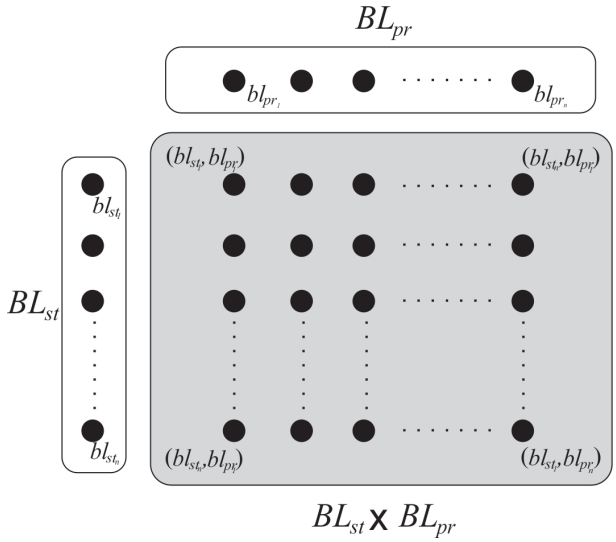

Figure 5.2: Representation of Cartesian product to generate of the combined blackout samples.

- Step 3: The blackout starting time and the blackout period in each day are determined and recorded.

- Step 4: The PDFs of the blackout starting time and the blackout period are calculated using KDE.

In this study, one blackout per day is considered, where the starting time and the period of this blackout are uncertain. Therefore, each daily blackout sample is a pair from the blackout starting time and blackout period (bl_{st}, bl_{pr}). The Cartesian product is used to combine the blackout starting time and the blackout period to generate produce all possible pairs that represent the daily blackouts. The generation of the combined blackout samples (bl_{st}, bl_{pr}) is illustrated in Fig. 5.2.

5.2.2 Solar Irradiance Uncertainty Model

The uncertainty of the solar irradiance has seasonal and diurnal patterns [194]. However, it was shown in [195] that the Beta PDF can describe the solar irradiance uncertainty with sufficient accuracy, which is given by [196, 195]

$$f_{G.x} = \frac{\Gamma(\psi + \varrho)}{\Gamma(\psi)\Gamma(\varrho)} G_x^{(\varrho-1)}(1 - G_x)^{(\psi-1)}, \qquad for \qquad \psi \geq 0, \quad \varrho \geq 0, \tag{5.5}$$

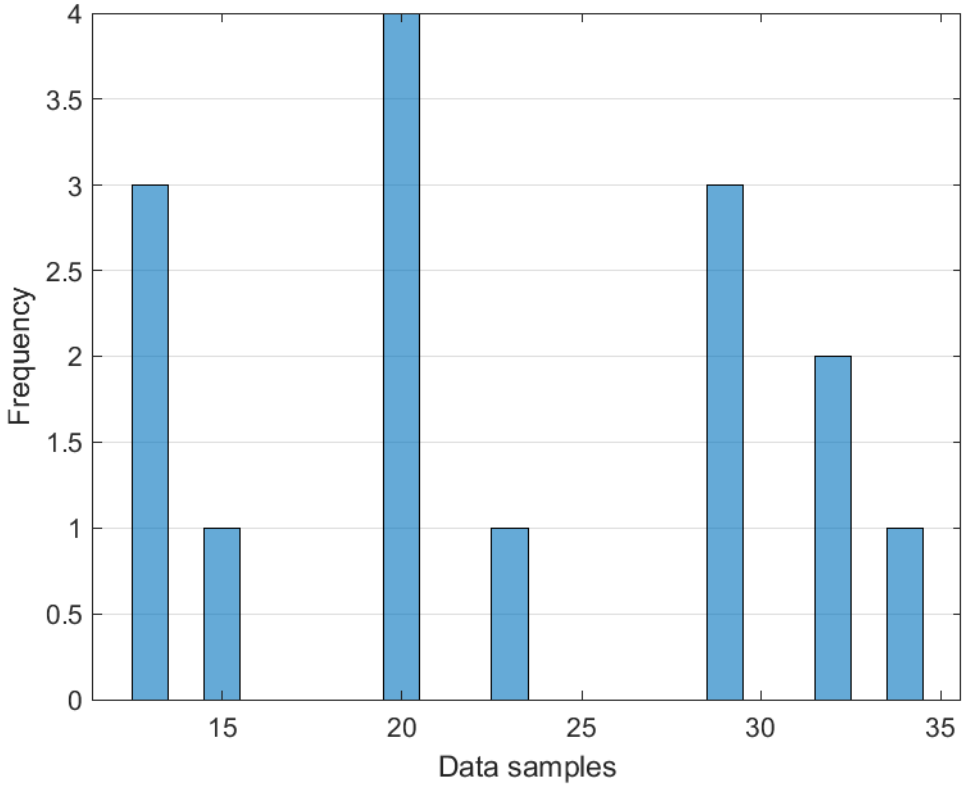

(a)

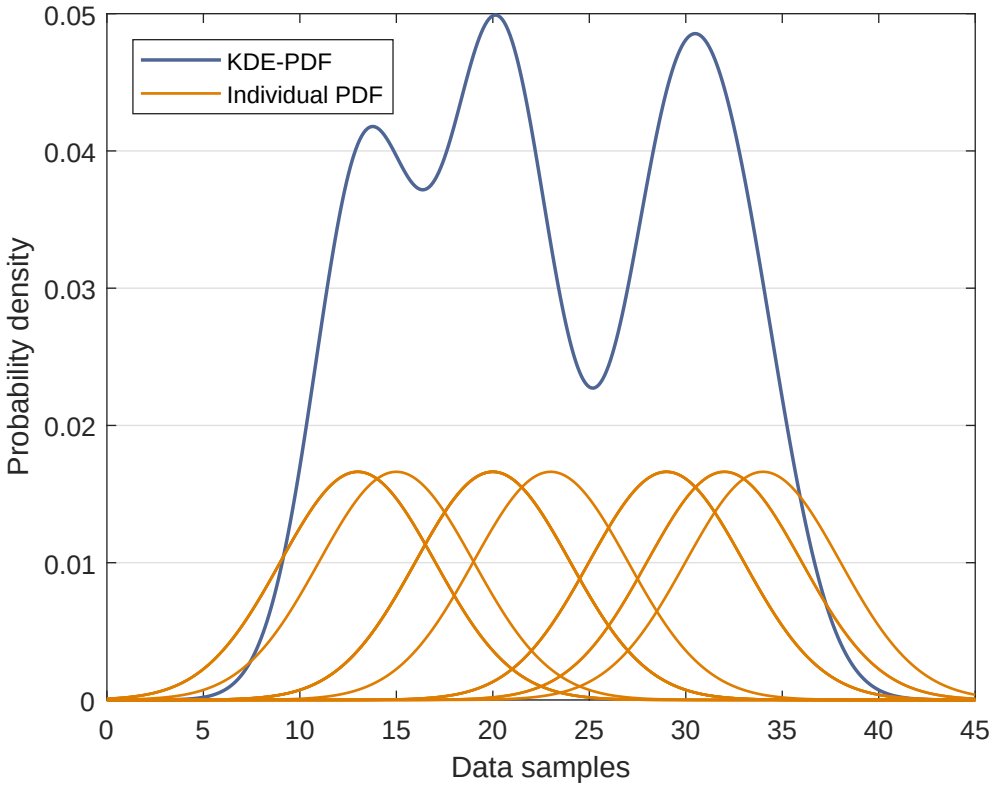

(b)

Figure 5.3: Kernel density estimator illustration. (a) Data representation as a histogram. (b) Individual probability density curve for each data value (orange curves) and the overall kernel distribution (blue curve).

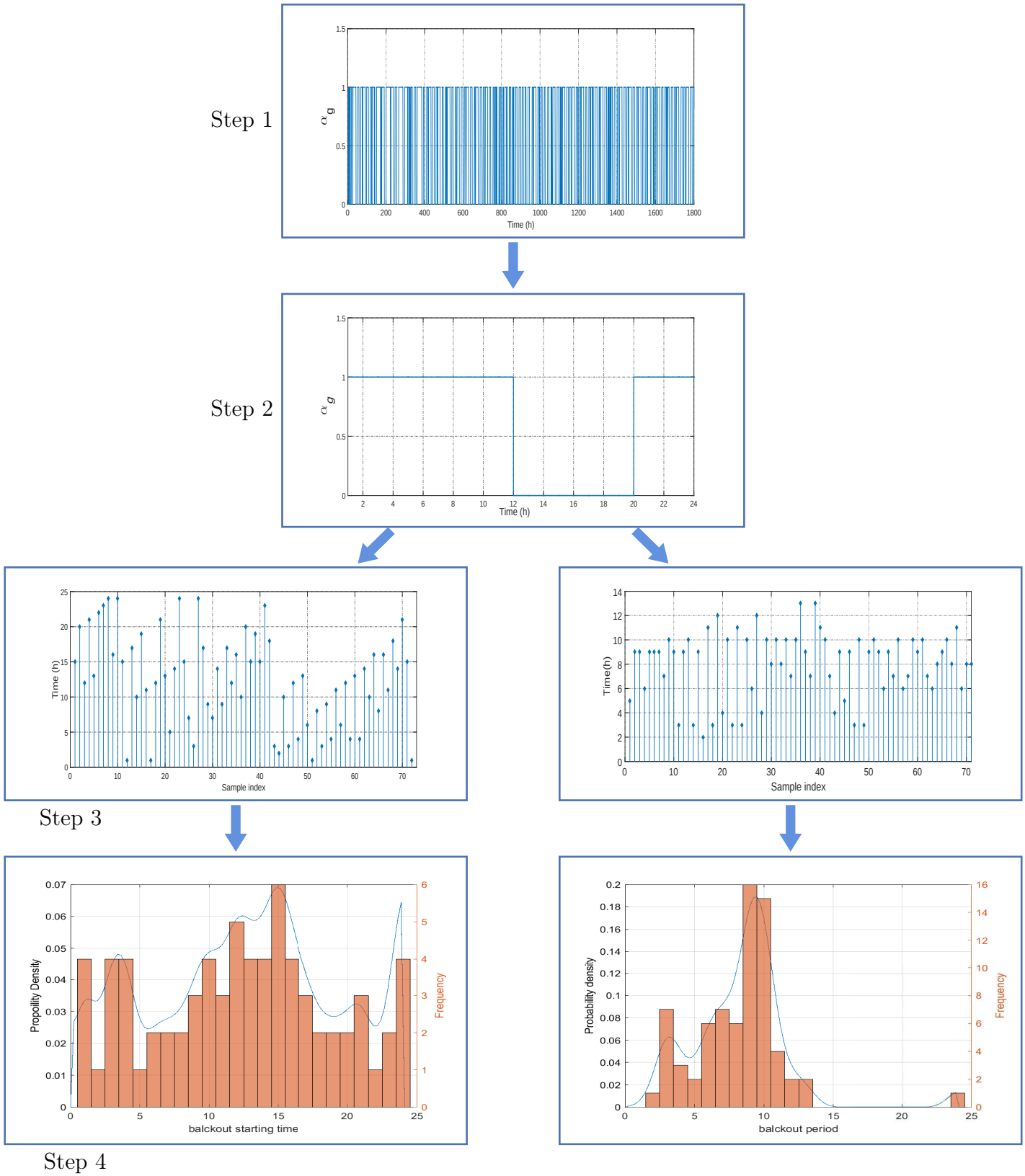

Figure 5.4: Representation of building the PDF of the blackout starting time and blackout period.

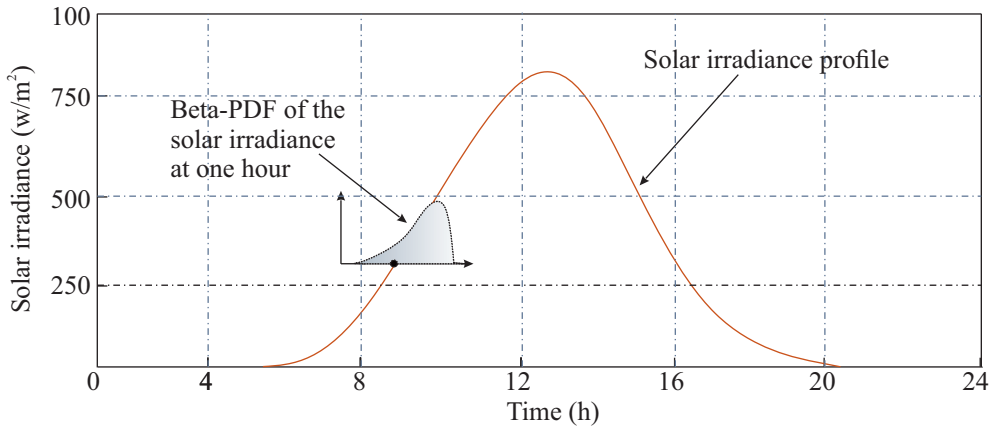

Figure 5.5: Illustration of solar irrdiance in one day.

where G_x is the solar irradiance, $f_{G.x}$ is the PDF of the solar irradiance, and x refers to the solar irradiance type that can be global, direct or diffused. Moreover. ψ and ϱ are the Beta-PDF parameters, which can be calculated from the mean value μ and the standard deviation σ of the historical data as [197]

$$\psi = (1-\mu)\Big(\frac{\mu(1+\mu)}{\sigma^2} - 1\Big), \tag{5.6}$$

$$\varrho = \frac{\psi\mu}{(1-\mu)}. \tag{5.7}$$

For an accurate representation of the solar irradiance uncertainty, a separate Beta-PDF for the solar irradiance at each hour is generated (see Fig. 5.5) considering the seasonal variation. The shown steps in Fig. 5.6 are followed to extract the needed hourly data for building the solar irradiance PDF from a yearly historical data as follows:

- Step 1: The yearly solar irradiance historical data for the PV-system installation site is collected [163].
- Step 2: The solar irradiance data for each season is extracted from the yearly data.
- Step 3: The solar irradiance data for each day is extracted from the seasonal data.
- Step 4: The solar irradiance data for each hour is extracted from the daily data.

- Step 5: The mean value and the standard deviation of the solar irradiance at each hour is calculated to build the Beta-distribution model for the specified hour.

It is to note that the above steps are repeated for the global, direct and diffused solar irradiance.

5.2.3 Ambient Temperature Uncertainty Model

It was reported in [198] that the normal (Gaussian) PDF is the best parametric distribution used to fit the ambient temperature uncertainty, which is given by [199]

$$f_t = \frac{1}{\sigma\sqrt{2\pi}} exp\Big(- \frac{(T_a - \mu_T)^2}{2\sigma_T^2} \Big), \tag{5.8}$$

where f_t is the PDF of the ambient temperature T_a, μ_T is the mean value, and σ_T the standard deviation of the ambient temperature historical data. A separate normal PDF for the ambient temperature at each hour is generated considering its seasonal variation (the same steps for extracting the hourly data that is explained in subsection 5.2.2 are followed to extract the hourly data of the ambient temperature).

5.3 Detailed Model for Lead-Acid Battery

Due to its low cost, high safety, and high recyclability rate, lead-acid battery is the most used electro-chemical energy storage system in various fields [83]. Furthermore, lead-acid battery is still an effective solution for a wide range of applications, such as back-up power supplies and hybrid PV systems, especially in the developing countries [85]. In this section, a comprehensive model that includes the battery current, the battery voltage and the battery state of charge (SOC) performances is applied to describe the battery operation. Moreover, the aging of the lead-acid battery is included considering the impact of SOC, the discharging current, the number of cycles, the acid stratification, and the sulfate-crystal structure on the battery lifetime.

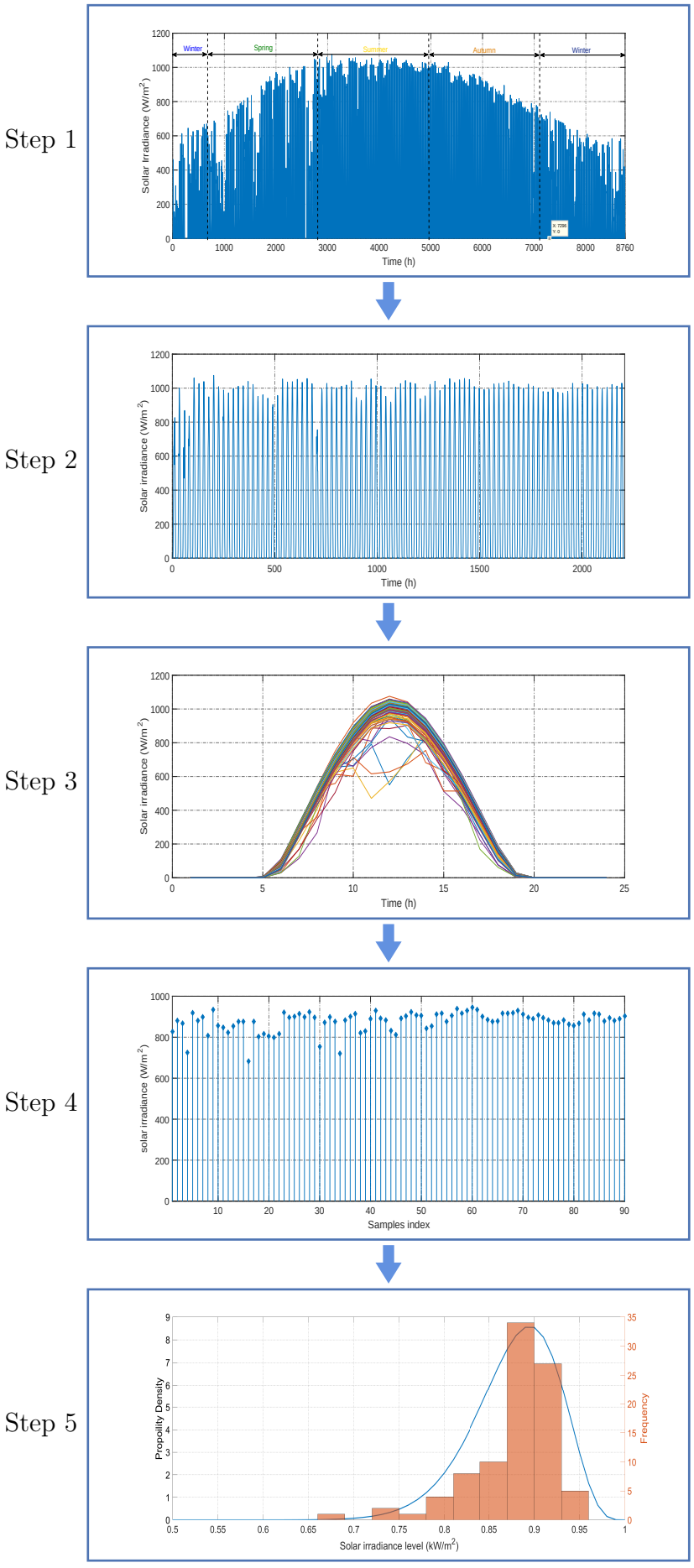

Figure 5.6: Representation of building the PDF of the hourly solar irradiance.

5.3.1 Operational Model of Lead-Acid Battery

In order to estimate the energy storage in a battery, an accurate model is required. Several models have been proposed to simulate the lead-acid battery performance. A basic model, which depends only on the amount of charging and discharging power to predict the SOC for the next time step was widely used [143]. However, this model does not take into account the battery technology characteristics and battery operation condition. Moreover, an equivalent electric circuit model was used to model the transient performance of the battery [200]. However, this model lacks accuracy due to the small number of adjustable parameters in the model. In this thesis, a detailed and accurate model for the lead-acid battery, which was proposed by [201] and adapted by [202] is used. This model takes into consideration the most physio-chemical process in the lead-acid battery [203].

The most relevant physical properties of the battery during its operation are the battery voltage $V_b(t)$ and its SOC [204]. In [202], the $V_b(t)$ and the SOC of each cell in the battery during charging and discharging are described based on the modified Shepherd equation [14] as follows

$$V_b(t) = V_{oc}(t) + I_b(t)R_{cell}(t), \tag{5.9}$$

where

$$V_{oc}(t) = \begin{cases} V_{0,c} - g_c(1 - SOC(t)), & \text{if} \quad I_b(t) > 0 \\ V_{0,d} - g_d(1 - SOC(t), & \text{if} \quad I_b(t) < 0 \end{cases}, \tag{5.10}$$

and

$$R_{cell}(t) = \begin{cases} \frac{\rho_c}{BC_{n.c}} + \frac{\rho_c}{BC_{n.c}} \frac{M_c SOC(t)}{C_c - SOC(t)}, & \text{if} \quad I_b(t) > 0 \\ \frac{\rho_d}{BC_{n.c}} + \frac{\rho_d}{BC_{n.c}} \frac{M_d(1-SOC(t))}{C_d - (1-SOC(t))}, & \text{if} \quad I_b(t) < 0, \end{cases} \tag{5.11}$$

where $V_{oc}(t)$ is the battery-cell open circuit voltage, $I_b(t)$ is the battery current, which is positive during charging and negative during discharging, $V_{0,c/d}$ is the open circuit cell voltage at full charge, $R_{cell}(t)$ is the battery cell internal resistance, and $BC_{n.c}$ is the nominal capacity of the battery cell. Moreover, $M_{c/d}$, $\rho_{c/d}$, and $g_{c/d}$ are lead-acid battery parameters , where their values are taken from [33].

By considering that the battery charging/discharging power $P_{ch/dis}(t)$ is a function

of battery current and voltage $\Big(P_{ch/dis}(t) = V_b(t)I_b(t)\Big)$, $I_b(t)$ can be calculated in terms of power and battery parameters by

$$I_b(t) = \frac{-V_{oc}(t) + \sqrt{V_{oc}^2(t) + 4P_X(t)R_{cell}(t)}}{2R_{cell}(t)}, \tag{5.12}$$

where $P_X(t)$ is positive during charging, and negative during discharging in which the superscript X can be ch/dis.

The battery cell SOC is calculated by considring the cell current [205] as

$$SOC(t) = SOC(t-1) + \frac{1}{BC_{n.c}}(I_{cell}(t) - I_{gas}(t))\Delta t, \tag{5.13}$$

where $I_{cell}(t)$ is the battery cell current, and $I_{gas}(t)$ is the gassing current. Note that, the battery cell current during the charging process depends on the applied charring method. Here, the constant current/constant voltage (CC/CV) method [206] is considered for battery charging. This mothed has two stages. In the first stage, a constant current is applied to charge the battery until the battery reaches the cut-off voltage. In the second stage, the voltage is kept constant while the current is decreased until the battery is fully charged. Based on the CC/CV charging method, the battery cell current can be calculated as follows [202]

$$I_{cell}(t) = \begin{cases} I_b(t) & if \quad V_b(t) \leq V_{b.max} \\ \min(I_b(t), \frac{V_b - V_{oc,c}(t)}{R_{cell,c}(t)}) & else, \end{cases} \tag{5.14}$$

where $V_{b.max}$ is the cut-off voltage, which is specified by the battery manufacturer datasheet. It is worthy to mention that $I_{cell}(t) = I_b(t)$ during discharging.

The gassing current in lead-acid batteries (caused by hydrogen and oxygen gassing inside the battery) depends on the applied voltage and the temperature and can be calculated using the following equation derived from the Tafel approximation [202]

$$I_{gas}(t) = \frac{BC_{n.c}}{100Ah} I_{gas,0}(t) exp(c_u(V_b(t) - V_{gas}) + c_T(T_b(t) - T_{gas}), \tag{5.15}$$

where $I_{gas,0}$, V_{gas}, and T_{gas} are the normalized gassing current, gassing voltage, and gassing temperature, respectively. Morover, c_u and c_T are the voltage and

temperature coefficients, respectively, while $T_b(t)$ is the battery temperature. Note that, $I_{gas,0}$ is the only parameter in Eq. (5.15) that changes during the battery's operation, while all other parameters can be assumed to be constant under normal operating conditions. Therefore, $I_{gas,0}(t)$ is given by

$$I_{gas,0}(t) = I_{gas,c} + I_{gas,r}\frac{\rho_{corr}(t)}{\rho_{corr.max}(t)}, \tag{5.16}$$

where $I_{gas,c}$ is the gassing current initial value, $I_{gas,r}$ is a gassing current parameter, $\rho_{corr.max}(t)$ is the maximum resistance of the corrosion, and $\rho_{corr}(t)$ is the corrosion layer resistance, which will be explained in the subsection 5.3.2. It is to note that $SOC(t)$ should be kept between the upper and lower bounds, i.e.,

$$SOC_{min} \leq SOC(t) \leq SOC_{max} \tag{5.17}$$

where $SOC_{min} = 1 - DOD$ and SOC_{max} is the normalized battery capacity.

5.3.2 Aging Model of Lead-Acid Battery

Estimating the battery lifetime is an essential issue in the energy system planning and operation. Therefore, many approaches have been worked out in the literature to estimate the battery lifetime [207]. The weighted Ah battery aging model that was introduced in chapter 3 is extended in this chapter to include the impact of the SOC, the discharge current and the acid stratification. The work in [205] proposed a detailed weighted Ah throughput model for lifetime estimation of a lead-acid battery based on the real operating conditions of the battery [208]. This model is used in this study to estimate the battery lifetime by considering the main effects that decrease the battery capacity. The corrosion of the positive electrode and the degradation of the active mass in the battery are the two critical aging mechanisms which were investigated in [205].

Corrosion has a direct effect on the battery cell resistance by adding a new corrosion coating with weaker conductivity, which increases the total internal resistance of the battery cell and decreases the conductivity between the battery grid and the active material. Meanwhile, battery degradation causes capacity loss due to changes in

the mechanical structure of the electrode. This leads to a decrease in the porosity of the electrode and reduces the surface area of the electro-chemical reaction [150]. Based on the above explanation, the remaining (rest) capacity of the battery $C_{rem.b}(t)$ is modeled by

$$C_{rem.b}(t) = C_{dis.0} - C_{corr}(t) - C_{deg}(t), \tag{5.18}$$

where $C_{dis.0}$ is the normalized discharge capacity of the battery, $C_{corr}(t)$ and $C_{deg}(t)$ are the battery capacity decrement due to corrosion and due to degradation, respectively. It is noteworthy to mention that the battery should be replaced when its remaining capacity is 80% of its nominal capacity [205]. The effect of battery corrosion and degradation is explained below in details.

Corrosion It happens when the lead of the positive electrode is converted to lead oxide, which has a lower conductivity. Moreover, the newly formed material has a lower density and a higher specific volume that increase the mechanical stress inside the battery. As a result, the contact between the active material and the positive electrode is decreased. Note that, the growth in the corrosion layer thickness $\Delta W(t)$ is correlated to the corrosion voltage $V_{corr}(t)$ [205] by

$$\Delta W(t) = K_s(t)\left(\frac{\Delta W(t-\Delta t)}{K_s(t)}\right)^{1/0.6} + \Delta t, \quad V_{corr} < 1.74 \tag{5.19}$$

$$\Delta W(t) = \Delta W(t-\Delta t) + K_s(t)\Delta t, \quad V_{corr} \geq 1.74, \tag{5.20}$$

where $V_{corr}(t)$ is the voltage of the positive electrode of the battery, which is given by

$$V_{corr}(t) = \begin{cases} V_{corr,0} - \frac{10}{13} g_c DOD(t) + I_b(t)\frac{\rho_c(t)}{2BC_{n.c}}\left(1 + M_c\frac{SOC(t)}{C_c - SOC(t)}\right), if \\ \qquad\qquad\qquad\qquad\qquad\qquad\qquad\qquad I_b(t) \geq 0, \\ V_{corr,0} - \frac{10}{13} g_d DOD(t) + I_b(t)\frac{\rho_d(t)}{2BC_{n.c}}\left(1 + M_d\frac{DOD(t)}{C_c - DOD(t)}\right), if \\ \qquad\qquad\qquad\qquad\qquad\qquad\qquad\qquad I_b(t) \leq 0, \end{cases} \tag{5.21}$$

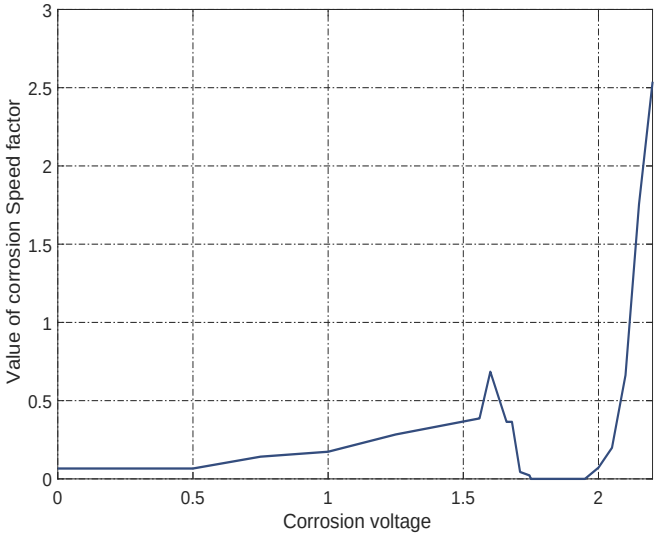

Figure 5.7: The relation between the corrosion speed factor and the corrosion voltage [202].

and $V_{corr,0}$ is the corrosion voltage of a fully charged battery without current flow. Moreover, $K_s(t)$ is the corrosion speed variable given by

$$K_s(t) = K_{s,f}(t)exp(K_{s,T}(T_b(t) - T_{corr})), \tag{5.22}$$

where $K_{s,T}$ is the temperature factor calculated by $K_{s,T} = \frac{ln(2)}{15}$, T_{corr} is the corrosion refrence temperature (T_{corr} = 298 [205]), $k_{s,f}(t)$ is the corrosion speed factor illustrated in Fig. 5.7. Based on the above calculation, the corrosion layer resistance $\rho_{corr}(t)$ and the capacity loss due to corrosion $C_{corr}(t)$ can be calculated as

$$\rho_{corr}(t) = \rho_{corr,max}\frac{\Delta W(t)}{\Delta W_{max}}, \tag{5.23}$$

$$C_{corr}(t) = C_{corr,max}\frac{\Delta W(t)}{\Delta W_{max}}, \tag{5.24}$$

where the parameters $\rho_{corr,max}$ and ΔW_{max} are the maximum resistance and thickness of the corrosion layer , respectively, when the battery cell reaches its maximum lifetime [205].

Degradation It describes the battery capacity loss due to the battery cycling. The nominal number of cycles is provided in the battery data-sheet, which is determined under the standard operating condition. However, the battery capacity deterioration

is affected by the real operating SOC and the discharging current values. Therefore, the weighted cycles number $Z_W(t)$ is used instead of its nominal value in calculating the degradation of the battery capacity $C_{deg}(t)$ [205] by

$$C_{deg}(t) = C_{deg,max} exp\left(- c_Z \left(1 - \frac{Z_W(t)}{1.6 Z_0} \right) \right), \tag{5.25}$$

where $C_{deg,max}$ is the maximum value of the battery capacity degradation, Z_0 is the nominal battery cycles number given in the data-sheet, and c_Z is a parameter (equal to 5.0 [205]). The weighted number of cycles is calculated by considering the discharging current, SOC, and acid stratification effects as

$$Z_W(t) = \frac{1}{BC_{n.c}} \int_0^t |I_d(\tau)| f_{SOC}(\tau) f_{acid}(\tau) d\tau \tag{5.26}$$

where $I_d(\tau)$ is the battery discharging current, f_{acid} is a factor that represents the effect of acid stratification, and f_{SOC} is a factor that includes the effect of SOC. It can be noticed from Eq. (5.26) that the Ah throughput ($= \int_0^t |I_d(\tau)|$) is not only integrated; but, it weighted by the factors that include the effects of the SOC and the acid stratification, which occurs due to the actual operating conditions of the battery. Here, the f_{SOC} is given by

$$f_{SOC}(t) = 1 + (c_{SOC,0} + c_{SOC_{min}} (1 - SOC_{min}(t)|_{t_0}^t) f_I(t)(t - t_0), \tag{5.27}$$

where c_{SOC_0} and $c_{SOC_{min}}$ are parameters taken from [205]. $(SOC_{min}(t))|_{t_0}^t$ is the lowest state of charge since the last full charge at time t_0. From Eq. (5.27), it can be noticed that the lower the SOC and the longer the battery remains at low SOC, the more the SOC impact increases. $f_I(t)$ is the current factor representing the effect of the discharged battery current, which is given by

$$f_I(t) = \sqrt{\frac{I_{ref}}{I_d(t)}} \sqrt[3]{\exp\left(\frac{n_{b.ch}(t)}{3.6}\right)}. \tag{5.28}$$

where I_{ref} is the discharge current at C_{10} (the current that the battery can discharge it continuously for 10 hours). From the first term in Eq. (5.28), it can be noticed that for lower discharge current, the impact of the current factor is increased. This was experimentally demonstrated in [209] that at a low discharge current, larger sulfate crystals are created, which are hard to be dissolved during the next charging process. Therefore, the crystals number increases at each cycle and remains at the negative electrode of the battery, which decreases its conductivity. The second term in Eq. (5.28) represents the influence of the number of ineffective charging processes $n_{b.ch}$, which is given by

$$n_{b.ch}(t) = \begin{cases} n_{b.ch}(t-1) + \frac{0.0025-(SOC_{ref}-SOC_{max.n})^2}{0.0025}, & \text{if} \quad SOC_{limit} \leq SOC(t) \leq 0.9999, \\ n_{b.ch}(t-1), & \text{else.} \end{cases} \tag{5.29}$$

where $SOC_{max.n}$ is the maximum SOC since the time that the SOC had reached its SOC_{ref}, where $SOC_{ref} = 0.95$ [205].

Acid stratification is caused by the inhomogeneous acid concentrations in the electrolyte that develops large sulphate crystals and strong aging effect [210]. The influence of acid stratification $f_{acid}(t)$ is calculated by [205]

$$f_{acid}(t) = 1 + f_{strat}\sqrt{\frac{I_{ref}}{|I_b(t)|}}, \tag{5.30}$$

where the degree of acid stratification $f_{strat}(t)$ is modeled by

$$f_{strat}(t) = f_{strat}(t-1) + f_{+}(t) - f_{-}(t), \tag{5.31}$$

here $f_{+}(t)$ and $f_{-}(t)$ represent the increment and decrement in the acid stratification, respectively. The $f_{+}(t)$ happens due to cyclic operation and is given by

$$f_{+}(t) = c_{plus}(1 - SOC_{min}(t)|_{t_0}^{t})exp(-3f_{strat}(t-1))\frac{|I_d(t)|}{I_{ref}}, \tag{5.32}$$

where c_{plus} is a factor for the increment of the acid stratification. Meanwhile, the acid stratification decreases by gassing at the battery cell voltage higher than 2.3

V. According to [205], the decrement in acid stratification $f_{-}(t)$ is given by

$$f_{-}(t) = c_{minus}\sqrt{\frac{100}{BC_{n.c}}}\frac{I_{gas}(t)}{I_{gas,0}}exp(c_u(V_{b.cell} - V_{ref}) + c_T(T_b(t) - T_{gas})) + \frac{8D}{z^2}f_{strat}(t-1)2^{(T_b(t)-20^oC)/10k}, \quad (5.33)$$

where c_{minus} is a factor for the decrement of the acid stratification, $V_{b.cell}$ is the battery cell voltage, and V_{ref} is the reference voltage, which equals to 2.5 V.

5.4 Optimization Problem Formulation

The main objective of this study is to find the optimal design for the MG to be able to provide a cost-effective and reliable power supply to the load in the long run. The objective function and the constraints of the optimization problem are formulated and explained in the following subsections.

5.4.1 Objective Function

The levelized Cost of Energy ($LCOE$) is the standard criterion for evaluating energy systems investments [211]. In $LCOE$, the costs of acquiring, owning, operating and maintaining the energy system over its lifetime are included [212]. Therefore, the objective function to be minimized in this context is defined as

$$\min_{\mathbf{u}} LCOE \quad (5.34)$$

where $\mathbf{u} = [N_{pv.m}, PV_{inv.size}, N_{batt}, DOD, N_{dg}, P_{r.dg_i}]$ is the decision variables vector. In $\mathbf{u}$, $N_{pv.m}$ is the number of PV-modules, $PV_{inv.size}$ is the size of the PV-inverter, N_{batt} is the number of batteries, N_{dg} is the number of DGs, and $P_{r.dg_i}$ is the DG rated power where $i \in 1, 2, ..., N_{dg}$.

The $LCOE$ is calculated by dividing the total annual cost of the dispatched power ($TAPC$) by the total annual dispatched power from the MG $P_{disp.t}$ [212],

which can be expressed as

$$\text{LCOE} = \frac{TAPC}{\sum_{t=1}^{T_{max}} P_{disp.t}}, \tag{5.35}$$

where

$$TAPC = ACC + AMOC + ARC, \tag{5.36}$$

and T_{max} is equal to 8760 (i.e. the total number of hours in one year), ACC is the annualized capital cost, $AMOC$ is the annualized maintenance and operation cost, and ARC is the annualized replacement cost.

Annualized Capital Cost It is the capital cost of the MG distributed over its lifetime. To consider this issue, the capital recovery factor (CRF) is used to share the total capital cost (TCC) of the MG over its lifetime considering the interest rate as

$$ACC = TCC \times CRF, \tag{5.37}$$

where

$$CRF = \frac{r_i(1+r_i)^{lt_{mg}}}{(1+r_i)^{lt_{mg}} - 1}, \tag{5.38}$$

and lt_{mg} is the total lifetime of the MG, and r_i is the real interest rate, which takes into account the inflation rate by

$$r_i = \frac{r_i^{'} - r_f}{1 + r_f}, \tag{5.39}$$

where $r_i^{'}$ and r_f are the nominal interest rate and the inflation rate, respectively. It is to note that the total capital cost TCC includes the cost of all components of the MG, i.e.,

$$TCC = CC_{pv} + CC_{b.b} + \sum_{i=1}^{N_{dg}} CC_{dg_i} + CC_{pv.inv} + CC_{b.inv}, \tag{5.40}$$

where CC_{pv}, and $CC_{b.b}$ are the PV-array and the battery bank capital cost, respectively, CC_{dg_i} is the i^{th} DG capital cost, $CC_{pv.inv}$, and $CC_{b.inv}$ are the PV-inverter and the battery-inverter capital cost, respectively.

However, installing the PV-panels and the battery bank requires many accessories that have to be added for fixing, protection, and electrical connections. The cost of these accessories can be included by adding the balance of system cost (BOS) as [14]

$$CC_{pv} = N_{pv.m} CC_{pv.m}(1 + BOS_{pv}), \tag{5.41}$$

and

$$CC_{b.b} = N_{batt} CC_{batt}(1 + BOS_{batt}), \tag{5.42}$$

where $N_{pv.m}$ is the total number of PV-modules in the PV-array and N_{batt} is the battery number in the battery bank. $CC_{pv.m}$ and CC_{batt} are the cost of a PV-module and the cost of a single battery, respectively.

Annualized Maintenance and Operation Costs The maintenance cost could be variable or fixed. The fixed cost comes from the scheduled maintenance actions that should be run based on the manufacturer recommendations. Meanwhile, the variable maintenance cost comes from the sudden disruptions during the operation. Because of the difficulty of predicting the variable maintenance cost, only the fixed cost is considered here. Besides, the amount of the dispatched power from each power source is considered in the operation cost calculation. The annual maintenance and operation cost is given by

$$AMOC = C_{m.pv} + C_{m.b} + C_g + C_{m.dg} + C_{a.op.dg}, \tag{5.43}$$

where $C_{m.pv}$ and $C_{m.b}$ are the annual maintenance cost of the PV-array and the battery bank, respectively, C_g is the annual cost of the dispatched energy from the grid tie-line, $C_{m.dg}$ and $C_{a.op.dg}$ are the total annual maintenance and operation costs of the diesel generator set, respectively.

The cost of the dispatched power from the grid is given by

$$C_g = C_{e.g} \sum_{t=1}^{T_{max}} P_{disp.g}(t), \tag{5.44}$$

where $C_{e.g}$ is the cost of each kWh dispatched from the grid, $P_{disp.g}(t)$ is the total dispatched power from the grid at time t. The operation costs of the diesel generator set include the fuel consumption cost as well as the startup and shutdown costs. $C_{a.op.dg}$ is formulated as

$$C_{a.op.dg}(t) = \sum_{t=1}^{T_{max}} \sum_{i=1}^{N_{dg}} (C_f f_{con.dg_i}(t) + C_{up} \xi_{up.dg_i}(t) + C_d \xi_{d.dg_i}(t))), \tag{5.45}$$

where C_f is the fuel cost in $\$/l$, $f_{con.dg_i}(t)$ is the diesel engine fuel consumption, C_{up} and C_d are the startup and shutdown costs, respectively. $\xi_{up.dg_i}(t)$ and $\xi_{d.dg_i}(t)$ are auxiliary binary variables that represent the changes at each diesel generator status (further details can be found in subsection 4.2.2). The fuel consumption function is approximated by a linear function [213] that can be expressed as

$$f_{con.dg_i}(t) = A_{dg} P_{disp.dg_i}(t) + B_{dg} P_{r.dg_i}, \tag{5.46}$$

where A_{dg} is a constant with the value of 0.246 l/kWh and B_{dg} is a constant with the value of 0.08415 l/kW.

Annualized Replacement Cost Some components in the MG have to be replaced once or multiple times through the MG lifetime, namely the battery bank, the battery inverter, the PV-inverter, and the DG. To calculate the replacement cost of each component, three steps are followed. Firstly, the lifetime of each component is separately estimated, then the present worth value (PWV) is used to convert the cost of the component at the replacement time to its present value, and the final step is distributing the estimated cost over the MG lifetime using the CRF. Therefore, the annualized replacement cost is defined as follows

$$ARC = CRF \times Comp_{size} \times PWV(N_{rep.x}, lt_x), \tag{5.47}$$

where $Comp_{size}$ is the component size, $N_{rep.x}$ is the number of replacement of the component during the MG lifetime, and lt_x is the estimated lifetime of it. The superscript x can be the battery bank, the diesel generator, the PV-inverter, or the

battery-inverter. Moreover, the PWV is given by [14]

$$PWV = \sum_{R=1}^{N_{rep.x}} Comp_{cost} \frac{1}{(1+i)^{R \times lt_x}}, \tag{5.48}$$

where

$$N_{rep.x} = \left\lceil \frac{lt_{mg}}{lt_x} \right\rceil - 1. \tag{5.49}$$

The battery lifetime is explained in details in subsection 5.3.2. The lifetime of the PV/battery-inverter is assumed to be fixed and equals 10 years. The diesel generator lifetime is defined by the maximum number of hours that can be operated, which is given by the manufacturer. Therefore, the lifetime of the DG is defined by

$$lt_{dg} = \frac{h_{dg.lt}}{h_{op.dg}}, \tag{5.50}$$

where $h_{dg.lt}$ is the maximum number of operation hours of the DG before reaching the end of its life and $h_{op.dg}$ is the total operation hours of the DG during one year.

5.4.2 Constraints

Finding the optimal solution of the MG design problem must be done while satisfying the financial and physical constraints of the problem as well as the required reliability level. Therefore, the following inequalities are added to the optimization problem:

$$0 \leq N_{pv.m} \leq N_{pv.m}^{max} \tag{5.51a}$$

$$0 \leq PV_{inv.size} \leq PV_{inv.size}^{max} \tag{5.51b}$$

$$0 \leq N_{batt} \leq N_{batt.max} \tag{5.51c}$$

$$0 \leq DOD \leq DOD_{max} \tag{5.51d}$$

$$0 \leq N_{dg} \leq N_{dg.max} \tag{5.51e}$$

$$0 \leq P_{r.dg_i} \leq P_{r.dg_i}^{max} \quad \forall i = 1, ..., N_{dg} \tag{5.51f}$$

$$0 \leq TCC \leq TCC_{max}. \tag{5.51g}$$

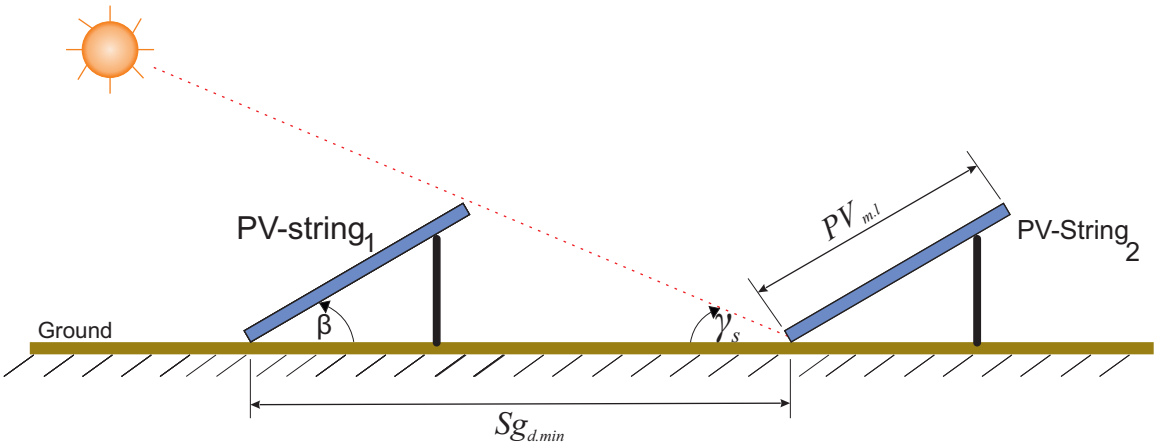

Figure 5.8: Illustration of a PV-array installation.

It is to note that the maximum number of the PV-modules $N_{pv.m}^{max}$ depends on the area of installation ($A_{pv.inst}$) for the PV-array. Consequently, the maximum numbers of the PV-modules can be calculated as follows [214]

$$N_{pv.m}^{max} = N_{sg} \times N_{m.sg}, \tag{5.52}$$

where

$$N_{sg} = \left\lfloor \frac{L_{inst}}{SG_{d.min}} \right\rfloor + 1, \tag{5.53a}$$

$$N_{m.sg} = \left\lfloor \frac{W_{inst}}{W_{pv.m}}, \right\rfloor \tag{5.53b}$$

where N_{sg} is number of the PV-strings, $N_{m.sg}$ is the maximum number of PV-modules per string, L_{inst} is the length of installation area, W_{inst} is the width of installation area, and $W_{pv.m}$ is the width of the PV-module. Moreover, $SG_{d.min}$ is the minimum distance between the PV-strings (see Fig. 5.8), which is very important to prevent the self-shading between the PV-strings and is given by [215]

$$SG_{d.min} = PV_{m.l} \times \frac{sin(\gamma_s + \beta)}{sin(\gamma_s)}, \tag{5.54}$$

where $PV_{m.l}$ is the module length (see Fig. 5.8) and γ_s is the angle of the sun. A role of thumb to calculate γ_s is that at noon on December 21 in the northern hemisphere must be no shading on the PV-strings [215].

In addition to the constraints stated in Eqs. (5.51a) - (5.51g), the following constraint is used to guarantee an acceptable annual loss of power supply $TLPS_{max}$ percentage during the MG operation

$$TLPS(\mathbf{x}, \mathbf{u}, \boldsymbol{\zeta}) \leq TLPS_{max} \tag{5.55}$$

where $TLPS$ is the annual total loss of power supply that happens when the available power from the MG is not enough to cover the load. Accordingly, the $TLPS$ is calculated by [70]

$$\text{TLPS} = \frac{\sum_{t=1}^{T_{max}} L_p(t)}{T_{max}} \times 100, \tag{5.56}$$

where T_{max} equals to 8760 hours and $L_p(t)$ is a binary variable, i.e., $L_p(t) = 1$ when the available power from the MG is lower than the required load, else $L_p(t) = 0$. Since the $TLPS$ value is affected by the uncertainty of the considered stochastic parameters, it will be uncertain to satisfy Eq. (5.55). Therefore, this constraint is formulated as a chance constraint

$$Pr\{TLPS(\mathbf{x}, \mathbf{u}, \boldsymbol{\zeta}) \leq TLPS_{max}\} \geq \alpha_{rel}. \tag{5.57}$$

Based on Eq. (5.57), the restriction of the $TLPS$ will be satisfied with a predefined probability level α_{rel}.

5.5 Solution Method

It was mentioned in section 5.1 that the stochastic optimal design problem is formulated as CCOPT to handle the uncertainties of the input parameters. There are two main approaches to solve CCOPT, namely, the analytic approximation and the numerical approximation approaches [216]. In both methods the chance constraints are converted into equivalent deterministic constraints. However, the analytic approximation methods use parameterized functions to represent the CCOPT problems as deterministic optimization problems. A state of the art analytic approximation approach consisting of an inner and an outer analytic approximation of chance constraints was proposed [217]. In this approach, the CCOPT is approximated by two parametric nonlinear programming (NLP) problems, which can readily be solved

by an NLP solver. On the other hand, in the numerical approximation methods, a set of samples for the random variables is used to compute the chance constraints by deterministic ones approximately [65]. Subsequently, the deterministic nonlinear optimization problem is solved to obtain an approximate solution to the CCOPT [218].

In this study, the formulated optimization problem is a stochastic MINLP problem, which cannot be solved using the available analytic approximation methods. Therefore, a numerical approximation method is utilized to convert the CCOPT to a deterministic mixed-integer nonlinear optimization problem. As a result, simulation-based optimization is used to give an approximate solution of the optimization problem.

5.5.1 Simulation-Based Optimization

Simulation-based optimization is commonly used to determine the optimal design parameters of the MG [65]. In this method, the model is used to evaluate and verify the effect of the design parameters given by the optimizer [66]. This iteratively continues until the iterates converge to the optimal solution. Applying this method to solve the problem of optimal design of a MG considering the battery lifetime requires the computation of the battery life at each iteration to calculate the replacement cost of the battery bank accurately (by utilizing the developed battery aging model in subsection 5.3.2).

Solving the deterministic optimal design problem of MGs by a simulation-based optimization method is summarized by the given flowchart in Fig. 5.9. At each iteration, the proposed decision variables by the optimizer are evaluated using the MG model. At first, the $TLPS$ of the design parameter is evaluated, if $TLPS \leq TLPS_{max}$ is satisfied, the objective function will be calculated. Otherwise, the given solution by the optimizer is considered unfeasible and the optimizer will give new design parameters. To calculate the value of the objective function, the annualized maintenance, and operation costs are calculated by hourly simulating the system model. Then, the simulation continues until the battery's remaining capacity reached 80 % of its nominal value to calculate the battery life. Finally, the $LCOE$ is calculated and

evaluated by the optimizer.

It is worthwhile to mention that the heuristic-based iterative optimization methods are widely utilized to solve such a simulation-based optimization problem [219]. In this study, the genetic algorithm (GA) is used to find the optimal design parameters because of its ability to solve complex optimization problems irrespective of the model of the system [160]. In GA, a population of candidate solutions is evolved toward better solutions by applying mutation, crossover and selection processes [159]. Meanwhile, the MG model is used to evaluate these solutions. However, it is noticed that some of the candidate solutions are evaluated multiple times through the optimization process, which increases the total solution time of the optimization problem. Therefore, the standard GA algorithm in MATLAB is modified by adding a temporary memory to store all the given solutions by the optimizer and the values of $LCOE$ and $TLPS$ related to them. In this way, each given solution by the optimizer is tested before it is evaluated by the MG model. If the solution already evaluated, the stored $LCOE$ and $TLPS$ values are called back directly without running the MG model.

5.5.2 Stochastic Simulation-Based Optimization

The solution of the CCOPT problem by a numerical approximation method requires the calculation of the probability of the chance constraint and the expected value of the objective function by a set of samples extracted from the PDFs of the uncertain parameters [65]. For this, Monte-Carlo Simulation (MCS) is used to evaluate the effect of the extracted samples using the MG model. MCS is a technique for estimating the value of an unknown quantity by running the simulation multiple times using random samples from the PDF of each uncertain parameter and analyzing the results [220] to obtain one representative value. Solving the CCOPT problem by a simulation-based optimization method is summarized by the given flowchart in Fig. 5.10. For each given solution by the optimizer, the battery lifetime is calculated using the mean values of the uncertain input parameters utilizing the explained battery aging model in subsection 5.3.2. Then, the MCS is used to calculate the $TLPS$ and $LCOE$ values for each extracted sample from the PDF of the uncertain

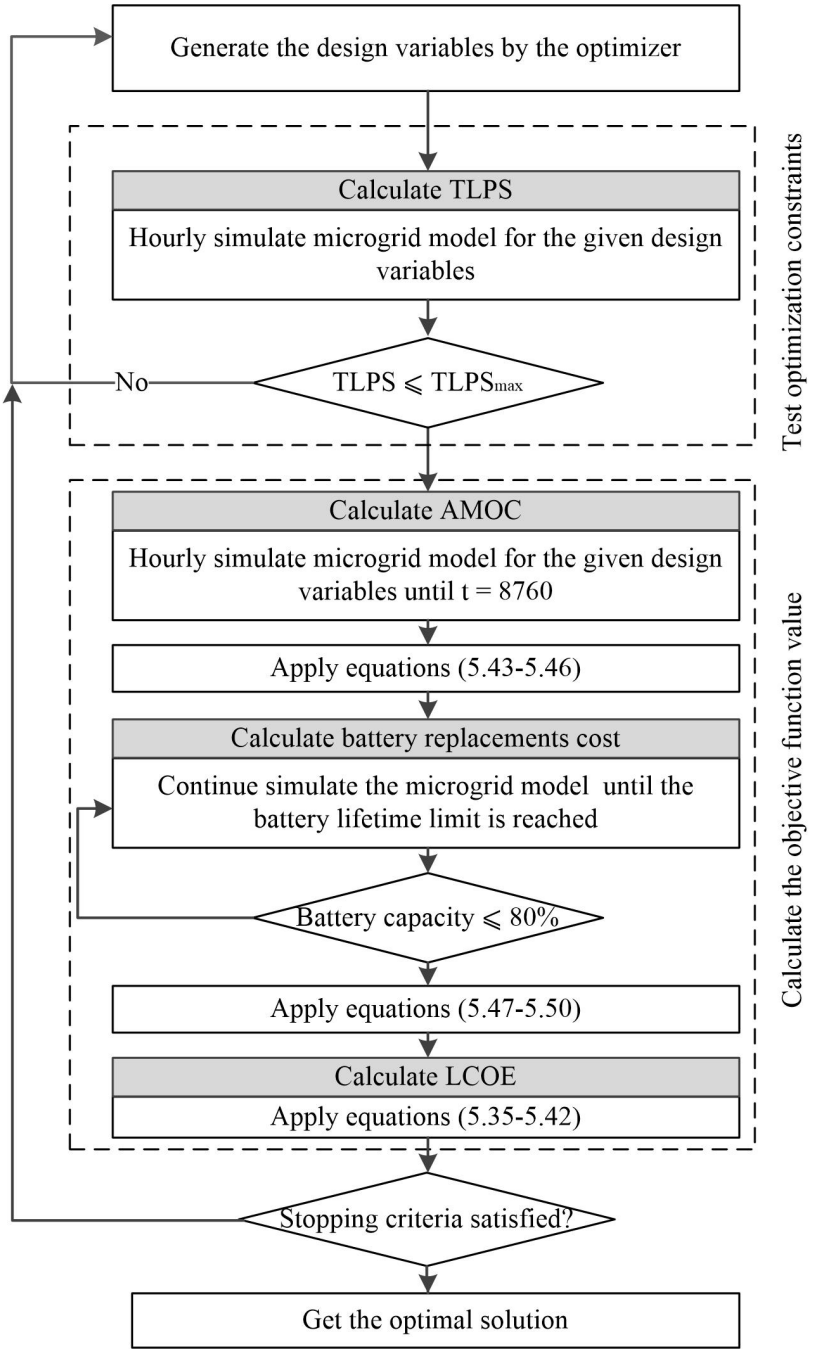

Figure 5.9: Flowchart of the deterministic simulation-based optimal design method.

input parameters. After that an approximated solution for the chance constraint reliability (see Eq. (5.57)) is calculated by

$$Pr\{TLPS(\mathbf{x}, \mathbf{u}, \boldsymbol{\zeta}) \leq TLPS_{max}\} = \frac{\text{Number of valid samples}}{\text{Total number of the simulated samples}}, \tag{5.58}$$

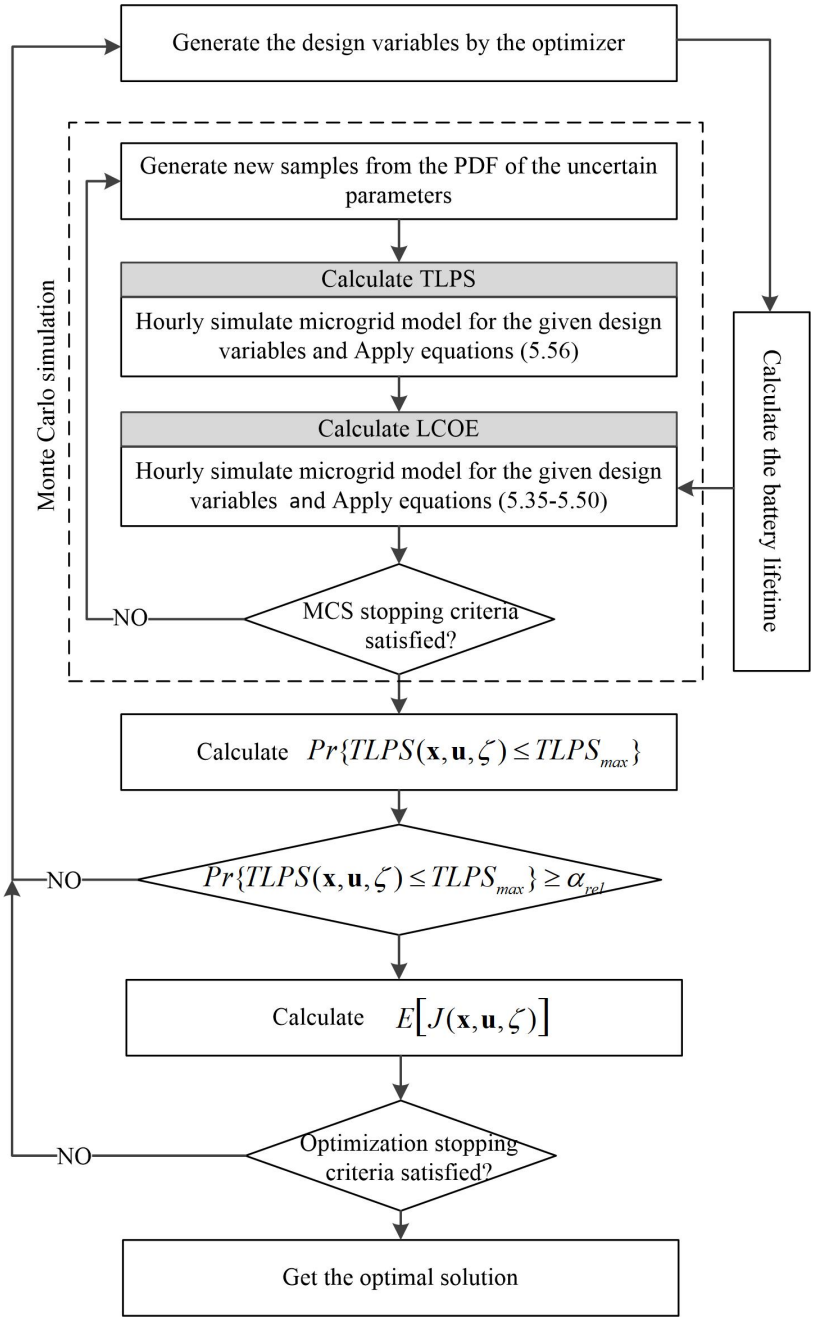

Figure 5.10: Flowchart of the stochastic simulation-based optimization.

where the value of $TLPS$ in the valid samples are lower than $TLPS_{max}$. Finally the expected value of the $LCOE$ is calculated and evaluated by the optimizer. These procedures repeated until the stopping criteria of the optimizer is satisfied.

It is worthwhile to mention that the iterations of MCS are stopped when the specified maximum number of iterates is reached. The iterations number in MCS is chosen so that both the simulation time and the change in the mean value of the $LCOE$ are acceptable.

5.6 Case Studies

The proposed optimal design method in this chapter is applied to optimize the residential and the industrial MGs that have been studied in chapter 3 and chapter 4, respectively. The proposed optimal design strategy is analyzed using a case study from Gaza city in Palestine (latitude=31.42° and longitude =34.38°) with a real solar irradiance data taken from [163] and grid blackout historical data that recorded in one installed project in Gaza city. The main parameters of the battery cell are given in Table 5.1; other parameters can be found in Table A.1. Besides, the main parameters of the economic model are listed in Table 5.2.

However, the optimal tilting angle of PV-panels is independent of the other design parameters for both MGs. Therefore, the optimum tilt angle is taken at which the irradiance on the titled PV-module becomes the maximum. The isotropic model (explained in subsection 3.2.2) is used to calculate the total solar radiation falling on the tilted PV-module at each tilt angle β from 0°to 90°, see Fig. 5.11. As shown in the mentioned figure, the highest solar irradiance can be captured by the PV-module when it is titled with 29.6 °.

As mentioned in subsection 5.2.1, the uncertainty of the starting time and the period of the grid blackout are modelled using KDE. Fig. 5.12. (a) shows the histogram of the blackouts starting times (orange bars) and the best PDF that fit the data probability (blue line). Similarly, Fig. 5.12. (b) shows the histogram of the blackouts periods (orange bars) and the best PDF that fit the data probability (blue

Table 5.1: Parameters of Lead-acid battery.

Parameter	$B_{n.c}$ (Ah)	Z_0 (-)	$C_{dis,0}$ (-)	$V_{0,c}$ (V)	$V_{0,d}$ (V)
Value	100	750	1.185	2.21	2.13

Table 5.2: Economic model parameters of MG design [221, 12].

Parameter	$r_i^{'}$ (-)	r_f (-)	C_f (\$/l)	C_g (\$/kWh)	lt_s (years)
Value	6.89%	3.16%	1.3%	0.15%	20

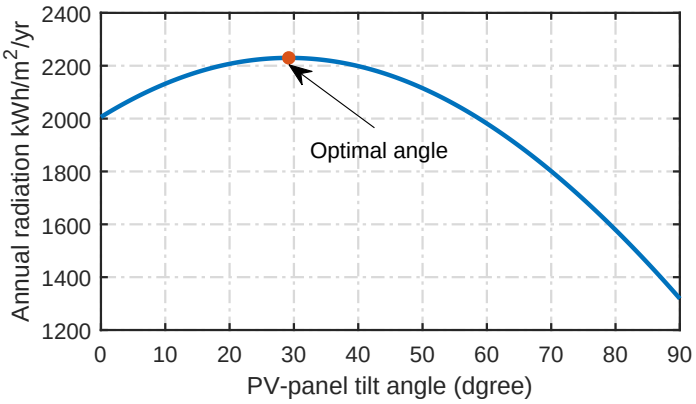

Figure 5.11: Relation between the PV-module tilt angle and the falling solar radiation.

line). On the other hand, the histogram solar irradiance data (orange bars) and the corresponding PDF (blue line) for each season are shown in Fig. 5.13. From Fig. 5.13 it can be shown that the Beta-PDF is able to model the solar irradiance uncertainty with accepted accuracy. This also corresponds to what was mentioned in [222].

All the computation is carried out on a Linux server with 64 processor of type AMD_Epyc7601 X86_64 using MATLAB 2018b software.

The optimal values of the design parameters and the sensitivity analysis of different parameter are investigated in details in the following subsection. It is to note that the confidence level in the optimization problem is chosen to be 98 %.

5.6.1 Optimal Design of the Residential MG

The size of the studied PV-battery MG in chapter 3 is considered here to be optimized. The decision variables in the introduced optimization problem in section 5.4 is changed to include only the PV-array and the battery bank size as well as the DOD value of the battery bank. Because of their small sizes, the power loss of power electronic devices in the MG is neglected. To consider the daily and seasonal variation in the residential load profile, four seasonal days in workdays and weekends are used, as shown in Fig. 5.14. The MG components' capital cost and maintenance cost are shown in Table 5.3. Moreover, the maximum value of the TCC is considered to be 3500 \$. The maximum $TLPS_{max}$ is selected to be 2% with a reliability level of 98 %.

The maximum and the minimum values of the decision variable in the optimiza-

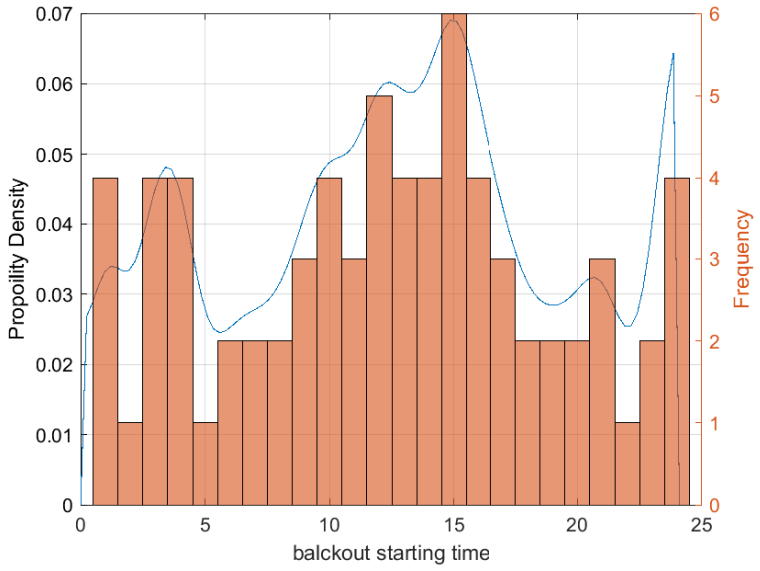

(a)

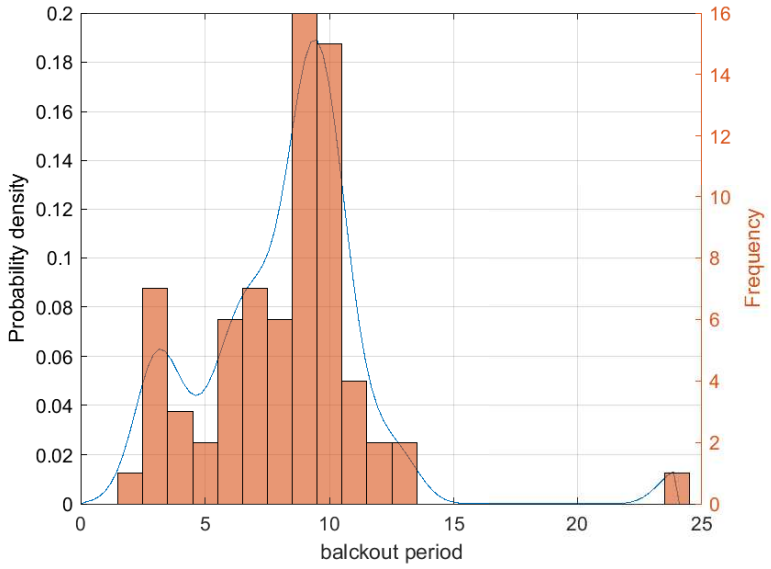

(b)

Figure 5.12: Representation of grid blackout starting time and grid blackout period. (a) histogram of the blackouts starting times (orange bars) and the best PDF that fit the data probability (blue line). (b) histogram of the blackouts periods (orange bars) and the best PDF that fit the data probability (blue line).

tion problem constraints are stated in Table 5.4. Here, the adjustment factors are added to Table 5.4. These factors are used to reduce the search space for the optimizer and to make the optimization results more compatible with the practical sizes of the components. As an example, the battery bank in the residential MG works with 24 v and the nominal voltage of a single battery is 12 v, that means the

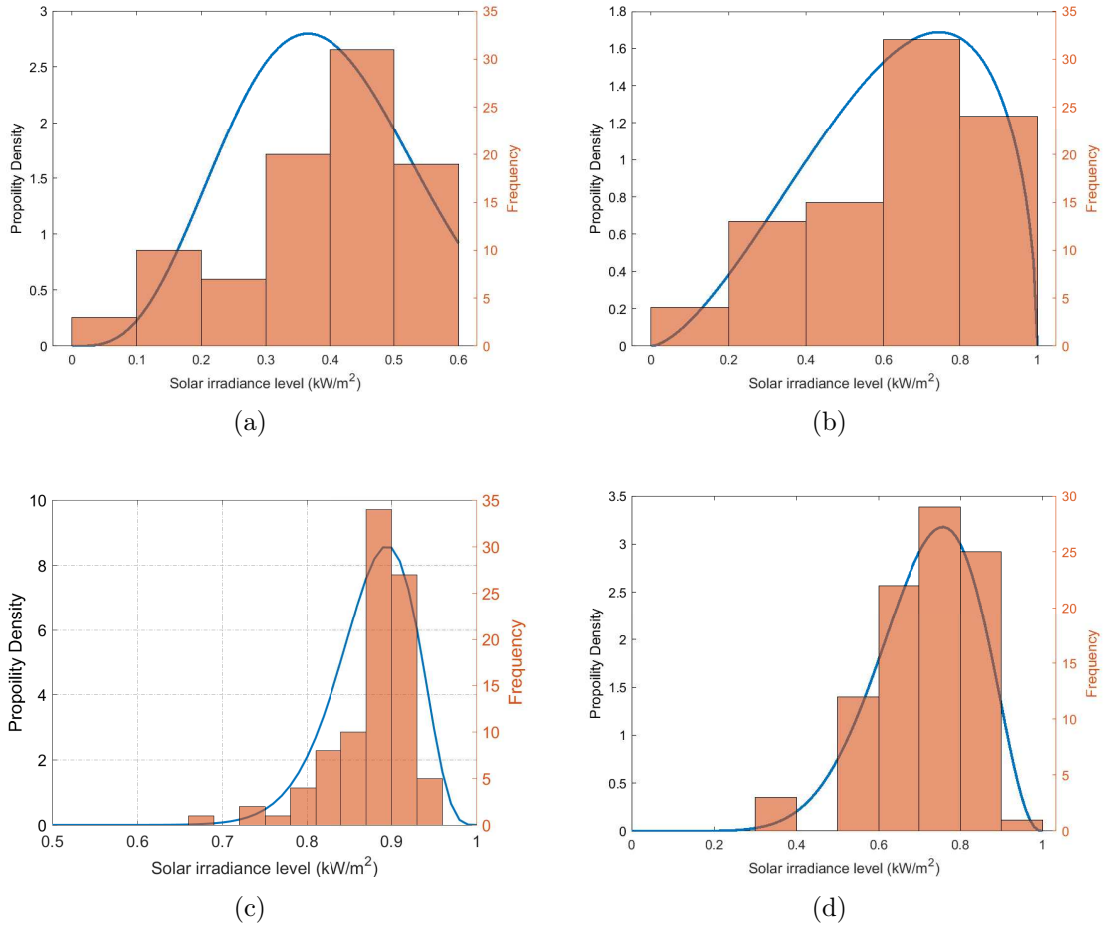

Figure 5.13: Solar irradiance data histogram (orange bars) and the corresponding PDF (blue line) for each season, (a) in winter, (b) in spring, (c) in summer, (d) in autumn.

minimum number of batteries to be installed should be 2, and the battery number must be an even number. Therefore, the decision variable of the number of batteries in the battery bank assigned to be an integer decision variable with minimum value 1 and the maximum value 10; meanwhile, the adjustment factor is 2. This means all possible numbers of batteries that will be evaluated by the MG model are [2, 4, 6, 8, 10, 12, 14, 16, 18, 20].

On the other hand the maximum number of the PV-modules is calculated based on the available area using Eq. (5.52) - (5.54). The latitude and longitude of the MG installation place are utilized to calculate the sun's angle (γ_s) at noon on December 21, using an online calculator available at [223], which gives $\gamma_s = 34.9°$. The used parameters and the calculation results of the calculation of the maximum number PV-modules are stated in Table 5.5.

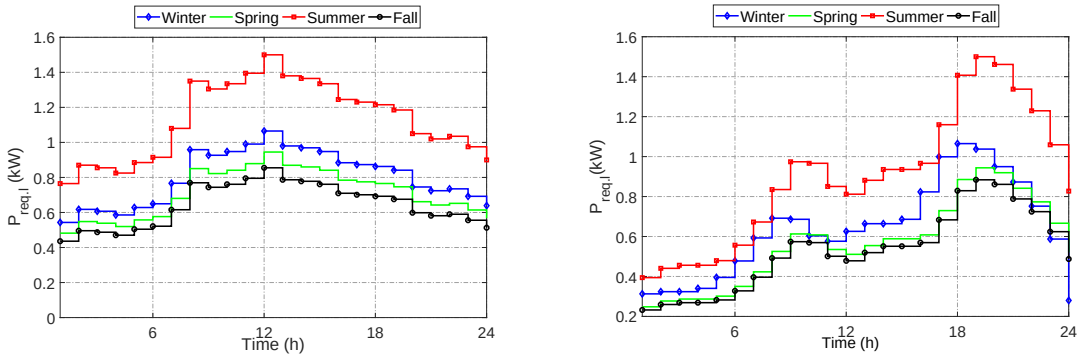

(a) load in weekends (b) load in workdays

Figure 5.14: The considered load profiles for a residential load

Table 5.3: Microgrid components' capital coat, maintenance cost and lifetime.

Parameter	unit capital cost	maintenance cost	lifetime
PV-array	550 \$/kW$_{\mathrm{p}}$	0.5%CC$_{\mathrm{pv}}$	20
Battery bank	150 \$/kWh	1%CC$_{\mathrm{b.b}}$	to be calculated.

Table 5.4: Decision variables maximum values, minimum values and adjustment factor in optimal design problem.

Parameter	Minimum value	Maximum value	**A**
Number of PV-modules	1	12	1
Number of Batteries	1	10	2
DOD	10	80	0.01

Table 5.5: Parameters and results of the maximum number of the PV-modules calculation.

Parameters	$L_{inst}(m)$	$W_{inst}(m)$	$PV_{m.l}(m)$	$W_{pv.m}(m)$
	7	4	1.65	0.99
Results	$SG_{d.min}$	N_{sg}	$N_{m.sg}$	$N_{pv.m}^{max}$
	2.63	3	4	12

It is worth to mention that the MG works according to a predefined rule-based operation strategy [14, 224] considering the operation constraints described in Chapter 3. The used operation strategy consists of two phases are summarized in algorithm 1. In *phase I*, the aim of the MG is to meet the load demand. If the available power from the PV-array is higher than the required load, it will be used to cover the load; otherwise, the battery bank and the PV-array will work together to cover the load. If the battery bank is not able to cover the deficit energy, the power from the main grid will be used if it is available; otherwise, the load will not be covered and the

Algorithm 1: The residential Microgrid operation algorithm.

Input: $G_T(t)$, $T_a(t)$, $\alpha_g(t)$.

Calculate the available power from the PV-array using the explained model in section 3.2;

Phase I, covering the load

if $P_{av.pv}(t) \geq P_{req.l}(t)$ **then**

  $P_{disp.pv}(t) = P_{req.l}(t)$;

else if $P_{dis.max}(t) + P_{av.pv}(t) \geq P_{req.l}(t)$ **then**

  $P_{disp.pv}(t) = P_{av.pv}(t)$;

  $P_{dis}(t) = P_{req.l}(t) - P_{disp.pv}(t)$;

  * Update the battery $SOC(t)$, see section 5.3.1;

  * Update the battery aging variables, see section 5.3.2;

else if $\alpha_g(t) == 1$ **then**

  $P_{disp.g}(t) = P_{req.l}(t)$;

else

  $L_p(t) = L_p(t-1) + 1$;

end

Phase II, charging the battery bank

if $SOC(t) \leq SOC_{max}$ & $P_{dis}(t) == 0$ **then**

  if $P_{av.pv}(t) - P_{disp.pv}(t) \geq 0$ **then**

    $P_{ch} = \min\left(P_{av.pv}(t) - P_{disp.pv(t)}, P_{ch.max}(t)\right)$;

  else if $\alpha_g(t) == 1$ **then**

    $P_{ch}(t) = P_{ch.max}$;

  else

    $P_{ch}(t) = 0$;

  end

  * Update the battery $SOC(t)$, see section 5.3.1;

  * Update the battery aging variables, see section 5.3.2;

end

$L_p(t)$ will be set to one. In *phase II*, if the battery needs to be charged, the extra power for the PV-array will be utilized to charge the battery bank; otherwise, the battery will be charged from the main grid if there is no blackout.

The Lead-Acid battery aging model that is explained in 5.3.2 is utilized here to sim-

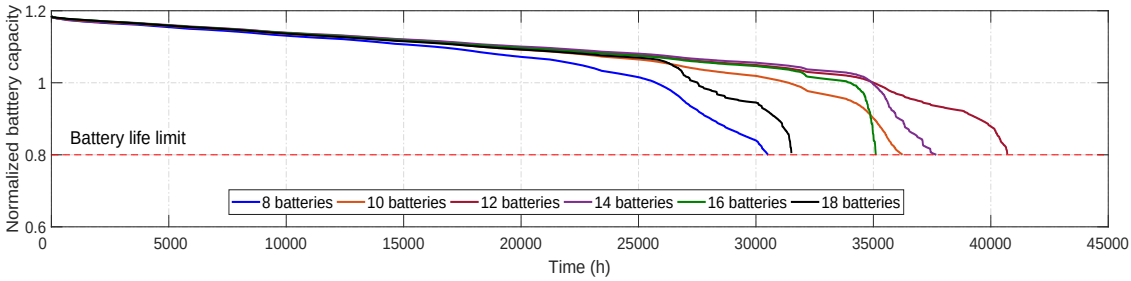

Figure 5.15: The impact of battery bank size on battery capacity.

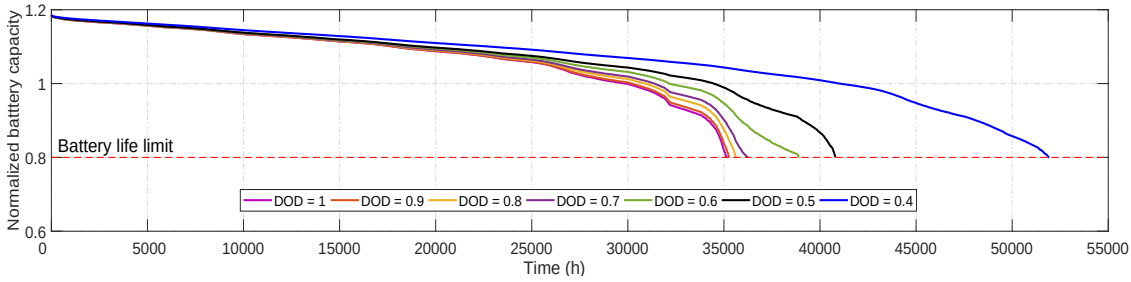

Figure 5.16: The impact of depth of discharge on battery capacity.

ulate the battery aging behavior. To study the impact of the battery bank size, the battery lifetime is calculated with different numbers of batteries. From Fig. 5.15, it can be seen that increasing the number of batteries will lead to an increase in the battery lifetime. However, at a specific number of batteries, this increment has a negative effect. The reason behind this is that increasing the number of batteries at the same operating conditions will decrease the discharged current from each battery cell, which will increase the influence of the current factor in the degradation of the battery capacity, see Eq. (5.28).

It was reported in [205] that the SOC has a high impact on the battery lifetime. Operating the battery at a low DOD value leads to an increase of the active mass degradation in the battery. Here, the effect of battery DOD is illustrated in Fig. 5.16. It can be seen that increasing the DOD value indeed decreases the battery lifetime. This effect arises due to the increased mechanical stress on the active masses and from the increasing size of the sulfate crystals [205].

To illustrate the importance of considering the input parameters uncertainties, two scenarios are considered in solving the problem of optimal design of the residential MG. In the first scenario, the problem is solved using the deterministic values of the input parameters. In this scenario, the mean values of the solar irradiance and the

Table 5.6: Optimal design results of the residential MG.

Parameter	N_{batt} (-)	$N_{pv.m}$ (-)	DOD (-)	$LCOE$ (\$/kWh)	α_{rel} (%)
Scenario 1 (deterministic)	8	10	0.56	0.1835	27.8
Scenario 2 (stochastic)	10	12	0.68	0.2059	98

ambient temperature in each season are calculated and used to build a yearly input data. Besides, the mean values for the starting time and the period of daily grid blackouts are used. Noting that the mean value of the blackout starting time and the blackout duration are 12 and 9, respectively. The deterministic simulation-based optimal design method that explained in subsection 5.5.1 is used in this scenario.
In the second scenario, the problem is solved using the stochastic models of the input parameters. Moreover, the stochastic simulation-based optimal design method explained in subsection 5.6.2 is used to solve the problem.
The optimal battery bank and the PV-array sizes, as well as the DOD optimal value, for both scenarios, are stated in Table 5.6. It can be noticed from the mentioned table that the size of the battery bank and the PV-array, as well as the DOD value, are larger in scenario 2. Moreover, the reliability level of the chance constraint is calculated for both scenarios. It can be said that neglecting the input parameters uncertainty leads to a considerable decrement in the reliability level of the MG.

The impact of the number of batteries and PV-modules on the reliability level is shown in Fig 5.17. Here, the number of batteries is increased gradually while fixing the other design parameters (taken from the optimal results of solving the stochastic optimization problem). Similarly, the effect of the number of PV-modules is tested. It can be noticed that the reliability level of the MG is increased by increasing the number of batteries and PV-modules. However, the number of batteries impact is higher than the impact of the PV-modules numbers. It is worth to mention that the increment in the level of reliability is directly proportional to the increment in $LCOE$, as demonstrated by Fig 5.18.

The effect of the design parameters on the $LCOE$ and $TLPS$ are studied separately (using the results of solving the deterministic optimization problem). From Fig. 5.19 it can be noticed that the number of batteries has the highest impact on

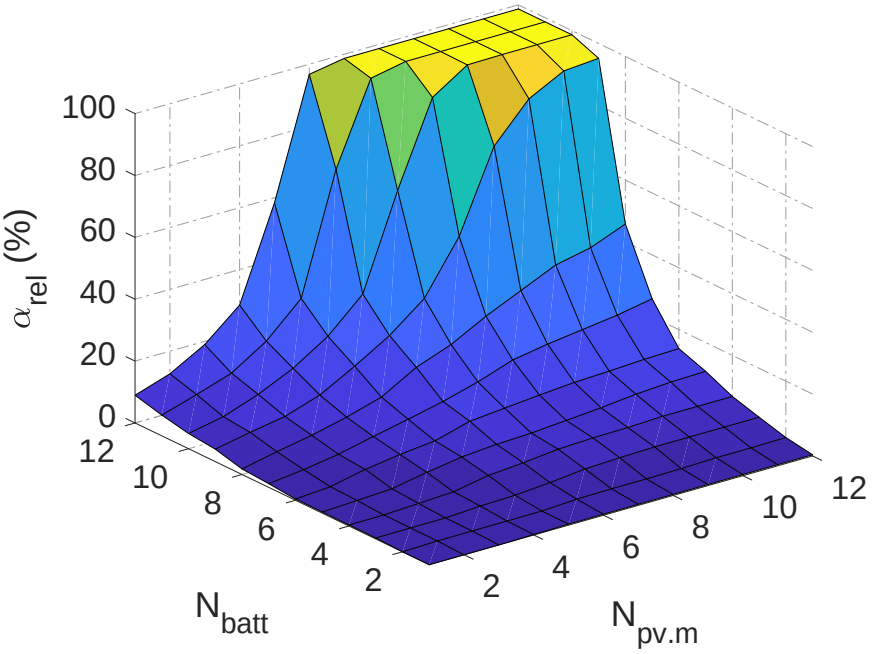

Figure 5.17: The impact of PV-modules and batteries number on the reliability level.

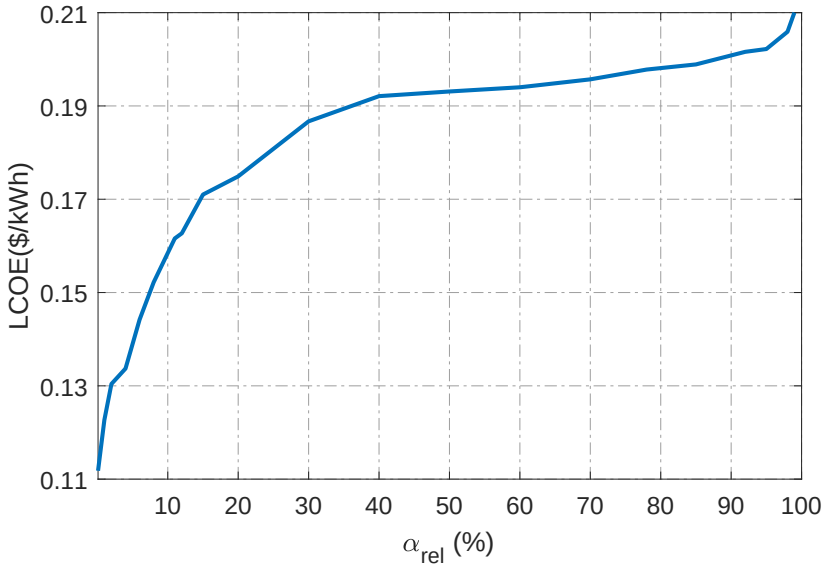

Figure 5.18: The relation between reliability level and the $LCOE$.

the $TLPS$. As shown in Fig. 5.19 (a), increasing the battery number, decreasing the $TLPS$; however, it increases the $LCOE$ due to the increment in the ACC and ARC. The effect of the number of PV-modules on the $LCOE$ is illustrated in Fig. 5.19 (b). It can be seen that increasing the PV-panel number decreases $LCOE$. However, when the number of PV-modules increases so that the energy generated

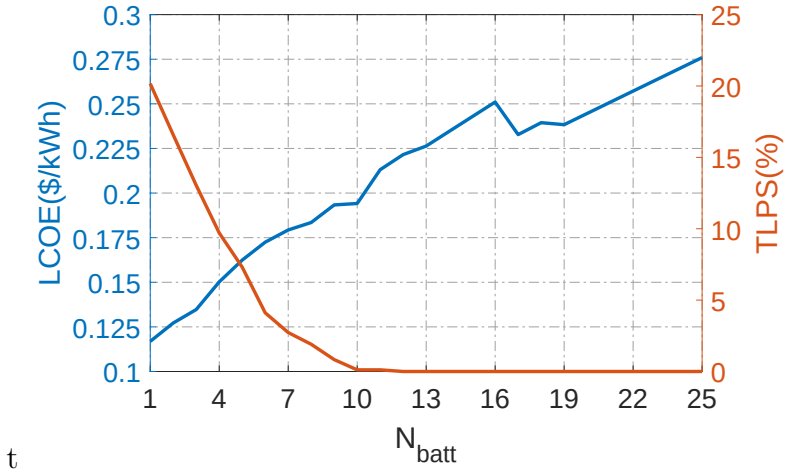

t

(a)

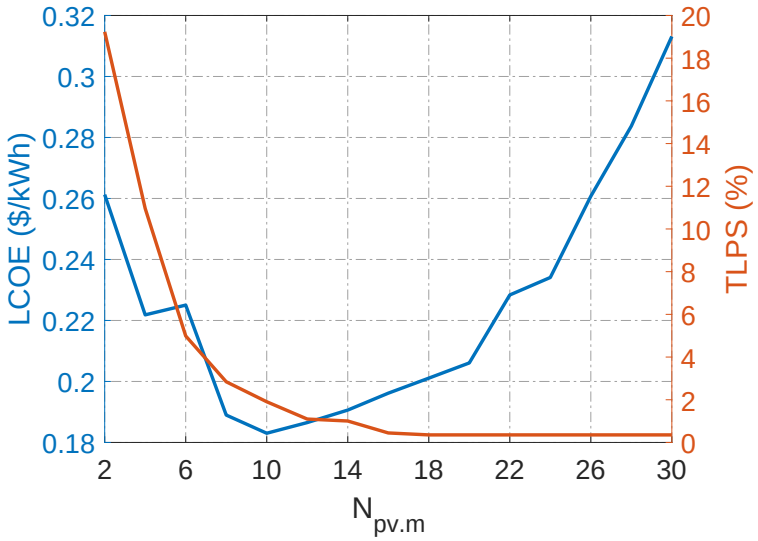

(b)

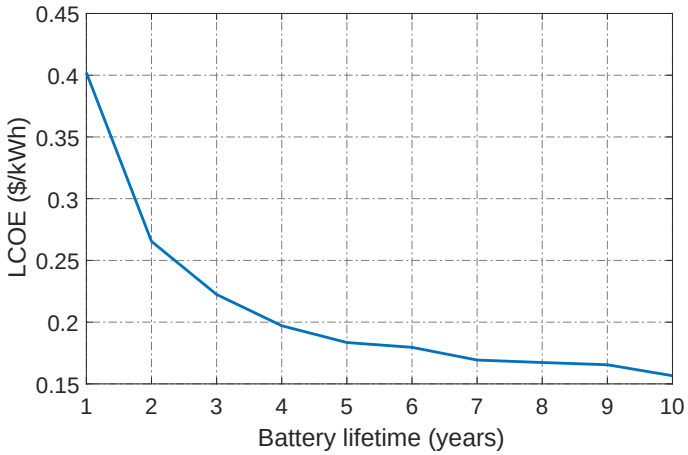

(c)

Figure 5.19: (a) Impact of Number of batteries on the $LCOE$ and the $TLPS$. (b) Impact of Number of PV-panels on the $LCOE$ and the $TLPS$. (c) Impact of battery lifetime on the $LCOE$.

Table 5.7: Decision variables maximum values, minimum values and adjustment factor.

Parameter	Minimum value	Maximum value	**A**
Number of PV-Modules	10	1450	1
PV-inverter size (kW)	1	50	10
Number of batteries	1	200	4
Size of diesel generator$_i$ (kW)	1	50	10
Number of diesel generators	0	3	1

Table 5.8: Parameters and results of the maximum number of the PV-modules calculation.

Parameters	$L_{inst}(m)$	$W_{inst}(m)$	$PV_{m.l}(m)$	$W_{pv.m}(m)$
	75	50	1.65	0.99
Results	$SG_{d.min}$	N_{sg}	$N_{m.sg}$	$N_{pv.m}^{max}$
	2.63	29	50	1450

by the panels becomes greater than the needed power to cover the load and to charge the battery bank, $LCOE$ is increased. Moreover, it can be seen from Fig. 5.19 (c) that increasing the battery lifetime has a considerable effect on the $LCOE$ that cannot be ignored. The reason behind is that the increase of the battery lifetime decreases the number of battery replacement, which decreases the replacement cost in $LCOE$, see subsection 5.4.1.

5.6.2 Optimal Design of the Industrial MG

In this section, the studied MG in chapter 4 is considered to be optimized. The PV-array size, the PV-inverter size, the battery bank size, the DOD value, the number of DGs, and the size of each DG are chosen to be the decision variables of the optimization problem. It is to note that the battery inverter size is chosen to be equal to the maximum allowable dispatched power from the battery bank (see, Eq. (4.5)).

The maximum and minimum values of the decision variables values, as well as their adjustment factors, are stated in Table 5.7. The maximum number of the PV-modules is calculated based on Eqs. (5.52) - (5.54) taking into account the available area for installing the PV-array. The used parameters and the calculation results of the PV-modules number calculation are stated in Table 5.8. Besides, the MG

Table 5.9: Microgrid components' capital coat, maintenance cost and lifetime.

Parameter	unit capital cost	maintenance cost	lifetime
PV-array	550 \$/kW$_{\text{p}}$	0.5 %	20 (years)
PV-inverter	300 \$/kW	0.5 %	10 (years)
Battery bank	150 \$/kWh	1 %	to be calculated
Batt-inverter	300 \$/kW	0.5 %	10 (years)
Diesel Generator	250 \$/kW	8 %	10000 (h)

components' capital cost, maintenance cost percentage from the capital cost and lifetime are shown in Table 5.9. Moreover, the maximum value of the TCC is considered to be 720000 \$.

It was proved in [11] that losing the power supply in industrial facilities is very costly. Therefore, the maximum $TLPS_{max}$ is selected to be 0% (i.e., there is no loss of power supply in the whole year) with a reliability level of 98 %. Moreover, to consider the daily and seasonal variations in the industrial load profile, four seasonal days in workdays and weekends are used, as shown in Fig. 5.20.

The MG works based on a predefined rule-based operation strategy considering the operation constraints described in chapter 4. The used operation strategy consists of two phases and summarized in algorithm 2. In *phase I*, the MG aims to meet the load demand and power losses. Hence, the PV-system has the priority to cover the load; if the $P_{av.pv}$ is not enough, the PV-inverter will work with the grid (if it is available) to utilize the $P_{av.pv}$ in covering the load. Otherwise, the PV-system and the battery storage system will work together to cover the load considering the limit of battery bank SOC and the $P_{av.pv}$. Else, the PV-inverter will work with the DGs to utilize the $P_{av.pv}$ considering the DGs operational limits. If the available power from all sources in the MG is not able to cover the load loss of power supply will occur, and the $L_p(t)$ will be set to one.

In *phase II*, if the battery bank needs to be charged, it will be charged from the DGs if and only if one of the DGs is working lower than its minimum operating load, see Eq. (4.16). Otherwise, the extra power for the PV-array will be utilized to charge the battery bank or the battery will be charged from the main grid if there is no blackout.

Since multiple DGs are used in the studied MG, it is essential to build an appropriate operation strategy to specify the dispatched power from each DG based on its

Algorithm 2: The industrial Microgrid operation algorithm.

Input: $G_T(t)$, $T_a(t)$, $\alpha_g(t)$.

Calculate the available power from the PV-array using the explained model in Section 3.2 ;

Phase I, covering the load

if $P_{av.pv}(t) \geq P_{req.l}(t)$ **then**

  $P_{disp.pv}(t) = P_{req.l}(t)$;

else if $\alpha_g(t) == 1$ **then**

  $P_{disp.pv}(t) = P_{av.pv}(t)$;

  $P_{disp.g}(t) = P_{req.l}(t) - P_{av.pv}(t)$;

else if $P_{dis.max}(t) + P_{av.pv}(t) \geq P_{req.l}(t)$ **then**

  $P_{disp.pv}(t) = P_{av.pv}(t)$;

  $P_{dis}(t) = P_{req.l}(t) - P_{disp.pv}(t)$;

  * Update the battery $SOC(t)$, see section 5.3.1;

  * Update the battery aging variables, see section 5.3.2;

else if $P_{req.l}(t) \leq P_{dg.max}$ **then**

  $P_{disp.pv}(t) = P_{av.pv}(t)$;

  $P_{disp.dg}(t) = P_{req.l}(t) - P_{disp.pv}(t)$;

else

  $L_p(t) = L_p(t-1) + 1$;

end

Phase II, charging the battery bank

if $SOC(t) \leq SOC_{max}$ & $P_{dis}(t) == 0$ **then**

  if $P_{disp.dg}(t) \leq P_{dg.min}$ **then**

    $P_{ch} = \min\left(P_{dg.limit}(t) - P_{dg.min}, P_{ch.max}(t)\right)$;

  else if $P_{av.pv}(t) - P_{disp.pv}(t) \geq 0$ **then**

    $P_{ch} = \min\left(P_{av.pv}(t) - P_{disp.pv(t)}, P_{ch.max}(t)\right)$;

  else if $\alpha_g(t) == 1$ **then**

    $P_{ch}(t) = P_{ch.max}$;

  else

    $P_{ch}(t) = 0$;

  end

  * Update the battery $SOC(t)$, see section 5.3.1;

  * Update the battery aging variables, see section 5.3.2;

end

Algorithm 3: Operation algorithm of multiple diesel generators.

Input: $P_{disp.dg}(t), \boldsymbol{DG_r}, N_{dg}$.

Phase I, selecting which DG will be turned on from $\boldsymbol{DG_r}$ vector;

$P_{req} = P_{disp.dg}(t)$

while $P_{req} > 0$ **do**

  if $P_{req} \leq \max[\boldsymbol{DG_r}]$ **then**

    % find all possible DGs that can cover the load.

    $\boldsymbol{DG_{min}} = find(P_{req} \leq \boldsymbol{DG_r})$

    % choose the smallest DG to cover the load and store it in the selected DGs vector $\boldsymbol{SL_{dg}}$.

    $\boldsymbol{SL_{dg}}(count) = \min[\boldsymbol{DG_{min}}]$

    %update the required power that have to be covered by the DGs.

    $P_{req} = P_{req} - \boldsymbol{SL_{dg}}(count)$

    % delete the selected DG from the DG vector to prevent double check.

    $find(\boldsymbol{DG_r} == \boldsymbol{SL_{dg}}(count)) = [\,]$

  else

    % find the smallest DG to cover the load with minimum difference between the DG size and the required load.

    $\boldsymbol{SL_{dg}}(count) = \min[\,|\boldsymbol{DG_r} - P_{req}|\,]$

    $P_{req} = P_{req} - \boldsymbol{SL_{dg}}(count)$

    $find(\boldsymbol{DG_r} == \boldsymbol{SL_{dg}}(count)) = [\,]$

  end

  $count = count + 1$

end

Phase II, distribute $P_{req.dg}(t)$ on the selected DGs

$\boldsymbol{DG_r}$ = sort($\boldsymbol{SL_{dg}}$,descend) % sort the vector $\boldsymbol{SL_{dg}}$ in descend order.

$P_{disp.dg_i}(t) = 0.3 \times \boldsymbol{SL_{dg}}$ % dispatch the minimum limit of $\boldsymbol{SL_{dg}}$.

% dispatch the rest of the required power from $\boldsymbol{SL_{dg}}$

for $i = 1 : length(\boldsymbol{SL_{dg}})$ **do**

  $P_{disp.dg_i}(t) = P_{disp.dg_i}(t) + 0.7 \times SL_{dg_i}$

  if $P_{req.dg}(t) \leq \sum_{k=1}^{i} P_{disp.dg_k}(t)$ **then**

    $P_{disp.dg_i}(t) = P_{req.dg}(t) - \sum_{k=1}^{i-1} P_{disp.dg_k}(t)$

    break

  end

end

* Update the DGs's status.

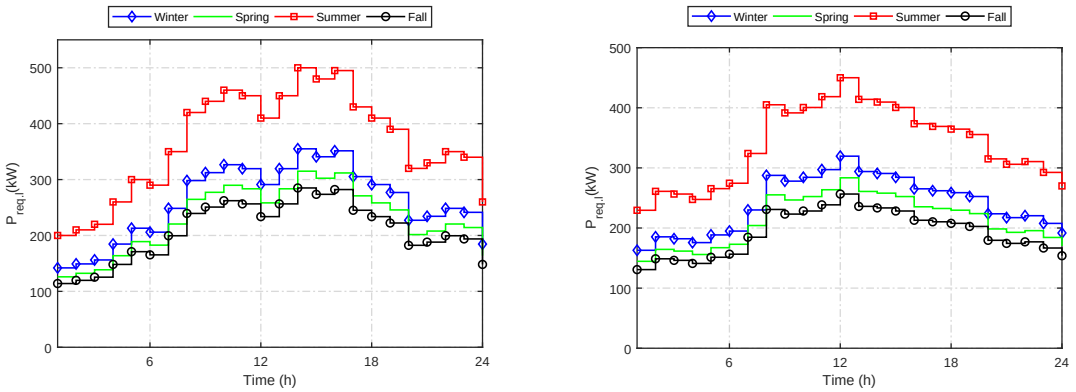

(a) load in workdays (b) load in weekends

Figure 5.20: The considered load profiles for an industrial load.

size. In this study, a separate operation method is implemented to select which DG has to be turned ON and to specify the dispatched power from it, considering the DG operation limits. The operation method consists of two phases and summarized in algorithm 3. In *phase I*, the DG to be operated is selected so that the priority is given to the DG with a size closest to the required load. In *phase II*, the amount of the dispatched power from each DG is determined so that it is ensured that the minimum operating limit of the DG is satisfied, and the DG is running as closely as possible to its full capacity.

To show the importance of considering input parameter uncertainties, the optimal design problem of PV-battery-diesel MG is solved in multiple scenarios, which are:

- Scenario 1: the optimal design problem of PV-battery-diesel MG is solved using deterministic simulation-based optimization employing the mean values of grid blackout starting time, grid blackout duration, solar irradiance and ambient temperature.
- Scenario 2: the optimal design problem of PV-battery-diesel MG is solved using stochastic simulation-based optimization considering the uncertainty of grid blackout starting time, grid blackout duration, solar irradiance and ambient temperature.
- Scenario 3: the optimal design problem of PV-battery-diesel MG is solved using simulation-based optimization employing the mean values of grid blackout duration, solar irradiance and ambient temperature. However, it is considered

Table 5.10: Optimal design results of the Industrial MG.

Parameter	Scenario 1	Scenario 2	Scenario 3	Scenario 4
PV-array	1450	1450	1450	1450
PV-inverter (Kw)	280	280	280	280
Battery size	568	568	464	488
DOD (%)	76	73	65	79
Diesel number	3	3	3	3
Diesel generator (Kw)	60	80	70	60
Diesel generator (Kw)	120	170	130	120
Diesel generator (Kw)	270	250	220	170
Battery life (year)	3.03	3.17	3.58	2.53
LCOE ($\$/Kw$)	0.1896	0.2169	0.1729	0.1643
$TLPS_{max}$ (%)	0 %	0 %	0 %	5 %
α_{rel} (%)	100 %	100 %	16.61 %	62.09 %

that the blackout starts at midnight to include the daily low load period in the grid blackout duration.

- Scenario 4: the optimal design problem of PV-battery-diesel MG is solved using simulation-based optimization using the mean values of grid blackout starting time, grid blackout duration, solar irradiance and ambient temperature. However, the $TLPS_{max}$ is considered to be 5 %.

The results of solving the mentioned four scenarios are stated in Table 5.10. It can be seen that there is no significant difference in the components' sizes in scenario 1 and scenario 2. Moreover, it can be noticed that the total rated capacity of the DGs in both scenarios is equal to the maximum load value (which is 500kW) which makes the MG able to cover the load at any time (i.e. $TLPS = 0$). Nonetheless, the difference in DGs sizes is due to the difference in load levels that require coverage by the DGs. Moreover, there is a notable difference in the $LCOE$ values in scenario 1 and scenario 2, even if the components' sizes are nearly equal. As a result, it can be said, if the uncertainties of the input parameters are not considered in optimizing the size of a PV-battery-diesel MG could lead to a wrong estimation for the output energy cost over the MG life, which could lead to wrong investment decisions.

It worth to mention that a lower $LCOE$ values can be achieved in scenario 1 and scenario 2 if the TCC constraint is neglected. As an example the effect of increasing the battery number is shown in Fig. 5.21, it can be noticed that a lower $LCOE$ can

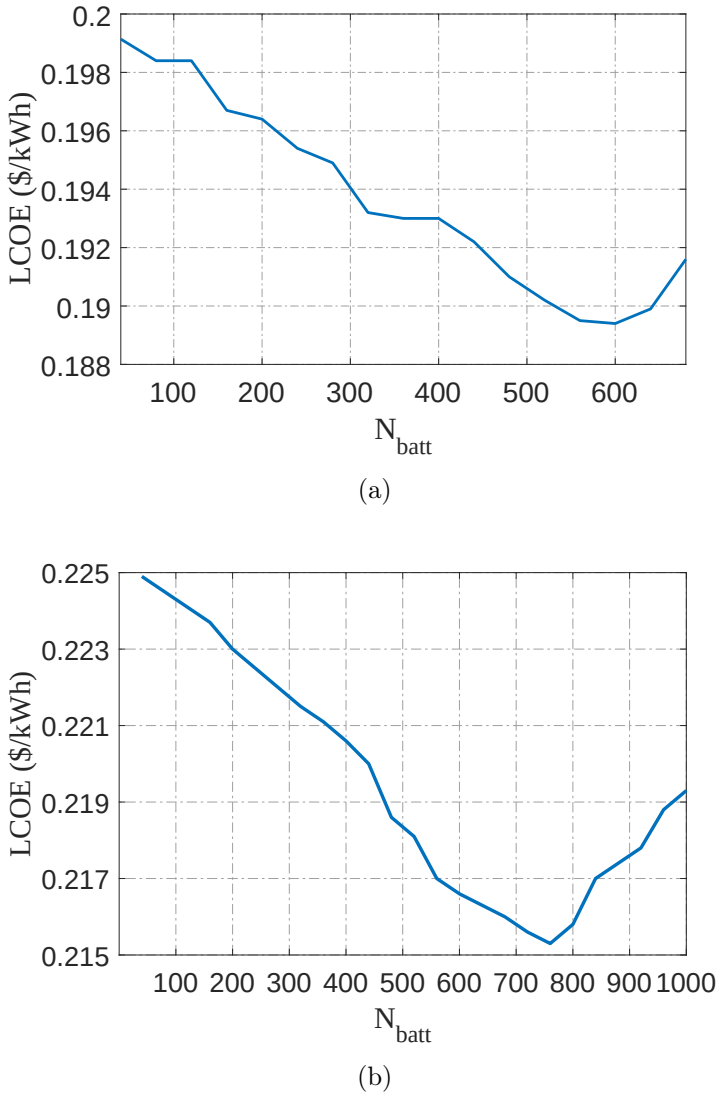

Figure 5.21: Impact of number of batteries design problem. (a) the relation between the number of batteries the $LCOE$ in scenario 1. (b) the relation between the number of batteries the $LCOE$ in scenario 2.

be reached with 600 and 760 batteries in scenario one and two, respectively. This leads to a remarkable result that a bigger size of the battery bank is required to decrease the $LCOE$ in case the input parameter uncertainties are considered.

In scenario 3, the blackout duration is shifted to include only a low load duration (from 0 to 8 o'clock, see Fig. 5.20). As shown in Table 5.10 the total rated capacity of the DGs is equal to the maximum load value in the specified period (which is 420kW) to cover the load at any time during the blackout duration (i.e. $TLPS = 0$). However, testing the reliability level of the chance constraint using the optimal solution of this scenario gives a very low-reliability percentage. This is because the

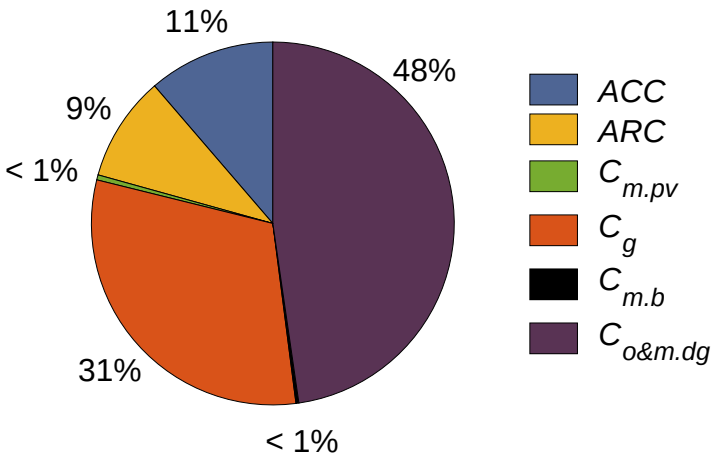

Figure 5.22: The annual cost analysis of the PV-battery-diesel MG.

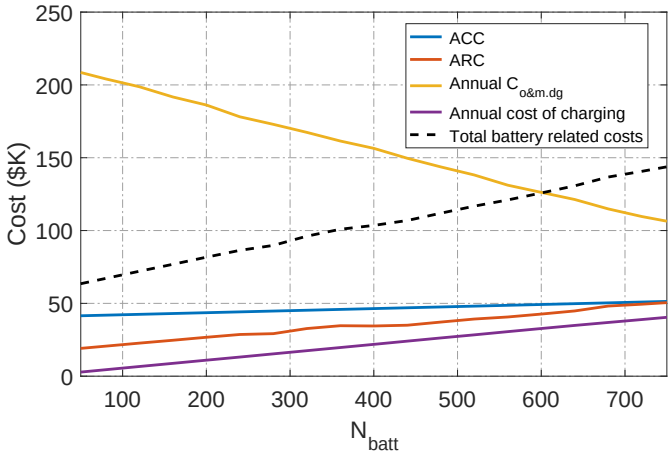

Figure 5.23: Analyze the effect of increasing the battery number on the annual costs.

MG is not able to cover loads higher than the size of the DGs in the event of a grid blackout in periods other than the specified period in the optimization problem. Therefore, it is highly essential to consider the grid blackout uncertainty to guarantee to cover the load at any time in the year.

In scenario 4, the value of $TLPS_{max}$ constraint is changed to be 5 %(i.e., the customer accept a loss of power supply of 5 % of the annual number of hours of operation). While, the mean values of grid blackout duration, solar irradiance and ambient temperature in solving the optimal design problem. As noted in Table 5.10, the sizes of the battery bank and the DG set are smaller than their sizes in scenario 1. Besides, testing the reliability level of the chance constraint (at $TLPS = 5$ %) using the optimal solution of this scenario gives a low-reliability percentage.

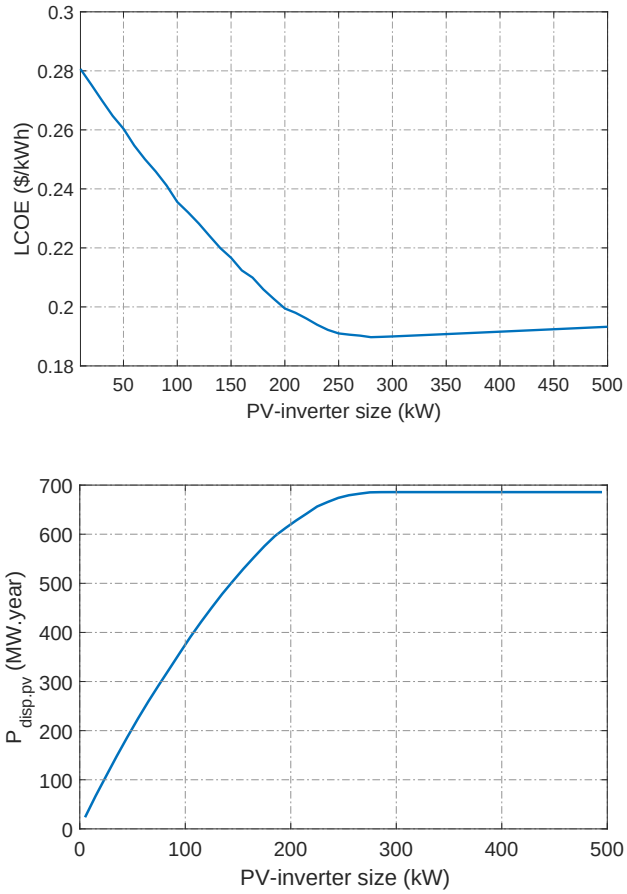

Figure 5.24: Impact of PV-inverter size on the design problem. (a) the relation between PV-inverter size and the $LCOE$. (b) the relation between PV-inverter size and the dispatched power from the PV-array.

The annual cost analysis of the MG (in scenario 1) is illustrated in Fig. 5.22. It can be seen that the cost of the dispatched power from the grid, and the DGs operation and maintenance costs $C_{o\&m.dg}$ are the substantial costs. Based on the followed operation strategy of the MG, these costs can be reduced by increasing the PV-system and the battery bank capacities. Therefore, the maximum number of PV-modules is selected by the optimizer as the optimal solution. In addition, increasing the number of batteries decreases the operation and maintenance cost of the DG (as shown in Fig. 5.23); however when the decrement in the DGs operation cannot compensate the increment in ACC, ARC, and battery charging costs (see, the dashed black line in Fig. 5.23), then the $LCOE$ start to rise as shown in Fig. 5.21.

The importance of considering the PV-array size in the design problem was heavily investigated in section 5.6.1. Here the PV-inverter is added to the optimization problem. Its size affects the $LCOE$ by its capital and replacement costs, see Fig.

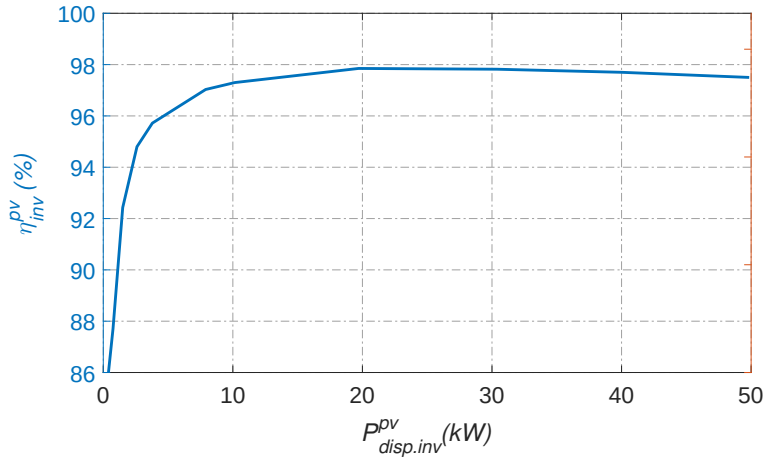

Figure 5.25: Efficiency curve of a 50 kVA PV-inverter [173].

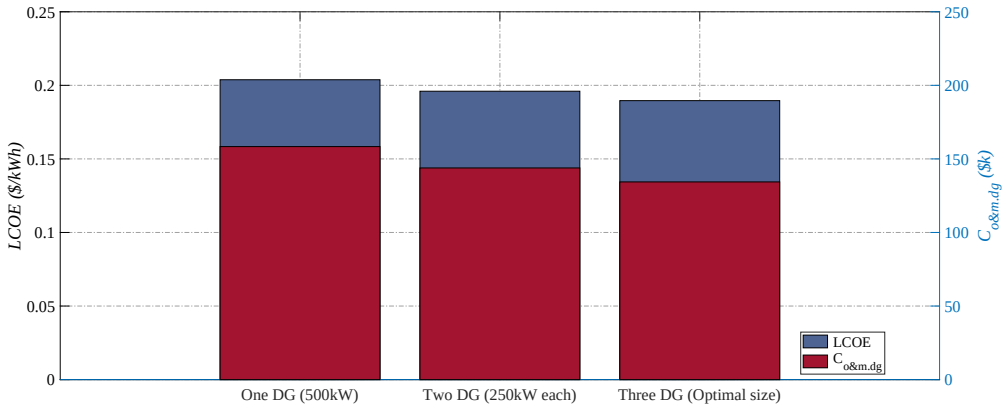

Figure 5.26: Effect of number of diesel generators.

5.24 (a). Moreover, it affects the $AMOC$ by specifying the maximum power that can be dispatched from the PV-array and the amount of the loosed power in the PV-inverter, see Fig. 5.24 (b). Besides, it can be shown in Fig. 5.25 that the behavior of the PV-inverter efficiency depends on the amount of the dispatched power from it. For instance, the PV-inverter works at high efficiency when the dispatched power is between 25 - 80% from it is nominal value; therefore, it is essential to optimize the PV-inverter size to keep it works in its high-efficiency range as much as possible.

It is worth to mention that several simple approaches have been used to size the PV-inverter; one standard method is selecting the PV-inverter to be equal to the nominal value of the PV-array. This method could lead to an oversized inverter which can cause an increment in the $LCOE$ and force the inverter to work in the low-efficiency region. Other studies proposed the array to inverter ratio (AISR) pa-

rameter that represents the relation between the PV-array size and the PV-inverter size. It was found in [225] that the AISR value is affected by the PV-module and the PV-inverter technology as well as the solar irradiance condition in the installation site. However, it has been found that the optimal AISR value between 1 and 1.6. Based on the optimal results in this study it is found that the AISR value is 1.29 in both cases.

From Eq. (5.46) it can be noticed that the fuel consumption of the DG is affected by the dispatched power from it and its rated power. Therefore, it is essential to select the DG size to be compatible with the connected load. Besides, the allowed power from the PV-system that can be shared with it can be limited to satisfy the minimum dispatched power from the diesel generator, see Eq. (4.16). Based on the initial results in [226], it was found that using multiple diesel generators with different sizes can increase the allowed dispatched power from the PV-array and decrease the total operation cost of the DGs. This is also demonstrated in Fig. 5.26; it can be noticed that increasing the number of DGs (with the same total rated capacity) decreases the total fuel consumption of the MG as well as the $LCOE$.

5.7 Conclusion

A comprehensive optimal design approach for PV-based MGs is proposed in this chapter to increase the reliability level of supplying the electrical energy to a load connected to the grid-tie line, which has long periods of blackouts. In this approach, the solar irradiance, ambient temperature, blackouts starting time, and blackouts duration uncertainties are modeled and considered in the optimization problem. A simulation-based optimization approach is used to solve the stochastic MINLP problem. The proposed approach is able to optimize the sizes of MG's components; meanwhile, the levelized Cost of Energy is minimized, and the required annual total loss of power supply is satisfied. Moreover, the proposed model takes into consideration the battery capacity deterioration due to the MG operating conditions. A detailed lead-acid battery aging model is used to estimate the battery lifetime in which the corrosion layer thickness and active material degradation are considered.

In addition, the impact of the depth of discharge and the battery bank size on the battery lifetime is investigated by computation study. Besides, the impacts of the uncertainties of the input parameters on the resulted solution are studied. The results showed that the uncertainties of the input parameters have a considerable effect on the optimal design problem's final solution and the value of the $LCOE$, especially in PV-battery MG. Moreover, it was shown that the uncertainty of grid blackout has a higher effect than the uncertainty of solar irradiance and ambient temperature.

Chapter 6

Conclusions and Future Challenges

To overcome the problem of grid blackouts, consumers relied on diesel generators and chemical batteries as an ideal solution to this problem. However, due to the pollutants resulting from the use of diesel generators and the short life of the batteries, it became essential to find a cheap and environmentally friendly solution.
Due to the high technology development in recent years, it has become feasible to integrate the PV-systems with conventional electrical power sources to build a local MG that can supply the required energy reliably and cost-effectively. Moreover, it is well recognized that optimizing the MG operation and design is a key solution to guarantee a low-cost and uninterrupted power supply. However, many technical and economic complexities have to be handled to achieve this goal. This leads to complex optimization problems, which are not easy to be solved.
In this thesis, a model-based optimal operation and design algorithms for a PV-based MGs considering the battery lifetime and the problem of a grid blackout was developed. For this, an accurate model for the proposed MGs was introduced, taking into account all operational constraints of the MG components. Besides, the differences between the residential and the industrial loads were considered. Therefore, different models were developed based on the type of the connected load.
To improve the operation efficiency of the residential MG, an OPD strategy was proposed to minimize the total operating cost of a PV-battery MG considering the battery lifetime and the grid blackout problem. A compersion between the traditional backup operation strategy and the EMPC-based OPD strategy was made.

The results showed that the proposed approach leads to a significant reduction in the cost of the total energy consumed from the grid while decreasing the curtailment of the generated power from the PV-array and maximizing the battery lifetime.

The proposed operation strategy was extended to optimize the active-reactive power dispatch in a PV-battery-diesel microgrid considering the battery lifetime cost, the reactive power cost, and the grid blackout issue. For this, a novel model was introduced to calculate the reactive power generation cost from the diesel generator. Moreover, the cost model of the dispatched reactive power from the PV-system and the battery bank was adapted. It was demonstrated by a real case study that considering the reactive power cost has a high impact on the optimal power flow in the MG. Moreover, it was proved that generating reactive power locally is more cost-effective than importing it from the main grid. The results showed that the PV-inverter could generate reactive power with a very low cost compared with the battery inverter. Finally, the results showed that the proposed operation strategy leads to a significant reduction in the total cost of the dispatched active and reactive power while maximizing the battery lifetime.

From another perspective, a new optimal design method for the introduced MGs was proposed to minimize the $LCOE$ while satisfying the required annual $TLPS$ percentage, where the battery lifetime and the problem of long term daily grid blackout were considered. A comprehensive lead-acid battery model that includes the battery current, voltage, and state of charge performances was applied to describe the battery operation. An improved method to calculate the $LOCE$ was developed utilizing an accurate model to estimate the lead-acid battery life. In this model, the impacts of SOC, discharging current, the number of cycles, acid stratification, and sulfate-crystal structure on the battery life were taken into account. Moreover, computation studies were made to reveal the effect of battery depth of discharge and the number of batteries on the battery lifetime.

It is well known that the deterministic design approaches highly depend on the given input parameters of the model as any deviation due to uncertainty could lead to a suboptimal solution. Therefore, a stochastic optimal design problem was formulated considering the uncertainties of solar irradiance, ambient temperature, blackouts

starting time, and blackouts duration. For this, a novel model is implemented to model the uncertainty of the grid blackout starting time and the blackout period using kernel density estimation. Besides, the stochastic optimal design problem was defined as a chance-constrained optimization problem. Accordingly, a stochastic simulation-based optimization method incorporating Monte-Carlo simulation was used to solve the optimal design problem to minimize the $LCOE$ considering a specific reliability level for the $TLPS$ constraint.

The results showed that the battery bank size has the highest impact on the $LCOE$ and the MG reliability. Moreover, it was proved that considering the uncertainties of the input parameters is essential to calculate the accurate annual cost of the dispatched energy for proper investment decisions.

Although a lot of question has been answered in this thesis, there is still space for further researches to improve the MG design and operation. The future research aspects related to this study can be summarized as follows:

- The developed MG model can be improved to incorporate several types of energy storage systems, such as super-capacitors and lithium-ion batteries.
- The developed optimal power dispatch framework can be extended to include the demand side management issue.
- The proposed operation strategy can be extended to consider the voltage and the frequency limitations at the point of connection with the main grid.
- Parameters estimation of the energy storage system can be included in the operation strategy for accurate estimation for the lifetime of the energy storage system.
- Selecting the type of energy storage system can be added as a decision variable in the optimal design problem.
- The proposed operation strategy can be adapted to be able to work on an embedded system. Also, the optimal design approach can be adapted to work with a graphical user interface for ease of use.

Appendix A

Parameters of the detailed lead-acid battery model

Table A.1: Parameters for detailed lead-acid battery model [202][205].

Parameter	Symbol	Value
Parameters for the operational model		
Open circuit cell voltage at full charge	$V_{0,c/d}$	2.21/2.13 V
Electrolyte proportional constant	$g_{c/d}$	0.08/0.2 V
Charge transfer over voltage	$\rho_{c/d}$	0.26/0.28 ΩAh
Charge transfer over voltage coefficient	$M_{c/d}$	0.4308/0.4308
Normalized capacity	$C_{c/d}$	1.004/1.185
Gassing voltage	V_{gas}	2.23 V
Gassing temperature	V_{gas}	298.15 K
Voltage coefficient of gassing current	C_v	11.513 1/K
Temperature coefficient of gassing current	C_T	0.0693 1/K
Gassing current initial value	$I_{gas,c}$	0.02 A
Gassing current parameter	$I_{gas,r}$	0.06 A
Parameters of corrosion effect calculation		
Corrosion voltage at full charge	$V_{corr,0}$	1.75 V
Maximum thickness of corrosion layer	ΔW_{max}	306.6 V
Maximum resistance of corrosion layer	$\rho_{corr,max}$	2.3713 ΩAh
Maximum corrosion capacity loss	$C_{corr,max}$	0.300822683568
Parameters of degradation effect calculation		
Maximum degradation capacity loss	$C_{deg,max}$	0.2344
Constant slope for the SOC factor	$C_{SOC,0}$	$6.614 \times 10^{-5} h^{-1}$
Impact of the minimum SOC on the SOC factor	$C_{SOC_{min}}$	$3.307 \times 10^{-3} h^{-1}$
Reference voltage	V_{ref}	2.5 V
Reference current	I_{ref}	-10 A
Factor for the increment of the acid stratification	C_{plus}	1/30
Factor for the decrements of the acid stratification	C_{minus}	0.1
Diffusion constant for sulfuric acid	D	$20 \times 10^{-9} m^2/s$
Battery height	z	30 cm

Bibliography

[1] D. J. Feldman and R. M. Margolis, "Q4 2018/q1 2019 solar industry update," National Renewable Energy Lab.(NREL), Golden, CO (United States), Tech. Rep., 2019.

[2] F. Katiraei, R. Iravani, N. Hatziargyriou, and A. Dimeas, "Microgrids management," *IEEE power and energy magazine*, vol. 6, no. 3, 2008.

[3] G. Masson and I. Kaizuka, "Trends in photovoltaic applications, international energy agency," 2019.

[4] K. Padiyar and A. M. Kulkarni, "Microgrids: Operation and control," 2019.

[5] R. Atia and N. Yamada, "Sizing and analysis of renewable energy and battery systems in residential microgrids," *IEEE Transactions on Smart Grid*, vol. 7, no. 3, pp. 1204–1213, 2016.

[6] M. Alramlawi, A. Gabash, E. Mohagheghi, and P. Li, "Optimal operation of PV-battery-diesel microgrid for industrial loads under grid blackouts," in *2018 IEEE International Conference on Environment and Electrical Engineering and 2018 IEEE Industrial and Commercial Power Systems Europe (EEEIC/I&CPS Europe)*. IEEE, 2018, pp. 1–5.

[7] V. Hau, M. Husein, I.-Y. Chung, D.-J. Won, W. Torre, and T. Nguyen, "Analyzing the impact of renewable energy incentives and parameter uncertainties on financial feasibility of a campus microgrid," *Energies*, vol. 11, no. 9, p. 2446, 2018.

[8] J. Li, Y. Liu, and L. Wu, "Optimal operation for community-based multiparty microgrid in grid-connected and islanded modes," *IEEE Transactions on Smart Grid*, vol. 9, no. 2, pp. 756–765, 2016.

[9] J. C. Vasquez, J. M. Guerrero, J. Miret, M. Castilla, and L. G. De Vicuna, "Hierarchical control of intelligent microgrids," *IEEE Industrial Electronics Magazine*, vol. 4, no. 4, pp. 23–29, 2010.

[10] J. Khoury, R. Mbayed, G. Salloum, and E. Monmasson, "Optimal sizing of a residential PV-battery backup for an intermittent primary energy source under realistic constraints," *Energy and Buildings*, vol. 105, pp. 206–216, 2015.

[11] G. Wacker and R. Billinton, "Customer cost of electric service interruptions," *Proceedings of the IEEE*, vol. 77, no. 6, pp. 919–930, 1989.

[12] M. Alramlawi, A. Gabash, E. Mohagheghi, and P. Li, "Optimal operation of hybrid PV-battery system considering grid scheduled blackouts and battery lifetime," *Solar Energy*, vol. 161, pp. 125–137, 2018.

[13] M. Hijjo and G. Frey, "Stochastic optimization framework for scheduling isolated microgrids," in *2018 19th IEEE Mediterranean Electrotechnical Conference (MELECON)*. IEEE, 2018, pp. 149–154.

[14] M. Alramlawi and P. Li, "Design optimization of a residential PV-battery microgrid with a detailed battery lifetime estimation model," *IEEE Transactions on Industry Applications*, pp. 1–1, 2020.

[15] M. Alramlawi, E. Mohagheghi, and P. Li, "Predictive active-reactive optimal power dispatch in PV-battery-diesel microgrid considering reactive power and battery lifetime costs," *Solar Energy*, vol. 193, pp. 529 – 544, 2019.

[16] G. Merei, *Optimization of off-grid hybrid PV-wind-diesel power supplies with multi-technology battery systems taking into account battery aging*. Shaker Verlag, 2016.

[17] A. Rabiee, H. Khorramdel, and J. Aghaei, "Retracted: A review of energy storage systems in microgrids with wind turbines," 2013.

[18] M. Faisal, M. A. Hannan, P. J. Ker, A. Hussain, M. B. Mansor, and F. Blaabjerg, "Review of energy storage system technologies in microgrid applications: Issues and challenges," *Ieee Access*, vol. 6, pp. 35 143–35 164, 2018.

[19] S. A. Arefifar, A.-R. M. Yasser, and T. H. El-Fouly, "Optimum microgrid design for enhancing reliability and supply-security," *IEEE Transactions on Smart Grid*, vol. 4, no. 3, pp. 1567–1575, 2013.

[20] B. Yan, P. B. Luh, G. Warner, and P. Zhang, "Operation and design optimization of microgrids with renewables," *IEEE Transactions on Automation Science and Engineering*, vol. 14, no. 2, pp. 573–585, 2017.

[21] A. G. Tsikalakis and N. D. Hatziargyriou, "Centralized control for optimizing microgrids operation," *IEEE Transactions on Energy Conversion*, vol. 23, no. 1, pp. 241–248, March 2008.

[22] J. M. Guerrero, M. Chandorkar, T.-L. Lee, and P. C. Loh, "Advanced control architectures for intelligent microgrids—part i: Decentralized and hierarchical control," *IEEE Transactions on Industrial Electronics*, vol. 60, no. 4, pp. 1254–1262, 2012.

[23] G. Vera, E. Yimy, R. Dufo-López, and J. L. Bernal-Agustín, "Energy management in microgrids with renewable energy sources: A literature review," *Applied Sciences*, vol. 9, no. 18, p. 3854, 2019.

[24] C. A. Hernandez-Aramburo, T. C. Green, and N. Mugniot, "Fuel consumption minimization of a microgrid," *IEEE Transactions on Industry Applications*, vol. 41, no. 3, pp. 673–681, May 2005.

[25] R. Rahmani, I. Moser, and M. Seyedmahmoudian, "Multi-agent based operational cost and inconvenience optimization of PV-based microgrid," *Solar Energy*, vol. 150, pp. 177–191, 2017.

[26] A. Chakir, M. Tabaa, F. Moutaouakkil, H. Medromi, M. Julien-Salame, A. Dandache, and K. Alami, "Optimal energy management for a grid connected PV-battery system," *Energy Reports*, 2019.

[27] K. Kusakana, "Operation cost minimization of photovoltaic-diesel-battery hybrid systems," *Energy*, vol. 85, pp. 645–653, 2015.

[28] S. Chalise, J. Sternhagen, T. M. Hansen, and R. Tonkoski, "Energy management of remote microgrids considering battery lifetime," *The Electricity Journal*, vol. 29, no. 6, pp. 1–10, 2016.

[29] L. Grüne and J. Pannek, *Nonlinear Model Predictive Control: Theory and Algorithms*. Springer, 2016.

[30] Y. Zhang, T. Zhang, R. Wang, Y. Liu, and B. Guo, "Optimal operation of a smart residential microgrid based on model predictive control by considering uncertainties and storage impacts," *Solar Energy*, vol. 122, pp. 1052–1065, 2015.

[31] A. Parisio, E. Rikos, and L. Glielmo, "A model predictive control approach to microgrid operation optimization," *IEEE Transactions on Control Systems Technology*, vol. 22, no. 5, pp. 1813–1827, 2014.

[32] R. Palma-Behnke, C. Benavides, F. Lanas, B. Severino, L. Reyes, J. Llanos, and D. Sáez, "A microgrid energy management system based on the rolling horizon strategy," *IEEE Transactions on Smart Grid*, vol. 4, no. 2, pp. 996–1006, 2013.

[33] J. Sachs and O. Sawodny, "A two-stage model predictive control strategy for economic diesel-PV-battery island microgrid operation in rural areas," *IEEE Transactions on Sustainable Energy*, vol. 7, no. 3, pp. 903–913, 2016.

[34] A. Núñez-Reyes, D. M. Rodríguez, C. B. Alba, and M. Á. R. Carlini, "Optimal scheduling of grid-connected PV plants with energy storage for integration in the electricity market," *Solar Energy*, vol. 144, pp. 502–516, 2017.

[35] C. Ju, P. Wang, L. Goel, and Y. Xu, "A two-layer energy management system for microgrids with hybrid energy storage considering degradation costs," *IEEE Transactions on Smart Grid*, vol. 9, no. 6, pp. 6047–6057, Nov 2018.

[36] M. Ellis, H. Durand, and P. D. Christofides, "A tutorial review of economic model predictive control methods," *Journal of Process Control*, vol. 24, no. 8, pp. 1156–1178, 2014.

[37] T. G. Hovgaard, K. Edlund, and J. B. Jørgensen, "The potential of economic mpc for power management," in *Decision and Control (CDC), 2010 49th IEEE Conference on*. IEEE, 2010, pp. 7533–7538.

[38] F. Tedesco, L. Mariam, M. Basu, A. Casavola, and M. F. Conlon, "Economic model predictive control-based strategies for cost-effective supervision of community microgrids considering battery lifetime," *IEEE Journal of Emerging and Selected Topics in Power Electronics*, vol. 3, no. 4, pp. 1067–1077, 2015.

[39] T. Broomhead, C. Manzie, P. Hield, R. Shekhar, and M. Brear, "Economic model predictive control and applications for diesel generators," *IEEE Transactions on Control Systems Technology*, vol. 25, no. 2, pp. 388–400, 2017.

[40] M. Zachar and P. Daoutidis, "Nonlinear economic model predictive control for microgrid dispatch," *IFAC-PapersOnLine*, vol. 49, no. 18, pp. 778–783, 2016.

[41] B. Zhao, X. Zhang, J. Chen, C. Wang, and L. Guo, "Operation optimization of standalone microgrids considering lifetime characteristics of battery energy storage system," *IEEE Transactions on Sustainable Energy*, vol. 4, no. 4, pp. 934–943, 2013.

[42] A. Das and Z. Ni, "A computationally efficient optimization approach for battery systems in islanded microgrid," *IEEE Transactions on Smart Grid*, vol. 9, no. 6, pp. 6489–6499, 2018.

[43] R. Dufo-López, L. A. Fernández-Jiménez, I. J. Ramírez-Rosado, J. S. Artal-Sevil, J. A. Domínguez-Navarro, and J. L. Bernal-Agustín, "Daily operation optimisation of hybrid stand-alone system by model predictive control considering ageing model," *Energy conversion and management*, vol. 134, pp. 167–177, 2017.

[44] A. Jayawardana, A. P. Agalgaonkar, D. A. Robinson, and M. Fiorentini, "Optimisation framework for the operation of battery storage within solar-rich microgrids," *IET Smart Grid*, vol. 2, no. 4, pp. 504–513, 2019.

[45] K. Thirugnanam, S. K. Kerk, C. Yuen, N. Liu, and M. Zhang, "Energy management for renewable microgrid in reducing diesel generators usage with multiple types of battery," *IEEE Transactions on Industrial Electronics*, vol. 65, no. 8, pp. 6772–6786, 2018.

[46] M. F. Zia, E. Elbouchikhi, and M. Benbouzid, "Optimal operational planning of scalable dc microgrid with demand response, islanding, and battery degradation cost considerations," *Applied Energy*, vol. 237, pp. 695–707, 2019.

[47] B. Venkatesh, G. Sadasivam, and M. A. Khan, "A new optimal reactive power scheduling method for loss minimization and voltage stability margin maximization using successive multi-objective fuzzy lp technique," *IEEE Transactions on power Systems*, vol. 15, no. 2, pp. 844–851, 2000.

[48] R. K. Varma, V. Khadkikar, and R. Seethapathy, "Nighttime application of PV solar farm as statcom to regulate grid voltage," *IEEE transactions on energy conversion*, vol. 24, no. 4, pp. 983–985, 2009.

[49] J. Schiffer, T. Seel, J. Raisch, and T. Sezi, "Voltage stability and reactive power sharing in inverter-based microgrids with consensus-based distributed voltage control." *IEEE Trans. Contr. Sys. Techn.*, vol. 24, no. 1, pp. 96–109, 2016.

[50] E. Mohagheghi, A. Gabash, M. Alramlawi, and P. Li, "Real-time optimal power flow with reactive power dispatch of wind stations using a reconciliation algorithm," *Renewable Energy*, vol. 126, pp. 509–523, 2018.

[51] Q. Jiang, M. Xue, and G. Geng, "Energy management of microgrid in grid-connected and stand-alone modes," *IEEE Trans. Power Syst*, vol. 28, no. 3, pp. 3380–3389, 2013.

[52] M. Et-Taoussi, H. Ouadi, and H. Chakir, "Hybrid optimal management of active and reactive power flow in a smart microgrid with photovoltaic generation," *Microsystem Technologies*, vol. 25, no. 11, pp. 4077–4090, 2019.

[53] A. Colet-Subirachs, A. Ruiz-Alvarez, O. Gomis-Bellmunt, F. Alvarez-Cuevas-Figuerola, and A. Sudria-Andreu, "Centralized and distributed active and reactive power control of a utility connected microgrid using iec61850," *IEEE Systems Journal*, vol. 6, no. 1, pp. 58–67, 2012.

[54] A. Bidram, A. Davoudi, and F. L. Lewis, "A multiobjective distributed control framework for islanded ac microgrids," *IEEE Transactions on industrial informatics*, vol. 10, no. 3, pp. 1785–1798, 2014.

[55] L. Meng, E. R. Sanseverino, A. Luna, T. Dragicevic, J. C. Vasquez, and J. M. Guerrero, "Microgrid supervisory controllers and energy management systems: A literature review," *Renewable and Sustainable Energy Reviews*, vol. 60, pp. 1263–1273, 2016.

[56] J. Llanos, D. E. Olivares, J. W. Simpson-Porco, M. Kazerani, and D. Sáez, "A novel distributed control strategy for optimal dispatch of isolated microgrids

considering congestion," *IEEE Transactions on Smart Grid*, vol. 10, no. 6, pp. 6595–6606, 2019.

[57] H. Han, Y. Liu, Y. Sun, M. Su, and J. M. Guerrero, "An improved droop control strategy for reactive power sharing in islanded microgrid," *IEEE Transactions on Power Electronics*, vol. 30, no. 6, pp. 3133–3141, 2015.

[58] H. Mahmood, D. Michaelson, and J. Jiang, "Accurate reactive power sharing in an islanded microgrid using adaptive virtual impedances," *IEEE Transactions on Power Electronics*, vol. 30, no. 3, pp. 1605–1617, 2015.

[59] Q. Li, C. Peng, M. Chen, F. Chen, W. Kang, J. M. Guerrero, and D. Abbott, "Networked and distributed control method with optimal power dispatch for islanded microgrids," *IEEE Transactions on Industrial Electronics*, vol. 64, no. 1, pp. 493–504, 2017.

[60] J. W. Lamont and J. Fu, "Cost analysis of reactive power support," *IEEE transactions on Power Systems*, vol. 14, no. 3, pp. 890–898, 1999.

[61] M. Braun, *Provision of ancillary services by distributed generators: Technological and economic perspective*. kassel university press GmbH, 2009, vol. 10.

[62] O. Gandhi, C. D. Rodriguez-Gallegos, N. B. Gorla, M. Bieri, T. Reindl, and D. Srinivasan, "Reactive power cost from PV inverters considering inverter lifetime assessment," *IEEE Transactions on Sustainable Energy*, 2018.

[63] O. Gandhi, C. D. Rodríguez-Gallegos, W. Zhang, D. Srinivasan, and T. Reindl, "Economic and technical analysis of reactive power provision from distributed energy resources in microgrids," *Applied Energy*, vol. 210, pp. 827–841, 2018.

[64] O. Gandhi, W. Zhang, C. D. Rodriguez-Gallegos, M. Bieri, T. Reindl, and D. Srinivasan, "Analytical approach to reactive power dispatch and energy arbitrage in distribution systems with ders," *IEEE Transactions on Power Systems*, 2018.

[65] U. M. Diwekar and J. R. Kalagnanam, "Efficient sampling technique for optimization under uncertainty," *AIChE Journal*, vol. 43, no. 2, pp. 440–447, 1997.

[66] W. Mefteh, "Simulation-based design: Overview about related works," *Mathematics and Computers in Simulation*, vol. 152, pp. 81–97, 2018.

[67] L. Zhou, Y. Zhang, X. Lin, C. Li, Z. Cai, and P. Yang, "Optimal sizing of PV and BESS for a smart household considering different price mechanisms," *IEEE Access*, vol. 6, pp. 41 050–41 059, 2018.

[68] R. Khalilpour and A. Vassallo, "Planning and operation scheduling of PV-battery systems: A novel methodology," *Renewable and Sustainable Energy Reviews*, vol. 53, pp. 194–208, 2016.

[69] O. Erdinc, N. G. Paterakis, I. N. Pappi, A. G. Bakirtzis, and J. P. Catalão, "A new perspective for sizing of distributed generation and energy storage for smart households under demand response," *Applied Energy*, vol. 143, pp. 26–37, 2015.

[70] H. Yang, Z. Wei, and L. Chengzhi, "Optimal design and techno-economic analysis of a hybrid solar–wind power generation system," *Applied Energy*, vol. 86, no. 2, pp. 163–169, 2009.

[71] M. Ghiasi, "Detailed study, multi-objective optimization, and design of an ac-dc smart microgrid with hybrid renewable energy resources," *Energy*, vol. 169, pp. 496–507, 2019.

[72] F. Benavente, A. Lundblad, P. E. Campana, Y. Zhang, S. Cabrera, and G. Lindbergh, "Photovoltaic/battery system sizing for rural electrification in bolivia: Considering the suppressed demand effect," *Applied energy*, vol. 235, pp. 519–528, 2019.

[73] U. Akram, M. Khalid, and S. Shafiq, "An improved optimal sizing methodology for future autonomous residential smart power systems," *IEEE Access*, vol. 6, pp. 5986–6000, 2018.

[74] I. A. Ibrahim, T. Khatib, and A. Mohamed, "Optimal sizing of a standalone photovoltaic system for remote housing electrification using numerical algorithm and improved system models," *Energy*, vol. 126, pp. 392–403, 2017.

[75] M. I. Hlal, V. K. Ramachandaramurthy, A. Sarhan, A. Pouryekta, and U. Subramaniam, "Optimum battery depth of discharge for off-grid solar PV/battery system," *Journal of Energy Storage*, vol. 26, p. 100999, 2019.

[76] T. M. Masaud and E. El-Saadany, "Correlating optimal size, cycle life estimation, and technology selection of batteries: A two-stage approach for microgrid applications," *IEEE Transactions on Sustainable Energy*, 2019.

[77] G. Ma, Z. Cai, P. Xie, P. Liu, S. Xiang, Y. Sun, C. Guo, and G. Dai, "A bi-level capacity optimization of an isolated microgrid with load demand management considering load and renewable generation uncertainties," *IEEE Access*, vol. 7, pp. 83 074–83 087, 2019.

[78] S. Barcellona, L. Piegari, V. Musolino, and C. Ballif, "Economic viability for residential battery storage systems in grid-connected PV plants," *IET Renewable Power Generation*, vol. 12, no. 2, pp. 135–142, 2017.

[79] I. Alsaidan, A. Khodaei, and W. Gao, "A comprehensive battery energy storage optimal sizing model for microgrid applications," *IEEE Transactions on Power Systems*, vol. 33, no. 4, pp. 3968–3980, 2018.

[80] H. Hesse, R. Martins, P. Musilek, M. Naumann, C. Truong, and A. Jossen, "Economic optimization of component sizing for residential battery storage systems," *Energies*, vol. 10, no. 7, p. 835, 2017.

[81] M. Astaneh, R. Roshandel, R. Dufo-López, and J. L. Bernal-Agustín, "A novel framework for optimization of size and control strategy of lithium-ion battery based off-grid renewable energy systems," *Energy conversion and management*, vol. 175, pp. 99–111, 2018.

[82] S. de la Torre, J. M. González-González, J. A. Aguado, and S. Martín, "Optimal battery sizing considering degradation for renewable energy integration," *IET Renewable Power Generation*, vol. 13, no. 4, pp. 572–577, 2018.

[83] K. Mongird, V. Fotedar, V. Viswanathan, V. Koritarov, P. Balducci, B. Hadjerioua, and J. Alam, "Energy Storage Technology and Cost Characterization Report," 2019.

[84] S. Few, O. Schmidt, and A. Gambhir, "Energy access through electricity storage: Insights from technology providers and market enablers," *Energy for sustainable development*, vol. 48, pp. 1–10, 2019.

[85] J. Yang, C. Hu, H. Wang, K. Yang, J. B. Liu, and H. Yan, "Review on the research of failure modes and mechanism for lead–acid batteries," *International Journal of Energy Research*, vol. 41, no. 3, pp. 336–352, 2017.

[86] G. Mavromatidis, K. Orehounig, and J. Carmeliet, "A review of uncertainty characterisation approaches for the optimal design of distributed energy systems," *Renewable and Sustainable Energy Reviews*, vol. 88, pp. 258–277, 2018.

[87] M. Aien, A. Hajebrahimi, and M. Fotuhi-Firuzabad, "A comprehensive review on uncertainty modeling techniques in power system studies," *Renewable and Sustainable Energy Reviews*, vol. 57, pp. 1077–1089, 2016.

[88] A. Zakaria, F. B. Ismail, M. H. Lipu, and M. Hannan, "Uncertainty models for stochastic optimization in renewable energy applications," *Renewable Energy*, 2019.

[89] A. Kamjoo, A. Maheri, and G. A. Putrus, "Chance constrained programming using non-gaussian joint distribution function in design of standalone hybrid renewable energy systems," *Energy*, vol. 66, pp. 677–688, 2014.

[90] A. Maleki, M. G. Khajeh, and M. Ameri, "Optimal sizing of a grid independent hybrid renewable energy system incorporating resource uncertainty, and load

uncertainty," *International Journal of Electrical Power & Energy Systems*, vol. 83, pp. 514–524, 2016.

[91] M. Bashir and J. Sadeh, "Optimal sizing of hybrid wind/photovoltaic/battery considering the uncertainty of wind and photovoltaic power using monte carlo," in *2012 11th International Conference on Environment and Electrical Engineering*. IEEE, 2012, pp. 1081–1086.

[92] P. Arun, R. Banerjee, and S. Bandyopadhyay, "Optimum sizing of photovoltaic battery systems incorporating uncertainty through design space approach," *Solar Energy*, vol. 83, no. 7, pp. 1013–1025, 2009.

[93] A. Roy, S. B. Kedare, and S. Bandyopadhyay, "Optimum sizing of wind-battery systems incorporating resource uncertainty," *Applied Energy*, vol. 87, no. 8, pp. 2712–2727, 2010.

[94] A. Kamjoo, A. Maheri, A. M. Dizqah, and G. A. Putrus, "Multi-objective design under uncertainties of hybrid renewable energy system using nsga-ii and chance constrained programming," *International Journal of Electrical Power & Energy Systems*, vol. 74, pp. 187–194, 2016.

[95] D. Yang, C. Jiang, G. Cai, and N. Huang, "Optimal sizing of a wind/solar/-battery/diesel hybrid microgrid based on typical scenarios considering meteorological variability," *IET Renewable Power Generation*, vol. 13, no. 9, pp. 1446–1455, 2019.

[96] J. Dong, F. Gao, X. Guan, Q. Zhai, and J. Wu, "Storage-reserve sizing with qualified reliability for connected high renewable penetration micro-grid," *IEEE Transactions on Sustainable Energy*, vol. 7, no. 2, pp. 732–743, 2016.

[97] N. Nguyen-Hong and H. Nguyen-Duc, "Optimal sizing of energy storage devices in wind-diesel systems considering load growth uncertainty," in *2016 IEEE International Conference on Sustainable Energy Technologies (ICSET)*. IEEE, 2016, pp. 54–59.

[98] S. Xia, K. Chan, X. Luo, S. Bu, Z. Ding, and B. Zhou, "Optimal sizing of energy storage system and its cost-benefit analysis for power grid planning with intermittent wind generation," *Renewable energy*, vol. 122, pp. 472–486, 2018.

[99] M. A. Abdulgalil, M. Khalid, and F. Alismail, "Optimal sizing of battery energy storage for a grid-connected microgrid subjected to wind uncertainties," *Energies*, vol. 12, no. 12, p. 2412, 2019.

[100] R. Dufo-Lopez, I. R. Cristobal-Monreal, and J. M. Yusta, "Stochastic-heuristic methodology for the optimisation of components and control variables of PV-wind-diesel-battery stand-alone systems," *Renewable Energy*, vol. 99, pp. 919–935, 2016.

[101] A. Sarkar and J. Singh, "Financing energy efficiency in developing countries—lessons learned and remaining challenges," *Energy Policy*, vol. 38, no. 10, pp. 5560–5571, 2010.

[102] H. Seyedi and M. Sanaye-Pasand, "New centralised adaptive load-shedding algorithms to mitigate power system blackouts," *IET generation, transmission & distribution*, vol. 3, no. 1, pp. 99–114, 2009.

[103] P. M. Murphy, S. Twaha, and I. S. Murphy, "Analysis of the cost of reliable electricity: A new method for analyzing grid connected solar, diesel and hybrid distributed electricity systems considering an unreliable electric grid, with examples in uganda," *Energy*, vol. 66, pp. 523–534, 2014.

[104] J. Khoury, R. Mbayed, G. Salloum, and E. Monmasson, "Optimal sizing of a residential PV-battery backup for an intermittent primary energy source under realistic constraints," *Energy and Buildings*, vol. 105, pp. 206–216, 2015.

[105] A. Hooshmand, B. Asghari, and R. Sharma, "A power management system for planned & unplanned grid electricity outages," in *Innovative Smart Grid Technologies Latin America (ISGT LATAM), 2015 IEEE PES*. IEEE, 2015, pp. 382–386.

[106] M. Hijjo, F. Felgner, and G. Frey, "Energy management scheme for buildings subject to planned grid outages," *Journal of Engineering Research and Technology*, vol. 3, pp. 58–65, 2016.

[107] C. V. Nayar, M. Ashari, and W. Keerthipala, "A grid-interactive photovoltaic uninterruptible power supply system using battery storage and a back up diesel generator," *IEEE Transactions on Energy Conversion*, vol. 15, no. 3, pp. 348–353, 2000.

[108] P. K. Ndwali, J. G. Njiri, and E. M. Wanjiru, "Optimal operation control of microgrid connected photovoltaic-diesel generator backup system under time of use tariff," *Journal of Control, Automation and Electrical Systems*, pp. 1–14, 2020.

[109] T. Zhang, S. Cialdea, J. A. Orr, and A. E. Emanuel, "Outage avoidance and amelioration using battery energy storage systems," *IEEE Transactions on Industry Applications*, vol. 52, no. 1, pp. 5–10, Jan 2016.

[110] A. Esmaeilian and M. Kezunovic, "Prevention of power grid blackouts using intentional islanding scheme," *IEEE Transactions on Industry Applications*, vol. 53, no. 1, pp. 622–629, Jan 2017.

[111] "Ieee guide for design, operation, and integration of distributed resource island systems with electric power systems," *IEEE Std 1547.4-2011*, pp. 1–54, July 2011.

[112] M. B. Najjar, A. Alameddine, and P. G. Horkos, "Supervisory control for sectored distributed generation during load shedding in lebanon's power grid," in *Renewable Energy Research and Applications (ICRERA), 2016 IEEE International Conference on.* IEEE, 2016, pp. 73–78.

[113] J. Mitra, "Reliability-based sizing of backup storage," *IEEE Transactions on Power Systems*, vol. 25, no. 2, pp. 1198–1199, 2010.

[114] J. Khoury, R. Mbayed, G. Salloum, and E. Monmasson, "Design and implementation of a real time demand side management under intermittent primary energy source conditions with a PV-battery backup system," *Energy and Buildings*, vol. 133, pp. 122–130, 2016.

[115] G. Pillai, J. Hodgson, C. Insaurralde, M. Pinitjitsamut, and S. Deepa, "The techno-economic feasibility of providing solar photovoltaic backup power," in *IEEE International Symposium on Technology and Society (ISTAS)*, vol. 20, 2016, p. 22.

[116] M. Mehrabankhomartash, M. Rayati, A. Sheikhi, and A. M. Ranjbar, "Practical battery size optimization of a PV system by considering individual customer damage function," *Renewable and Sustainable Energy Reviews*, vol. 67, pp. 36–50, 2017.

[117] S. A. Arefifar and Y. A.-R. I. Mohamed, "*dg* mix, reactive sources and energy storage units for optimizing microgrid reliability and supply security," *IEEE Transactions on Smart Grid*, vol. 5, no. 4, pp. 1835–1844, 2014.

[118] M. Hijjo, F. Felgner, and G. Frey, "PV-battery-diesel microgrid design for buildings subject to severe power outages," in *2017 IEEE PES PowerAfrica.* IEEE, 2017, pp. 280–285.

[119] J. Dong, L. Zhu, Y. Su, Y. Ma, Y. Liu, F. Wang, L. M. Tolbert, J. Glass, and L. Bruce, "Battery and backup generator sizing for a resilient microgrid under stochastic extreme events," *IET Generation, Transmission & Distribution*, vol. 12, no. 20, pp. 4443–4450, 2018.

[120] J. Zhou, S. Tsianikas, D. P. Birnie III, and D. W. Coit, "Economic and resilience benefit analysis of incorporating battery storage to photovoltaic array generation," *Renewable energy*, vol. 135, pp. 652–662, 2019.

[121] S. Tsianikas, J. Zhou, D. P. Birnie III, and D. W. Coit, "Economic trends and comparisons for optimizing grid-outage resilient photovoltaic and battery systems," *Applied Energy*, vol. 256, p. 113892, 2019.

[122] S. J. Hossain, T. P. George, R. Bisht, A. Suresh, and S. Kamalasadan, "An integrated battery optimal power dispatch architecture for end-user driven micro

grid in islanded and grid connected mode of operation," *IEEE Transactions on Industry Applications*, 2018.

[123] M. Hijjo and G. Frey, "Forecast-driven power planning approach for microgrids incorporating smart loads using stochastic optimization," in *2018 International Conference on Smart Energy Systems and Technologies (SEST)*. IEEE, 2018, pp. 1–6.

[124] I. M. Syed and K. Raahemifar, "Predictive energy management and control system for PV system connected to power electric grid with periodic load shedding," *Solar Energy*, vol. 136, pp. 278–287, 2016.

[125] A. A. Lazou and A. D. Papatsoris, "The economics of photovoltaic stand-alone residential households: a case study for various european and mediterranean locations," *Solar Energy Materials and Solar Cells*, vol. 62, no. 4, pp. 411–427, 2000.

[126] J. Weniger, T. Tjaden, and V. Quaschning, "Sizing of residential PV battery systems," *Energy Procedia*, vol. 46, pp. 78–87, 2014.

[127] J. J. Justo, F. Mwasilu, J. Lee, and J.-W. Jung, "Ac-microgrids versus dc-microgrids with distributed energy resources: A review," *Renewable and sustainable energy reviews*, vol. 24, pp. 387–405, 2013.

[128] E. I. Batzelis and S. A. Papathanassiou, "A method for the analytical extraction of the single-diode PV model parameters," *IEEE Transactions on Sustainable Energy*, vol. 7, no. 2, pp. 504–512, 2015.

[129] S. Bana and R. Saini, "A mathematical modeling framework to evaluate the performance of single diode and double diode based SPV systems," *Energy Reports*, vol. 2, pp. 171–187, 2016.

[130] E. Lorenzo, *Solar electricity: engineering of photovoltaic systems*. Earthscan/James & James, 1994.

[131] J.-Y. Park and S.-J. Choi, "A novel datasheet-based parameter extraction method for a single-diode photovoltaic array model," *Solar Energy*, vol. 122, pp. 1235–1244, 2015.

[132] G. Wang, *Technology, Manufacturing and Grid Connection of Photo-voltaic Solar Cells*. Wiley Online Library, 2018.

[133] W. De Soto, S. Klein, and W. Beckman, "Improvement and validation of a model for photovoltaic array performance," *Solar energy*, vol. 80, no. 1, pp. 78–88, 2006.

[134] S. A. Rahman, R. K. Varma, and T. Vanderheide, "Generalised model of a photovoltaic panel," *IET Renewable Power Generation*, vol. 8, no. 3, pp. 217–229, 2014.

[135] Y. Zhang, S. Gao, and T. Gu, "Prediction of iv characteristics for a PV panel by combining single diode model and explicit analytical model," *Solar Energy*, vol. 144, pp. 349–355, 2017.

[136] *YGE 60 cell series 2*, Yingli Solar, December 2019. [Online]. Available: www.yinglisolar.com

[137] H. Häberlin, *Photovoltaics: system design and practice*. John Wiley & Sons, 2012.

[138] J. A. Duffie and W. A. Beckman, *Solar engineering of thermal processes*. John Wiley & Sons, 2013.

[139] A. K. Yadav and S. Chandel, "Tilt angle optimization to maximize incident solar radiation: A review," *Renewable and Sustainable Energy Reviews*, vol. 23, pp. 503–513, 2013.

[140] B. Y. Liu and R. C. Jordan, "A rational procedure for predicting the long-term average performance of flat-plate solar-energy collectors," in *Solar Energy*. Citeseer, 1963.

[141] J. A. Duffie, W. A. Beckman, and N. Blair, *Solar Engineering of Thermal Processes, Photovoltaics and Wind*. John Wiley & Sons, 2020.

[142] S. Semaoui, A. H. Arab, S. Bacha, and B. Azoui, "The new strategy of energy management for a photovoltaic system without extra intended for remote-housing," *Solar Energy*, vol. 94, pp. 71–85, 2013.

[143] M. Alramlawi, A. Gabash, and P. Li, "Optimal operation strategy of a hybrid PV-battery system under grid scheduled blackouts," in *Environment and Electrical Engineering (EEEIC), 2017 IEEE 17th International Conference on*. IEEE, 2017, pp. 1–5.

[144] E. Koutroulis and K. Kalaitzakis, "Novel battery charging regulation system for photovoltaic applications," *IEE Proceedings-Electric Power Applications*, vol. 151, no. 2, pp. 191–197, 2004.

[145] Z. Wu and X. Xia, "Optimal switching renewable energy system for demand side management," *Solar Energy*, vol. 114, pp. 278–288, 2015.

[146] D. U. Sauer and H. Wenzl, "Comparison of different approaches for lifetime prediction of electrochemical systems—using lead-acid batteries as example," *Journal of Power sources*, vol. 176, no. 2, pp. 534–546, 2008.

[147] T. B. Reddy, *Linden's handbook of batteries*. McGraw-hill New York, 2011, vol. 4.

[148] A. Jossen, J. Garche, and D. U. Sauer, "Operation conditions of batteries in PV applications," *Solar energy*, vol. 76, no. 6, pp. 759–769, 2004.

[149] M. Amiri, M. Esfahanian, M. R. Hairi-Yazdi, and V. Esfahanian, "Minimization of power losses in hybrid electric vehicles in view of the prolonging of battery life," *Journal of Power Sources*, vol. 190, no. 2, pp. 372–379, 2009.

[150] H. Bindner, T. Cronin, P. Lundsager, J. F. Manwell, U. Abdulwahid, and I. Baring-Gould, *Lifetime modelling of lead acid batteries*, 2005.

[151] D. Jenkins, J. Fletcher, and D. Kane, "Lifetime prediction and sizing of lead–acid batteries for microgeneration storage applications," *IET Renewable Power Generation*, vol. 2, no. 3, pp. 191–200, 2008.

[152] J. M. Maciejowski, *Predictive control: with constraints*. Pearson education, 2002.

[153] E. F. Camacho and C. B. Alba, *Model predictive control*. Springer Science & Business Media, 2013.

[154] C. Bordons, F. Garcia-Torres, and M. A. Ridao, "Model predictive control of microgrids," 2019.

[155] D. Angeli, R. Amrit, and J. B. Rawlings, "On average performance and stability of economic model predictive control," *IEEE transactions on automatic control*, vol. 57, no. 7, pp. 1615–1626, 2012.

[156] J. B. Rawlings, D. Angeli, and C. N. Bates, "Fundamentals of economic model predictive control," in *Decision and Control (CDC), 2012 IEEE 51st Annual Conference on*. IEEE, 2012, pp. 3851–3861.

[157] J. H. Holland, *Adaptation in natural and artificial systems*. Univ. Michigan Press, 1975.

[158] D. E. Goldberg, "Genetic algorithms in search, optimization, and machine learning, 1989," *Reading: Addison-Wesley*, 1989.

[159] A. Zilouchian and M. Jamshidi, *Intelligent control systems using soft computing methodologies*. CRC Press, Inc., 2000.

[160] G. Stojanovski and M. Stankovski, *Model predictive controller employing genetic algorithm optimization of thermal processes with non-convex constraints*. INTECH Open Access Publisher, 2012.

[161] MATLAB, *Global Optimization Toolbox Version 3.4*. Natick, Massachusetts: The MathWorks Inc., 2016.

[162] A. Khiareddine, C. B. Salah, and M. F. Mimouni, "Power management of a photovoltaic/battery pumping system in agricultural experiment station," *Solar Energy*, vol. 112, pp. 319–338, 2015.

[163] Solar energy services for professionals. [Online]. Available: http://www.soda-pro.com

[164] M. A. Muñoz-García, O. Marin, M. C. Alonso-García, and F. Chenlo, "Characterization of thin film PV modules under standard test conditions: Results of indoor and outdoor measurements and the effects of sunlight exposure," *Solar Energy*, vol. 86, no. 10, pp. 3049–3056, 2012.

[165] A. Gabash, M. Alkal, and P. Li, "Impact of allowed reverse active power flow on planning PVs and bsss in distribution networks considering demand and evs growth," *Power & Energy Student Summit (PESS) 2013, IEEE Student Branch Bielefeld*, pp. 11–16, 2013.

[166] J. Tant, F. Geth, D. Six, P. Tant, and J. Driesen, "Multiobjective battery storage to improve PV integration in residential distribution grids," *IEEE Transactions on Sustainable Energy*, vol. 4, no. 1, pp. 182–191, 2013.

[167] S. Benhamed, H. Ibrahim, K. Belmokhtar, H. Hosni, A. Ilinca, D. Rousse, A. Chandra, and D. Ramdenee, "Dynamic modeling of diesel generator based on electrical and mechanical aspects," in *2016 IEEE Electrical Power and Energy Conference (EPEC)*. IEEE, 2016, pp. 1–6.

[168] S. Chapman, *Electric machinery fundamentals*. Tata McGraw-Hill Education, 2005.

[169] S. Pelland, D. Turcotte, G. Colgate, and A. Swingler, "Nemiah valley photovoltaic-diesel mini-grid: System performance and fuel saving based on one year of monitored data," *IEEE Transactions on Sustainable Energy*, vol. 3, no. 1, pp. 167–175, 2012.

[170] Cummins. Diesel engine technical data sheet. [Online]. Available: www.cummins.com/g-drive-engines/diesel-qsl9-series

[171] ——, "Diesel QSB-series." [Online]. Available: https://www.cummins.com/g-drive-engines/diesel-qsb-series

[172] ——. Alternator technical data sheet. [Online]. Available: https://stamford-avk.com/data-sheets?field_model_value_selective=All&field_core_value_selective=All&field_poles_value_selective=All&field_winding_value_selective=All

[173] SMA. SMA PV-inverter data sheet. [Online]. Available: https://www.sma.de/en/products/solarinverters.html

[174] ——. SMA battery-inverter data sheet. [Online]. Available: https: //www.sma.de/en/products/battery-inverters.html

[175] Cummins. Diesel generator set specification sheet. [Online]. Available: https://www.cummins.com/generators

[176] M. Sharafi and T. Y. ELMekkawy, "Multi-objective optimal design of hybrid renewable energy systems using pso-simulation based approach," *Renewable Energy*, vol. 68, pp. 67–79, 2014.

[177] A. Charnes and W. W. Cooper, "Chance-constrained programming," *Management science*, vol. 6, no. 1, pp. 73–79, 1959.

[178] H. Zhang and P. Li, "Chance constrained programming for optimal power flow under uncertainty," *IEEE Transactions on Power Systems*, vol. 26, no. 4, pp. 2417–2424, 2011.

[179] M. Klöppel, A. Gabash, A. Geletu, and P. Li, "Chance constrained optimal power flow with non-gaussian distributed uncertain wind power generation," in *2013 12th International Conference on Environment and Electrical Engi-neering*. IEEE, 2013, pp. 265–270.

[180] E. Mohagheghi, A. Geletu, N. Bremser, M. Alramlawi, A. Gabash, and P. Li, "Chance constrained optimal power flow using the inner-outer approximation approach," in *2018 IEEE International Conference on Environment and Electrical Engineering and 2018 IEEE Industrial and Commercial Power Systems Europe (EEEIC/I&CPS Europe)*. IEEE, 2018, pp. 1–6.

[181] L. Andrieu, R. Henrion, and W. Römisch, "A model for dynamic chance constraints in hydro power reservoir management," *European journal of opera-tional research*, vol. 207, no. 2, pp. 579–589, 2010.

[182] P. Li, M. Wendt, H. Arellano-Garcia, and G. Wozny, "Optimal operation of distillation processes under uncertain inflows accumulated in a feed tank," *AIChE Journal*, vol. 48, no. 6, pp. 1198–1211, 2002.

[183] C. Feng, F. Dabbene, and C. M. Lagoa, "A kinship function approach to robust and probabilistic optimization under polynomial uncertainty," *IEEE Transactions on Automatic Control*, vol. 56, no. 7, pp. 1509–1523, 2010.

[184] L. Blackmore and M. Ono, "Convex chance constrained predictive control without sampling," in *AIAA Guidance, Navigation, and Control Conference*, 2009, p. 5876.

[185] M. Alramlawi and P. Li, "Chance constrained optimal design of pv-based microgrids considering grid blackout uncertainties," 2020, under review in IEEE Transactions on Industry Applications.

[186] C. Soize, "Stochastic modeling of uncertainties in computational structural dynamics—recent theoretical advances," *Journal of Sound and Vibration*, vol. 332, no. 10, pp. 2379–2395, 2013.

[187] H. Farzin, M. Fotuhi-Firuzabad, and M. Moeini-Aghtaie, "Stochastic energy management of microgrids during unscheduled islanding period," *IEEE Transactions on Industrial Informatics*, vol. 13, no. 3, pp. 1079–1087, 2016.

[188] R. N. Allan *et al.*, *Reliability evaluation of power systems*. Springer Science & Business Media, 2013.

[189] Y.-C. Chen, "A tutorial on kernel density estimation and recent advances," *Biostatistics & Epidemiology*, vol. 1, no. 1, pp. 161–187, 2017.

[190] A. W. Bowman and A. Azzalini, *Applied smoothing techniques for data analysis: the kernel approach with S-Plus illustrations*. OUP Oxford, 1997, vol. 18.

[191] A. Voskrebenzev, S. Riechelmann, A. Bais, H. Slaper, and G. Seckmeyer, "Estimating probability distributions of solar irradiance," *Theoretical and applied climatology*, vol. 119, no. 3-4, pp. 465–479, 2015.

[192] MATLAB, *Statistics Toolbox User's Guide*. Natick, Massachusetts: The MathWorks Inc., 2004.

[193] "The humanitarian impact of gaza's electricity and fuel crisis," 2015.

[194] G. Mavromatidis, K. Orehounig, and J. Carmeliet, "Uncertainty and global sensitivity analysis for the optimal design of distributed energy systems," *Applied Energy*, vol. 214, pp. 219–238, 2018.

[195] R. Mena, M. Hennebel, Y.-F. Li, C. Ruiz, and E. Zio, "A risk-based simulation and multi-objective optimization framework for the integration of distributed renewable generation and storage," *Renewable and Sustainable Energy Reviews*, vol. 37, pp. 778–793, 2014.

[196] F. Y. Ettoumi, A. Mefti, A. Adane, and M. Bouroubi, "Statistical analysis of solar measurements in algeria using beta distributions," *Renewable Energy*, vol. 26, no. 1, pp. 47–67, 2002.

[197] E. Chia and M. Hutchinson, "The beta distribution as a probability model for daily cloud duration," *Agricultural and forest meteorology*, vol. 56, no. 3-4, pp. 195–208, 1991.

[198] B. R. Prusty and D. Jena, "A sensitivity matrix-based temperature-augmented probabilistic load flow study," *IEEE Transactions on Industry Applications*, vol. 53, no. 3, pp. 2506–2516, 2017.

[199] N. Nikmehr and S. N. Ravadanegh, "Optimal power dispatch of multi-microgrids at future smart distribution grids," *IEEE Transactions on Smart Grid*, vol. 6, no. 4, pp. 1648–1657, 2015.

[200] I. A. Azzollini, V. Di Felice, F. Fraboni, L. Cavallucci, M. Breschi, A. Dalla Rosa, and G. Zini, "Lead-acid battery modeling over full state of charge and discharge range," *IEEE Transactions on Power Systems*, vol. 33, no. 6, pp. 6422–6429, 2018.

[201] D. U. Sauer, "Optimierung des einsatzes von blei-säure-akkumulatoren in photovoltaik-hybrid-systemen unter spezieller berücksichtigung der batteriealterung," Ph.D. dissertation, Universität Ulm, 2009.

[202] J. Sachs, *Model-based Optimization of Hybrid Energy Systems*. Shaker Verlag, 2016.

[203] B. Homan, V. Marnix, J. L. Hurink, and G. J. Smit, "A realistic model for battery state of charge prediction in energy management simulation tools," *Energy*, vol. 171, pp. 205–217, 2019.

[204] F. A. Farret and M. G. Simões, *Integration of renewable sources of energy*. John Wiley & Sons, 2017.

[205] J. Schiffer, D. U. Sauer, H. Bindner, T. Cronin, P. Lundsager, and R. Kaiser, "Model prediction for ranking lead-acid batteries according to expected lifetime in renewable energy systems and autonomous power-supply systems," *Journal of Power sources*, vol. 168, no. 1, pp. 66–78, 2007.

[206] C.-C. Hua and M.-Y. Lin, "A study of charging control of lead-acid battery for electric vehicles," in *ISIE'2000. Proceedings of the 2000 IEEE International Symposium on Industrial Electronics (Cat. No. 00TH8543)*, vol. 1. IEEE, 2000, pp. 135–140.

[207] R. Dufo-López, J. M. Lujano-Rojas, and J. L. Bernal-Agustín, "Comparison of different lead–acid battery lifetime prediction models for use in simulation of stand-alone photovoltaic systems," *Applied Energy*, vol. 115, pp. 242–253, 2014.

[208] M. Mohsin, A. Picot, and P. Maussion, "Lead-acid battery modelling in perspective of ageing: a review," in *2019 IEEE 12th International Symposium on Diagnostics for Electrical Machines, Power Electronics and Drives (SDEMPED)*. IEEE, 2019, pp. 425–431.

[209] D. Schulte, D. U. Sauer, E. Ebner, A. Börger, S. Gose, and H. Wenzl, ""stratifiability index"–a quantitative assessment of acid stratification in flooded lead acid batteries," *Journal of Power Sources*, vol. 269, pp. 704–715, 2014.

[210] M. Kwiecien, M. Huck, J. Badeda, C. Zorer, K. Komut, Q. Yu, and D. U. Sauer, "Variation of impedance in lead-acid batteries in the presence of acid stratification," *Applied Sciences*, vol. 8, no. 7, p. 1018, 2018.

[211] M. Bruck, P. Sandborn, and N. Goudarzi, "A levelized cost of energy (lcoe) model for wind farms that include power purchase agreements (ppas)," *Renewable energy*, vol. 122, pp. 131–139, 2018.

[212] T. Tezer, R. Yaman, and G. Yaman, "Evaluation of approaches used for optimization of stand-alone hybrid renewable energy systems," *Renewable and Sustainable Energy Reviews*, vol. 73, pp. 840–853, 2017.

[213] B. Wu, A. Maleki, F. Pourfayaz, and M. A. Rosen, "Optimal design of stand-alone reverse osmosis desalination driven by a photovoltaic and diesel generator hybrid system," *Solar Energy*, vol. 163, pp. 91–103, 2018.

[214] N. N. Castellano, J. A. G. Parra, J. Valls-Guirado, and F. Manzano-Agugliaro, "Optimal displacement of photovoltaic array's rows using a novel shading model," *Applied energy*, vol. 144, pp. 1–9, 2015.

[215] K. Mertens, *Photovoltaics: fundamentals, technology, and practice*. John Wiley & Sons, 2018.

[216] N. Tran *et al.*, "Limit and shakedown analysis of structures under stochastic conditions," Ph.D. dissertation, 2019.

[217] A. Geletu, M. Klöppel, A. Hoffmann, and P. Li, "A tractable approximation of non-convex chance constrained optimization with non-gaussian uncertainties," *Engineering Optimization*, vol. 47, no. 4, pp. 495–520, 2015.

[218] B. K. Pagnoncelli, S. Ahmed, and A. Shapiro, "Sample average approximation method for chance constrained programming: theory and applications," *Journal of optimization theory and applications*, vol. 142, no. 2, pp. 399–416, 2009.

[219] A.-T. Nguyen, S. Reiter, and P. Rigo, "A review on simulation-based optimization methods applied to building performance analysis," *Applied Energy*, vol. 113, pp. 1043–1058, 2014.

[220] J. Guttag, *Introduction to computation and programming using Python: With application to understanding data*. MIT Press, 2016.

[221] Trading economics. [Online]. Available: http://www.tradingeconomics.com

[222] L. Luo, W. Gu, X.-P. Zhang, G. Cao, W. Wang, G. Zhu, D. You, and Z. Wu, "Optimal siting and sizing of distributed generation in distribution systems with PV solar farm utilized as statcom (PV-STATCOM)," *Applied Energy*, vol. 210, pp. 1092–1100, 2018.

[223] 3D sun-path - andrewmarsh.com. [Online]. Available: http://andrewmarsh.com/apps/staging/sunpath3d.html

[224] M. Alramlawi, Y. Souidi, and P. Li, "Optimal design of PV-battery microgrid incorporating lead-acid battery aging model," in *2019 IEEE International Conference on Environment and Electrical Engineering and 2019 IEEE Industrial and Commercial Power Systems Europe (EEEIC/I&CPS Europe)*. IEEE, 2019, pp. 1–6.

[225] J. Väisänen, A. Kosonen, J. Ahola, T. Sallinen, and T. Hannula, "Optimal sizing ratio of a solar PV inverter for minimizing the levelized cost of electricity in finnish irradiation conditions," *Solar Energy*, vol. 185, pp. 350–362, 2019.

[226] M. Alramlawi, A. F. Timothy, A. Gabash, E. Mohagheghi, and P. Li, "Optimal operation of PV-diesel microgrid with multiple diesel generators under grid blackouts," in *2018 IEEE International Conference on Environment and Electrical Engineering and 2018 IEEE Industrial and Commercial Power Systems Europe (EEEIC/I&CPS Europe)*. IEEE, 2018, pp. 1–6.